BILINGUAL PUBLISHING GROUP

Journal of Electronic & Information Systems

Volume 5 • Issue 2 • October 2023 ISSN 2661-3204 (Online)

Volume 5 Issue 2 • October 2023 • ISSN 2661-3204 (Online)

Journal of Electronic & Information Systems

BILINGUAL PUBLISHING GROUP

BILINGUAL PUBLISHING GROUP

Volume 5 | Issue 2 | October 2023 | Page1-66

Journal of Electronic & Information Systems

Contents

Articles

BILINGUAL PUBLISHING GROUP

Journal of Electronic & Information Systems
https://journals.bilpubgroup.com/index.php/jeis

ARTICLE

Stressed Coral Reef Identification Using Deep Learning CNN Techniques

***S.P. Aruna*[1], *M. Thamarai*[2*]**

[1] *Skilltroniks Technologies, Tadepalligudem, Andhra Pradesh, 534101, India*
[2] *ECE Department, Sri Vasavi Engineering College, Tadepalligudem, Andhra Pradesh, 534102, India*

ABSTRACT

Deep learning is a machine learning technique that allows the computer to process things that occur naturally to humans. Today, deep learning techniques are commonly used in computer vision to classify images and videos. As a result, for challenging computer vision problems, deep learning provides state of the art solutions to it. Coral reefs are an essential resource of the earth. A new study finds the planet has lost half of its coral reefs since 1950. It is necessary to restore and prevent damage to coral reefs as they play an important role in maintaining a balance in the marine ecosystem. This proposed work helps to prevent the corals from bleaching and restore them to a healthy condition by identifying the root cause of the threats. In the proposed work, using deep learning CNN techniques, the images are classified into Healthy and Stressed coral reefs. Stressed coral reefs are an intermediate state of coral reef between healthy and bleached coral reefs. The pre-trained models Resnet50 and Inception V3 are used in this study to classify the images. Also, a proposed CNN model is built and tested for the same. The results of Inception V3 and Resnet50 are improved to 70% and 55% by tuning the hypermeters such as dropouts and batch normalisation. Similarly, the proposed model is tuned as required and obtains a maximum of up to 90% accuracy. With large datasets, the optimum amount of neural networks and tuning it as required brings higher accuracy than other methods.

Keywords: Stressed coral reef; Deep learning; Convolutional neural network; Pre-trained models

1. Introduction

The ocean is a large resource that supports life, fights climate crises, and is home to large biodiversity. Unlike landforms, oceans are one continuous body that connects every corner of our planet. Ocean

*CORRESPONDING AUTHOR:
M. Thamarai, ECE Department, Sri Vasavi Engineering College, Tadepalligudem, Andhra Pradesh, 534102, India; Email: mthamarai2014@gmail.com

ARTICLE INFO
Received: 27 June 2023 | Revised: 29 August 2023 | Accepted: 30 August 2023 | Published Online: 8 September 2023
DOI: https://doi.org/10.30564/jeis.v5i2.5808

CITATION
Aruna, S.P., Thamarai, M., 2023. Stressed Coral Reef Identification Using Deep Learning CNN Techniques. Journal of Electronic & Information Systems. 5(2): 1-9. DOI: https://doi.org/10.30564/jeis.v5i2.5808

ecosystems are the largest of Earth's aquatic ecosystems which support many lives and also benefit human beings in many ways. Coral ecosystems are part of marine ecosystems formed up of coral reefs. These coral reefs provide shelter to millions of marine species and protect the land coastline from storms and erosions. It provides rich aquatic life for fishing and other purposes. Increasing ocean temperature and rapid global warming are some of the risks of coral reef bleaching. Human activities such as water pollution also affect the quality and life of the corals. So, it is necessary to prevent the coral from damage detect the early signs of coral damage and restore it. In this method, we are detecting whether the coral is stressed or not using a CNN deep learning algorithmThe ocean is a large resource that supports life, fights climate crises, and is home to large biodiversity. Unlike landforms, oceans are one continuous body that connects every corner of our planet. Ocean ecosystems are the largest of Earth's aquatic ecosystems which support many lives and also benefit human beings in many ways. Coral ecosystems are part of marine ecosystems formed up of coral reefs. These coral reefs provide shelter to millions of marine species and protect the land coastline from storms and erosions. It provides rich aquatic life for fishing and other purposes. Increasing ocean temperature and rapid global warming are some of the risks of coral reef bleaching. Human activities such as water pollution also affect the quality and life of the corals. So, it is necessary to prevent the coral from damage detect the early signs of coral damage and restore it. In this method, we are detecting whether the coral is stressed or not using a CNN deep learning algorithm.

1.1 Coral reef biodiversity

Coral reefs are formed of colonies of hundreds to thousands of tiny individual corals commonly known as polyps. These marine invertebrate animals have hard exoskeletons made of calcium carbonate and are sessile. The large coral reef (Great Barrier Reef) is found in Queensland, Australia. These corals are colourless in nature. The microscopic algae named Zooxanthellae that live in it, adds different colours. Corals and algae have a mutual relationship. The coral offers the zooxanthellae a safe environment as well as the substances essential for photosynthesis. The zooxanthellae create oxygen and aid the coral in removing trash as payment. Millions of zooxanthellae produce pigments that add colours to coral. Depending on the colour of the coral image, we can predict using CNN whether the coral is stressed or not. It is an advantage for us, at this point the damage made is minimal we can prevent it from bleaching.

1.2 Coral bleaching

The corals are classified into the following stages.

Healthy Coral: Healthy coral reefs are bright corals filled with microscopic algae called zooxanthellae that live in their tissues. These algae give bright colors to coral reefs.

Stressed Coral: Stressed coral reefs are less bright compared to healthy coral reefs. Due to the temperature rise, it loses its color as algae tend to leave the coral reefs.

Bleached Coral: Bleached coral reefs are empty coral reefs with any algae present in them. It is white because only the coral skeleton is present.

The Healthy Coral, Stressed Coral and Bleached Coral are shown in **Figures 1a. and 1b. and 1c.** respectively.

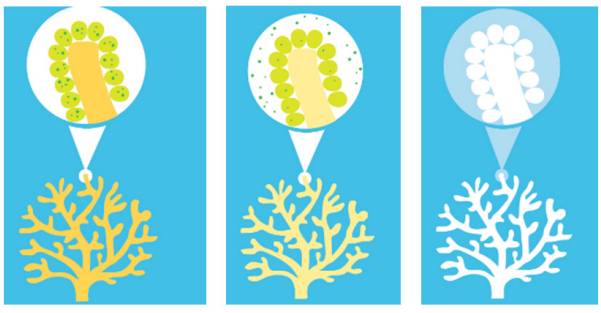

a. Healthy coral b. Stressed coral c. Bleached coral

Figure 1. Coral reefs.

Causes for bleaching

Climate change causes a rise in the ocean temperature that results in coral bleaching. Industrial pollutants and fertilizer wastes that drain into the ocean

also change its environment and cause coral bleaching. Direct exposure to sunlight in shallow waters also causes coral bleaching. Low tides and exposure to air may also cause bleaching. When water gets too warm for corals, corals release their colorful microalgae, turning skeletal white. If bleaching events are prolonged or happen too frequently with not enough time to recover in between, significant coral mortality can occur, sealing the fate of coral reefs.

The Global Coral Reef Monitoring Network (GCRMN) is a network of the International Coral Reef Initiative (ICRI) that has published a report titled The Status of Coral Reefs of the World: 2020. Its findings illustrate that, between 2009 and 2018, there was a progressive loss of 14% of the corals brought on by frequent, massive bleaching events. More hard coral was destroyed than is currently present on Australia's coral reefs, totalling around 11,700 square kilometres. Similar to the decline in hard coral throughout this time period, the amount of algae on coral reefs around the world has increased by roughly 20% since 2010. The report depicts four decades of falling coral abundance, increased bleaching, and rising algae levels, which are indicators of deteriorating reef health. The paper also highlights the remarkable capacity of coral reefs to recover in the absence of local and global threats. Both conclusions ought to spur immediate action. Coral reefs are largely invisible, but environmental protection must prioritize their health. Global Coral Reef Monitoring Network (GCRMN) is a network that maintains and operates the international coral reef and provides information about it [1]. GCRMN divides it into ten regional nodes. They are Australia, the Caribbean, ETP, etc, GCRMN collects the database, monitors it from time and time, and publishes its status. It states that almost all the coral reefs are extinct due to global warming and local human activities. Also, some parts of coral reefs proved to remain resilient and can recover from damage by taking appropriate measures. There are more than 600 subspecies in just the Great Barrier Reef in Australia. They come in a wide range of sizes, shapes, and colours, making them a diversified species. Hard corals and soft corals are the two main types of corals. Soft corals are flexible and frequently mistaken for plants because they lack the Skelton, which hard corals have. The best coral reef health indicator is hard coral. The most crucial factor in quantifying the coral population is the hard coral cover percentage.

Coral reefs that are dominated by algae lose some of their architectural complexity and structural integrity. The goal of NOAA's Coral Health and Monitoring Programme (CHAMP), which was established to help protect and preserve the health of coral reefs around the world, is to offer resources and services to researchers and the general public.

The proposed work comprises the following:

· Pre-trained models such as InceptionV3 and Resnet50 are fine-tuned by adding batch normalization and dropout layers to eliminate overfitting parameter problems and improve the stressed coral reef identification accuracy.

· An efficient low-complexity CNN architecture is proposed for stressed coral reef identification.

· The performance of the pre-trained models and proposed CNN model are analysed using performance metrics such as classification accuracy, F1 score, precision and Recall.

The paper is organized as follows. Section 1 describes the introduction to coral reefs and the importance of coral reef identification. Section 2 reviews deep learning and previous work on coral reef classification using convolution neural networks. Section 3 describes the proposed work for stressed coral reef identification using pre-trained models and proposed low-complexity CNN architecture. Section 4 discusses the results and Section 5 concludes the paper.

2. Deep learning

Deep learning networks, which are advanced neural networks with a lower error rate, are crucial for solving prediction and classification problems. Deep learning networks, a subtype of artificial intelligence, are employed for a number of tasks, including image identification, speech to text conversion, scene description, drug discovery, face detection and recognition, weather forecasting, and more [2,3].

2.1 Convolutional neural network

A convolutional neural network is a network architecture of deep learning algorithms [4]. It has high performance and accuracy in image classifications by finding or recognizing required patterns in the images. It breaks the pixels of the image into smaller pixels and detects the required data in them. A typical convolutional neural network has the following layers and the architecture is shown in **Figure 2**.

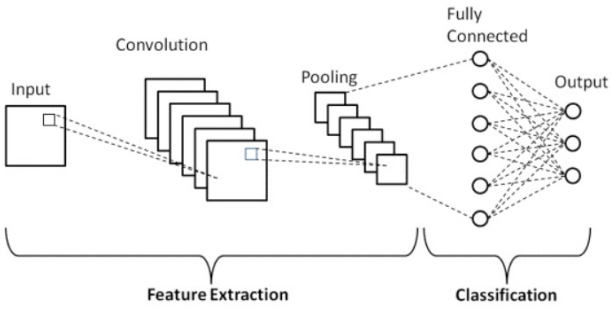

Figure 2. Typical convolution neural network architecture.

Convolutional layer

The convolution layer is the mathematical layer that processes the image segment by segment and filters it as given. The input image is divided into three for an RGB image and one for a grey image. The filter filters the input image with the provided kernel size. Using the Dot product, the value of the input image and filter is multiplied and stored in them.

Pooling layer

The pooling layer is next to the convolution layer. There are two types of pooling, max pooling, and average pooling. Max pooling returns the max value in the feature map. Average pooling returns the average value of the feature map. For example, the kernel size is 2 × 2, and its values are 34, 56, 78, and 23. If max pooling is selected, it returns the value 78 from the feature map. If the average pooling is selected, it returns the value 48. Between the convolutional layer and the fully linked layer, the pooling layer frequently acts as an intermediate.

Fully connected layer

The fully connected layer is the layer that connects one neutral network to the output neutral network. It connects the weights and biases of previous neurons to the weights and biases of the next neurons. The final layers of CNN are used to summarize the network by flattening and connecting it to the output layer. The flattening layer reduces the dimension of the network to one. Here, based on the type of problem, the output layer is provided. For example, if it is classification, then it is Sigmoid.

Activation functions

The activation function is an essential function of the CNN model. It identifies and transfers the variables from one neuron to another neuron. It decides what should be transferred and what should be not. This network is non-linear. Activation functions like ReLu, Sigmoid, Tanh, and Softmax are used in it. ReLu connects the value of the variable from zero to infinity. If any negative value is present in the ReLu, it is considered zero. The tanh connects from a negative one to a positive one. Sigmoid is for binary classification problems and Softmax is for multiclass classification problems.

2.2 Deep learning in coral reef classification

This section describes the previous work done in the coral reef classification using deep learning.

Automated underwater vehicles (AUVs) have been successfully used to monitor these reefs in recent years. These computers can be improved to categorise many coral species, though, by integrating neural networks [5,6].

Additionally, poor picture quality is a constant problem, resulting in hazy and blurry images. This is because the sediments in the water make it difficult to take high-quality pictures, even though the coral photos transect uses this technique for image capture and processing. Then, it generates photos of excellent quality and makes it noticeably simpler to see the characteristics of corals [7].

Elawadyetal. developed a machine vision algorithm to enable underwater robots to locate coral reefs and pick them up using CNN [8]. The shape and texture features are added as supplementary channels along with basic spatial color channels of coral input images and used for classification. Raphael et al. developed an automated DL classification scheme for

11 species of corals present in the Eilat Gulf regio [9]. Chindapol et al.used advection diffusion equations to model the effects of flow on coral reef colony growth and shape [10]. Mahmood et al. used neural networks and deep learning to distinguish various coral species and live corals from bleached corals. The author used VGGNet with a 2-layer MLP classifier for the classification of corals in their work [11]. Mahmood et al. discussed the power of deep learning for monitoring coral reefs in their survey work [12]. Mahmood et al. combined CNN images and handcrafted features for coral classification, but this approach is computationally expensive and not suitable for large datasets [12]. Mahmood et al. used VGGNet for the classification of unlabeled coral mosaics [13].

Gómez-Ríos et al. used three various CNN architectures—Inception V3, ResNet, and Densenet and data augmentation techniques to obtain high accuracy in coral texture image classification [14]. Mary et al. used improved local derivative patterns for submarine coral reef image classification [15]. Lumini et.al.developed ensemble-based different convolution neural network models for underwater imagery analysis [16].

3. Proposed work

The proposed work pre-trained models have been trained using the transfer learning concept and tested. The pre-trained CNN models Inception V3 and Resnet50 are fine-tuned to improve the performance in stressed coral reef identification. In addition to it, a new CNN model was also built and studied and compared its performance with the pre-trained models.

3.1 Resnet50 architecture

The pre-trained model, Resnet50 architecture is shown in **Figure 3**. The architecture has 50 layers and is specially designed to eliminate training errors. The network has a special block called residual block which is shown in **Figure 3**. A residual block also referred to as a "bottleneck", uses 11 convolutions to cut down on the number of parameters and matrix multiplications. This makes each layer's training significantly faster.

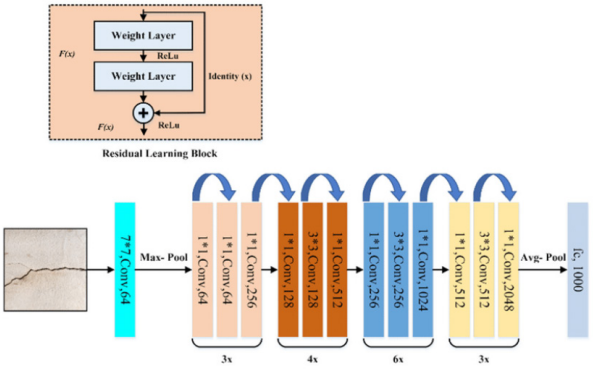

Figure 3. Resnet50 architecture.

3.2 Inception V3 architecture

The important milestone in CNN development is the inception network which is shown in **Figure 4**. Convolutional neural network model Inception V3 has 48 layers and was pre-trained. It is an Inception network variant that has been trained on more than a million images from the image net collection. It is the third iteration of Google's Inception CNN model.

A popular image recognition algorithm called Inception V3 has demonstrated improved accuracy on the ImageNet dataset.

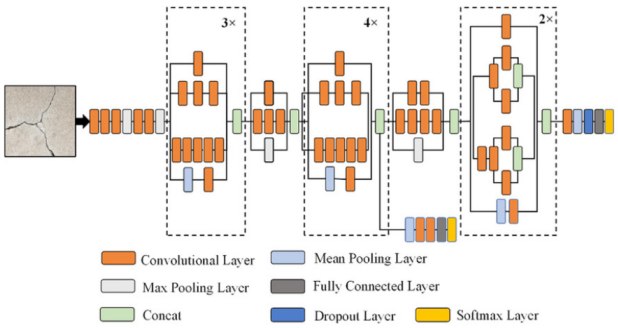

Figure 4. Inception network.

3.3 Fine-tuning the pre-trained models

For the models, the pre-trained models of InceptionV3 and Resnet50 are inherited using the keras library. For InceptionV3, the base model is loaded and then fine-tuned with the required parameters. Using the GlobalAveragePooling3D() function, the dimensions of the inputs given are adjusted cause

channels_last corresponds to inputs with shape (batch, height, width, channels) while channels_first corresponds to inputs with shape (batch, channels, height, width). To extend the base model, GlobalAveragePooling3D is used and also to avoid dimension conflicts. In the case of InceptionV3, the model is trained with more accuracy and it is in an overfitting condition. To avoid this condition, a Dropout(0.1) of weights is added to improve the model efficiency and avoid overfitting. Dropout is the layer of keras that is used to remove the weights that are overtrained based on the percentage given. Then, it is connected to the intermediate dense layer with "Relu" activation and connected to the output layer with softmax activation. After the changes are made, the model is trained with train and test datasets. It is compiled using Adam optimizers and then fitted with the validation data as 20% and batch size as 32.

Similarly, the works are done for the Resnet50 model. The base model is loaded and then fine-tuned with the required parameters. Using the GlobalAveragePooling3D() function, the dimensions of the inputs given are adjusted cause channels last correspond to inputs with shape (batch, height, width, channels) while channels first correspond to inputs with shape (batch, channels, height, width). To extend the base model, GlobalAveragePooling3D is used and also to avoid dimension conflicts. In the case of Restnet50, our model is learning too slowly and also reaches a steady learning rate. Once the model reaches a steady learning rate, adjusting the learning rate may not give significant results. So, the Batchnormalisation function is added to the neutral network to improve the model efficiency. Like InceptionV3, it is also connected to an intermediate dense layer with "Relu" activation and connected to the output layer as Softmax activation. After the changes are made, the model is trained with train and test datasets. It is compiled using Adam optimizers and then fitted with the validation data as 20% and batch size as 32.

3.4 Proposedlow complexity CNN model

In the proposed CNN model, we trained the data separately and created a sequential model using keras. Inside the model, we added two convolution2D layers with the required parameters. RELU activation is used in each neutral network as shown in **Figure 5**. Also, dropouts and Batchmormalisation hypermeters and adjusted as required to improve the model efficiency. It is connected to output layers with dense = 1 and activation = Sigmoid since it is the binary class classification. The model size is very small when compared to the Resnet50 and Inception V3 pre-trained models. The proposed model is memory efficient with less number of training parameters. The model is compiled and fitted with the validation data as 20% and batch size as 4.

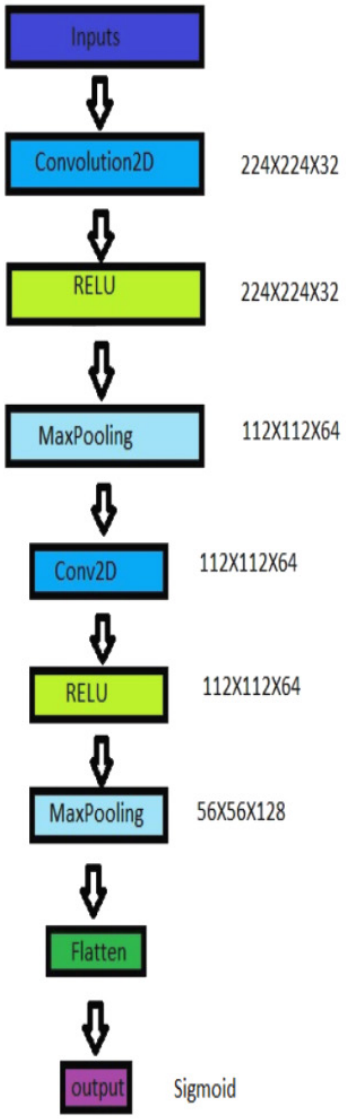

Figure 5. Proposed CNN model.

4. Results and metrics

The pre-trained models and proposed CNN model are trained and tested with our dataset collected from internet sources. The dataset contains 120 images. The dataset has an equal number of healthy and stressed coral images(healthy coral reef images: 60, stressed coral reef images). All the models are compiled and fitted with the validation data as 20% and different batch sizes.

The sample input images in the two categories (healthy and stressed coral reef images) are shown in **Figure 6**. The healthy coral images used in the training dataset are shown in **Figures 6a and 6b** and stressed coral reefs used in the dataset are shown in **Figures 6c and 6d** respectively.

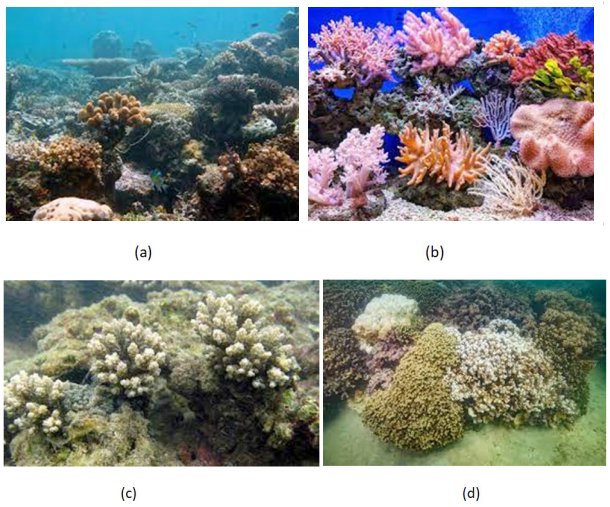

Figure 6. Input coral reef images. (a) and (b) represent the healthy coral reef images used in the dataset. (c) and (d) represent the stressed coral reef images used in the dataset.

The confusion matrix of each model is extracted for the test images. Then, the precision, recall, and accuracy of each model are calculated.

The confusion matrix for our model is represented in **Table 1**.

Precision = True Positive/(True Positive + False Positive)

Precision gives us the quality of positive predictions.

Recall Formula = True Positive/(True Positive + False Negative)

Recall, also known as sensitivity gives us the proportion of actual positives that were identified correctly.

Accuracy Formula = (True Positive +True Negative)/(True Positive + False Positive + False Negative + True Negative)

Table 1. Confusion matrix for the coral reef classification (proposed) model.

True positive—The image of stressed coral reefs are identified correctly.	False positive—The image of stressed coral reef is identified as healthy coral reef. (Type II error)
False Negative—The image of healthy coral reef is identified as stressed coral reef. (Type I error)	True Negative—The image of coral reefs are found not stressed.

Accuracy gives us the number of correct predictions that the trained model achieves.

Comparing the precision, recall, and accuracy for the three models, based on the correct predictions of stressed coral reefs and healthy coral reefs, the values are calculated and given in **Table 2**. The dataset is collected from coral website images in Google. Totally 120 images are in the dataset. The training images are 100 (Healthy: 50 images; stressed: 50 images). The sample test images given are 20 images, 10—healthy coral reef images and 10—stressed coral reef images. The performance of the proposed CNN in classifying stressed coral is 90%, which is the highest accuracy when compared to the fine tuned pre-trained models. The accuracy is 15% higher than the Inception V3 model and 35% higher than the Resnet50 model. The proposed model CNN model predicts the healthy and stressed coral with the same accuracy (90%).

Table 2. Performance comparison of the proposed CNN model with pre-trained models.

CNN model	Test data	Precision	Recall	F1 score
Inception V3 (Pretrained fine tuned model using transfer learning concept)	Healthy	0.67	0.80	0.73
	Stressed	0.75	0.60	0.67
Resnet50 (Pretrained finetuned model using transfer learning concept)	Healthy	0.56	0.50	0.53
	Stressed	0.55	0.60	0.57
Proposed CNN model	Healthy	**0.90**	**0.90**	**0.90**
	Stressed	**0.90**	**0.90**	**0.90**

The classification accuracy is computed as follows for sample 20 input test images.

Accuracy of Inception V3 model is(8+6)/(8+2+4+6)= 0.7

Accuracy of Resnet50 model is (5+6)/(5+5+4+6)= 0.55

Accuracy of proposed CNN model is (9+9)/(9+1+9+1)= 0.9

5. Conclusions

Action needs to be taken after identifying stressed corals.

Once the stressed coral reef is identified in a particular area. Scientists can analyse the reasons behind its decay and its root causes. If the coral is stressed, it tends to lose its pigmentation causing the algae that are living together to start to move away from it, due to some natural causes or man-made pollution. Natural causes involve ocean temperature rise, climate change, etc. Man-made causes involve water pollution, global warming, etc. Once the scientists analysed and found its root cause, it would be easy to restore the coral reef to a healthy stressed state. It would take a lot of effort to restore it from a bleached state. Which is why, we are identifying it in the stressed state itself.

Prevention is better than cure. The coral reef forms a major economic source of ocean resources for a country or a state. It is necessary to maintain it in its state of health. Because a healthy coral reef enhances fish production, healthy aquatic life such as seaweeds has economic value. That's why it is significant to prevent the coral from bleaching. In our models, we are identifying in our early bleaching stage (i.e. stressed stage) and helping them to restore it to a healthy state.

The proposed work describes an efficient low computational complexity CNN model to predict the stressed corals and the model classification accuracy is 90% which is 15% higher than the Inception V3 model accuracy and 35% higher than the Resnet50 model. In the future, the pre-processing techniques will be applied to overcome the underwater image blur and colour balancing and then the proposed method will be suitable for real-time applications.

Author Contributions

Author 1: Concept, writing, execution and results.
Author 2: Writingand result analysis.

Conflict of Interest

There is no conflict of interest.

References

[1] Status of Coral Reefs of the World: 2020 [Internet]. Available from: https://gcrmn.net/2020-report/

[2] Chandrasekar, V., Sureshkumar, V., Kumar, T.S., et al., 2020. Disease prediction based on micro array classification using deep learning techniques. Microprocessors and Microsystems. 77, 103189.
DOI: https://doi.org/10.1016/j. micpro.2020.103189

[3] Chen, K.C.J., Ebrahimi, M., Wang, T.Y., et al., 2020. A NoC-based simulator for design and evaluation of deep neural networks. Microprocessors and Microsystems. 77, 103145.
DOI: https://doi.org/10.1016/j.micpro.2020.103145

[4] O'Shea, K., Nash, R., 2015. An introduction to convolutional neural networks. arXiv preprint arXiv: 1511.08458.

[5] Moniruzzaman, M., Islam, S.M.S., Bennamoun, M., et al. (editors), 2017. Deep learning on underwater marine object detection: A survey. Advanced Concepts for Intelligent Vision Systems: 18th International Conference, ACIVS 2017; 2017 Sep 18-21; Antwerp, Belgium. p. 150-160.

[6] Borbon, J., Javier, J., Llamado, J., et al. (editors), 2021. Coral health identification using image classification and convolutional neural networks. 2021 IEEE 13th International Conference on Humanoid, Nanotechnology, Information Technology, Communication and Control, Environment, and Management (HNICEM); 2021 Nov 28-30; Manila, Philippines. New York: IEEE. p. 1-6.

[7] Marks, K., 2013. PVC Paparazzi [Internet]. Living Oceans Foundation [cited 2014 Feb 25]. Available from: https://www.livingoceansfoundation.org/pvc-paparazzi/

[8] Elawady, M., 2015. Sparse coral classification using deep convolutional neural networks. arXiv preprint arXiv: 1511.09067.

[9] Raphael, A., Dubinsky, Z., Iluz, D., et al., 2020. Deep neural network recognition of shallow water corals in the Gulf of Eilat (Aqaba). Scientific Reports. 10(1), 12959.

[10] Chindapol, N., Kaandorp, J.A., Cronemberger, C., et al., 2013. Modelling growth and form of the scleractinian coral Pocillopora verrucosa and the influence of hydrodynamics. PLoS Computational Biology. 9(1), e1002849.

[11] Mahmood, A., Bennamoun, M., An, S., et al. (editors), 2016. Coral classification with hybrid feature representations. 2016 IEEE International Conference on Image Processing (ICIP); 2016 Sep 25-28; Phoenix, AZ, USA. New York: IEEE. p. 519-523.

[12] Mahmood, A., Bennamoun, M., An, S., et al., 2017. Deep learning for coral classification. Handbook of neural computation. Academic Press: Cambridge. pp. 383-401.

[13] Mahmood, A., Bennamoun, M., An, S., et al. (editors), 2016. Automatic annotation of coral reefs using deep learning. Oceans 2016 MTS/IEEE Monterey; 2016 Sep 19-23; Monterey, CA, USA. New York: IEEE. p. 1-5.

[14] Gómez-Ríos, A., Tabik, S., Luengo, J., et al., 2019. Towards highly accurate coral texture images classification using deep convolutional neural networks and data augmentation. Expert Systems with Applications. 118, 315-328.

[15] Mary, N.A.B., Dharma, D., 2017. Coral reef image classification employing improved LDP for feature extraction. Journal of Visual Communication and Image Representation. 49, 225-242.

[16] Lumini, A., Nanni, L., Maguolo, G., 2020. Deep learning for plankton and coral classification. Applied Computing and Informatics. (ahead-of-print).

BILINGUAL PUBLISHING GROUP

Journal of Electronic & Information Systems
https://journals.bilpubgroup.com/index.php/jeis

ARTICLE

The Application of Information Systems to Improve Ambulance Response Times in the UK

Alan Slater

University of Huddersfield, Huddersfield, HD13DH, UK

ABSTRACT

Emergency ambulance services in the UK are tasked with providing pre-hospital patient care and clinical services with a target response time between call connect to on-scene attendance. In 2017, NHS England introduced four new response time categories based on patient needs. The most challenging is to be on-scene for a life-threatening situation within seven minutes of the call being connected when such calls are random in terms of time and place throughout a large territory. Recent evidence indicates emergency ambulance services regularly fall short of achieving the target ambulance response times set by the National Health Service (NHS). To achieve these targets, they need to undertake transformational change and apply statistical, operations research and artificial intelligence techniques in the form of five separate modules covering demand forecasting, plus locate, allocate, dispatch, monitoring and re-deployment of resources. These modules should be linked in real-time employing a data warehouse to minimise computational data and generate accurate, meaningful and timely decisions ensuring patients receive an appropriate and timely response. A simulation covering a limited geographical area, time and operational data concluded that this form of integration of the five modules provides accurate and timely data upon which to make decisions that effectively improve ambulance response times.

Keywords: Ambulance response times; Demand forecasting; Geo-location models; Simulation

1. Introduction

Management in the UK Ambulance Service has accepted the challenge to develop the ability to collect and apply information innovatively. However, the focus has been on rapidly changing technology

*CORRESPONDING AUTHOR:
Alan Slater, University of Huddersfield, Huddersfield, HD13DH, UK; Email: alan@contactslater.co.uk

ARTICLE INFO
Received: 5 August 2023 | Revised: 28 August 2023 | Accepted: 29 August 2023 | Published Online: 21 September 2023
DOI: https://doi.org/10.30564/jeis.v5i2.5881

CITATION
Slater, A., 2023. The Application of Information Systems to Improve Ambulance Response Times in the UK. Journal of Electronic & Information Systems. 5(2): 10-24. DOI: https://doi.org/10.30564/jeis.v5i2.5881

and solving stand-alone issues such as crew scheduling rotas rather than linking opportunities together to improve overall efficiency and productivity. The centre of attention for management since the COVID-19 pandemic has been arresting a significant decline in ambulance response time (also known as 'clock-time'). This paper addresses the need to understand how identifying, upgrading and linking together several focused micro-information modules will create a macro information system that offers a foundation for improved ambulance response times.

The ambulance response time process is seen by management as the most significant issue in their service to critically ill patients because response time is both challenging and the key performance indicator by which the service is judged by both politicians and the public. This paper focuses upon an alternative approach to improving the ambulance dispatch process by utilising the combination of several real-time information systems which the ambulance service control directly on a day-to-day basis. There are, however, other influences on response times that cannot be controlled by the ambulance service on a day-to-day basis including vehicle design, vehicle maintenance, driver training, traffic management and public awareness. Attention to such issues may be combined with dispatch information to improve ambulance response times.

Attention to the information systems which support the ambulance response system could be the first step in the creation of a 'smart ambulance operation' which uses a set of rules incorporated in an 'artificial intelligence' system to recommend appropriate actions to call-handlers and dispatchers.

2. Operating environment

The objective of the ambulance service is to provide 'out-of-hospital' early medical assistance to 'save lives' by causing 'no further harm' before and during transporting a patient to a relevant hospital facility. Cooke [1] speculated that delays in pre-hospital care could lead to poorer patient outcomes and patient satisfaction increased when response was rapid.

In England, the public believes there is equality of access to appropriate pre-hospital care from the ambulance service based upon national ambulance response time targets—which are the time taken in minutes from an emergency call being connected to the ambulance service and the on-scene attendance by appropriate staff. The UK public has been encouraged by both the NHS management and the press to judge the ambulance service by its response to 'life-threatening' calls. Indicating that when they make a call for an ambulance one will be dispatched immediately (with 'blue lights and sirens') implying that resources are always available to answer every call and that each call is equally important and taken in priority of receipt.

In reality, ambulance managers prioritise calls using various response times according to patient needs. This means that calls classified as 'life-threatening' have a short response time target, whereas calls classified as 'urgent' have a longer response time target. This practice creates a tiered system of requirements to respond which allows resources to be allocated throughout the territory as 'ready to respond' thus maximising the response time target achievement with limited resources. However, short-term peaks in demand may lead to a lack of resources to respond to patient calls. In the event of a shortage of resources, an outbound crew on less urgent calls may be diverted to a life-threatening call.

The public may be unaware and do not recognise that there is a variation in response times although call handlers normally quote a forecast on-scene arrival time either when a despatcher has allocated a resource or alternatively they quoted a forecast waiting time before a resource will be allocated. The public is not made aware of the contributory factors behind any change in response time performance. Only since COVID-19 has such factors as traffic delays, hand-over delays at Accident and Emergency, or staff and vehicle availability been cited as causes for response time delays.

Unfortunately, recent press reporting concentrates upon failures to attend 'life-threatening emergencies' within the 7-minute response time target even though such situations represent less than 10% of all calls.

In reality, emergency ambulance services are tasked with reaching patients, by category of clinical need, as defined by the Advanced Medical Priority System (AMPDS), with suitably qualified staff. The response time targets, rather than the patient outcome, have become the key performance measure by which the press and public judge the success of ambulance services. However, Heath and Radcliffe [2,3] have criticised the NHS for concentrating only on ambulance service response times when the ambulance service offers a greater range of skills.

The NHS has over recent years reviewed the AMPDS and adjusted the provisional patient diagnosis categories, which are accessed by the call-handlers, such that the target response time is more appropriate to the patient pathway measured in terms of potential further harm and probability of a successful outcome. The NHS is currently developing response time targets for some specific conditions for the full clinical pathway from initial call to treatment in hospital and discharge to community care. These changes are based on data gathered by the NHS on patient outcomes from particular clinical pathways. Such applied information systems are available to the ambulance service to target and improve the management of ambulance response times.

When the NHS was first formed in 1947 the ambulance service was tasked with providing out-of-hospital care by attending on-scene emergencies providing patients with first-aid and transport to a suitable medical facility. In recent years the ambulance service provision has been expanded into other areas of NHS social care provision including situations that arise from mental health, alcohol or drugs and homelessness. These situations have arisen from a combination of changes in primary care strategy and shortages in the provision of social care. Privately, ambulance service managers indicate that many of their calls now relate to emergencies derived from a lack of social care where the ambulance service is the patient's last port of call.

This increase in workload placed pressure on the service by expanding demand, increasing on-scene time and increasing patient hand-over time at medical facilities. In addition, Gething, University of Wales, Health Board [4] reported a substantial increase in emergency calls mainly due to an expanding elderly population and the widespread misunderstanding amongst the general public of the ambulance service offering that all calls would obtain an immediate response.

The nature of a medical emergency indicates that demand for the ambulance service will be somewhat random in terms of 'time', 'place', and the 'required response'. The operational complexity of the ambulance response time problem is one of the most complex logistics tasks. The main difficulty is that in certain life-threatening situations there is an extremely short time before a patient may suffer further harm if no first-aid is administered. **Figure 1** outlines a process flow chart and the related urgency of responses required for certain conditions. With average demand for the busiest ambulance services at over one call per minute with demand emphasised by seasonal variations and event escalations the logistics requirements to achieve the response time targets are particularly difficult to manage. The challenge for operations managers is to recognise the urgency of the need, allocate appropriate resources, and achieve the target response time 24 hours/7 days a week/52 weeks a year at any location in the territory served whatever the traffic or weather conditions.

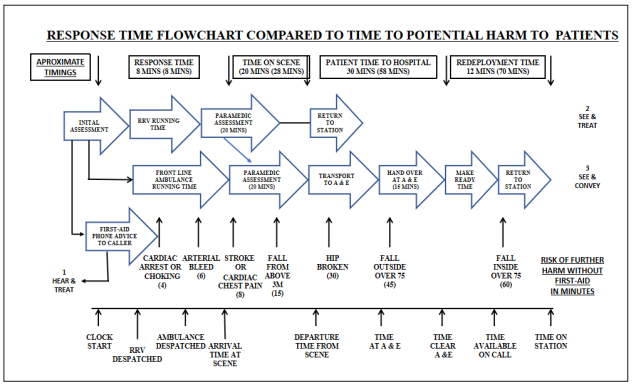

Figure 1. Response time flowchart compared to time to potential harm to patients.

3. Response time targets

Price [5] and Wankhade [6] indicated that ambu-

lance services could not keep pace with demand and were managing the 'response time' target by dispatching more than one resource to life-threatening calls rather than considering overall patient needs. Cooke [1] concluded that response time targets had been the main motivator for service restructuring although ambulance service management recognised that targets themselves do not save lives, more significantly ambulance availability, staff training and communications throughout the patient pathway would improve service and save lives.

Following a study into ambulance response times by Sheffield University, NHS England [7,8] established the Ambulance Response Programme with new integrated performance level and response time targets for all emergency calls based upon a combination of triage time by call handlers and ambulance response time by suitable crews for four categories of patient need:

Category 1—defined as 'life threatening' cases where the triage time is the earliest of 30 seconds from the call being connected, an ambulance being dispatched, or the patient needing to be identified. These cases require a 7-minute mean response with 90% of the calls responded to within 15 minutes or less. In addition, suitable transport must be available to convey the patient within 15 minutes of the call being connected.

Category 2—defined as 'emergency cases' where the triage time is the earliest of 240 seconds from the call being connected, an ambulance being dispatched, or the patient needing to be identified. These cases require an 18-minute mean response time with 90% of the calls responded to within 40 minutes or less. The 'clock' is only stopped by the arrival of a suitable vehicle to convey the patient, or if a vehicle is not required the first staff on the scene.

Category 3—defined as 'urgent cases' where the triage time is the earliest of 240 seconds from the call being connected or an ambulance being dispatched. These cases require a 90% response within 120 minutes by suitable transport, but if the patient does not require transport then the first staff on-scene stops the 'clock'.

Category 4—defined as 'non-urgent' cases where the triage time is 240 seconds from the call being connected, an ambulance being dispatched, or the patient needs to be identified. 90% of these cases should be responded to within 180 minutes and the 'clock' is only stopped by the arrival of a vehicle suitable to transport the patient, but if the patient does not require transport then the arrival of the first staff is on-scene.

Further integrated targets were also defined. For example, by 2022 90% of eligible heart attack patients should receive definitive treatment at a specialist heart centre within 150 minutes of the call being connected. These targets imply that ambulances take patients with certain defined conditions directly to the relevant hospital facility rather than Accident and Emergency (A & E).

4. Earlier theoretical solutions

In the past, operations research algorithms have offered a range of potential solutions addressing specific topics such as ambulance numbers and locations. Such studies have included Toregas et al. [9] who used optimisation to minimise the number of ambulances used to cover a defined geographical area. Whereas, Church and ReVelle [10] and Repede and Bernardo [11] indicated how fixed ambulance numbers could be located to obtain maximum geographical coverage. Gendreau et al. [12] and Dorner et al. [13] combined these two ideas to provide the minimum number of ambulances over a maximum geographical coverage. Daskin [14,15] modelled the impact of ambulance unavailability and Carter et al. [16] used queuing theory with fixed locations to tackle a similar problem. Larson [17] developed a 'hypercube' queuing model to select ambulances to respond from a fixed fleet. Lubicz and Meielczarek [18], Savas [19], Fitzsimmons [20], Swoveland et al. [21], Erkut et al. [22] and Inakawa et al. [23] have all used queuing and simulation techniques to predict ambulance response times in specific cities or geographical areas. Brotcorne et al. [24] provide a comprehensive review of ambulance location models. Similar specific parameters have been modelled by Fitch et al. [25], Blackwell

and Kaufman [26] and Shane et al. [27]. These operations research techniques were employed to tackle location and historic deployment issues rather than address the end-to-end tasks of managing a short lead time 24/7 emergency ambulance service supporting populations in a substantial territory

In addition, early operation research models were weak on input data and underlying operating assumptions and failed to provide credible solutions that represented an improvement upon existing operations. When these models were compared with real-time ambulance deployment planning there were several significant weaknesses. Furthermore, these models failed to consider significant real-time opportunities such as the re-deployment of returning ambulances to alternative locations, staggered crew shift times, diverting ambulances from less non-urgent tasks to life-threatening tasks, or the short-term use of alternative or third-party ambulance services for non-urgent cases.

Brotcorne et al. [24] indicated that several comments had been made by both users and reviewers of these techniques. Firstly, the data sets employed are historic, time-limited and do not account for a dynamic starting position, or peaks and troughs in demand on a seasonal, monthly, weekly, daily or hourly basis. Secondly, as shown by Carson and Batta [28], the travel time differences throughout the day are ignored and the travel time is either calculated on a straight-line distance at a constant speed or distance is calculated on the 'square root law' devised by Kolesar [29], leading to significant inaccuracies when compared with actual ambulance travel times. Thirdly, each model limited its scope by addressing only the significant issues of either location or fleet size, although Naoum-Sawaya and Elhedhli [30] considered a continuous-time chain to redeploy ambulances to a location upon completion of a task.

None of the models quoted coped with dynamic operational practices such as the use of deployment locations only on specific days or times of day; variable road speeds on different roads and the same road throughout the day. In addition, variations in on-site timings at different medical facilities including handover delays were not considered. Furthermore, they do not consider what has now become the operational practice in terms of dispatching more than one ambulance from different locations to a single call; the use of hubs (main ambulance stations) with satellites and despatch points (temporary standby ambulance locations), and the use of crews when returning from a task or extending crew shift times.

5. Operational issues

The shortfall in the operations research models indicates that problems facing the ambulance service are extremely complex and not those which could be solved by models which combine location selection with vehicle routing and scheduling because they involve a combination of several real-time operational issues including:

· Call pick-up delays at the call-centre when busy

· Insufficient or incorrect information to categorise patient needs correctly

· The immediate or subsequent availability of suitable crews

· Outbound (and inbound) traffic conditions

· Ability to obtain relevant patient information

· Selection or diversion to a suitable medical facility

· Waiting time and handover delays at hospital facilities

· Make ready and/or crew break before returning to a standby location

· Knowledge of current resources deployed on which category of task

· Progress of each deployment and potential crew reassignment time

· Currently available resources by type and skill level

· Number of patients on-scene at each location

· Data on the changing condition of the patient(s)

· Location of the incident and access to the patient(s)

· Time of day, traffic conditions, weather conditions

These issues delay the process flow of attending, on-site treatment and delivery of a patient to a suitable medical facility and may risk failing to achieve the target response time for the complete task. Lord Carter [31] suggested the reality of ambulance service

operations is currently very different from the optimum process due to the combination of increased demand and a need to substantially improve productivity. In addition to response times the ambulance service has a wider set of financial and operating key performance measures to report to NHS England monthly. However, in practice, there is real operational concentration on response times because both the general public and the national press highlight timing failures regularly.

Following receipt of an emergency call current practice is to follow one of three pathways—see **Figure 1** (where patient pathways are numbered 1, 2 and 3). Initially, the patient's need is categorised using AMPDS then call-centre staff will either deploy a suitable resource or provide telephone advice (known as 'hear and treat' 1). Some emergency and urgent calls may be concluded on scene employing treatment or advice from the crew (known as 'see and treat' 2). For life-threatening and emergency calls (known as 'see and convey' 3). one or more resources may be despatched immediately (if available) or existing outbound crews servicing urgent or less urgent calls may be diverted.

To assist with achieving target response times, call-centre staff have the electronic mapping of the territory which is combined with the use of full postcodes, or the compass on a caller's mobile phone, to give an accurate location of the patient. They have vehicle tracking and tracing to locate vehicles and coding to determine if vehicles are available and the category of the task they are undertaking. Workforce planning indicates the remaining shift time available to staff on duty and the potential availability of crews about to start a shift. On the local map, they have the locations of all medical facilities, on-call staff, community first responders, members of the hazardous area response team, the helicopter emergency medical service (HEMS), mountain rescue teams (MRT) and the location of static public access defibrillators and bleed control packs.

Call-centre staff also know about handover delays at each medical facility, vehicles out of service and crews on shift potentially taken out of service for operational reasons. On-scene staff need to know if they have multiple patients to consider at one site and the nature of any hazard that may impede staff either traveling to the site or at the site plus whether any other emergency service has been called out to assist and is a rendezvous arranged with anyone. Despatchers will monitor both the progress and requirement for those resources where they have despatched more than one resource to enable them to achieve the response time; so that they could stand down duplicated resources at the first opportunity.

In the event of severe life-threatening trauma being recognised by staff they may in addition despatch support in the form of a mobile critical care team consisting of a paramedic and/or doctor or the helicopter emergency medical service if suitable and available.

6. Alternative approach

The key issues to facilitate improving ambulance response times and staff productivity are the collection, analysis and availability of relevant timely information. To overcome the deficiencies encountered when using operations research techniques to optimise specific issues an alternative approach would be the combination of solutions from five real-time modules all of which could be integrated using a data-warehouse—see **Figure 2**.

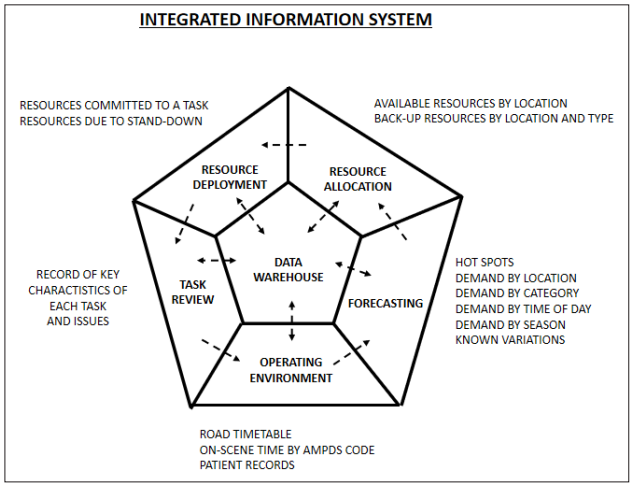

Figure 2. Integrated in formation system.

In this instance, a module is represented by one or more algorithms that obtain real-time or historic data from a directly linked data-warehouse to either

answer a specific question or add further processed data to the data warehouse.

6.1 Demand forecasting from historic data

Traditionally, the ambulance service has collected a large quantity of real-time data reflecting demand parameters including location of demand, timing of calls, classification of requirement, age of patients, operational conditions and short-term outcome for patients. This data indicates that calls are in essence random both in location and nature but analysis over an extended period of 3 years shows similar macro patterns if one-off factors such as mass-casualty incidents, pandemics, events or severe weather are discounted.

By combining ambulance service data with data from public services such as postcodes [32] and population data (see Office of National Statistics 2022) it is possible to determine some basic demand parameters. Pidd et al. [33] showed that mapping volume data by location and time using a geographic information system (GIS) would highlight demand 'hot spots'. Such analysis of both ambulance service and GIS data shows demand by postcode sector (defining area), showing potential forecasting variations, and defining demand by category of call, time of day and age of the population—see **Table 1**.

The profile may differ in each selected territory, however, data will be more accurate for Functional Urban Areas (FUA) which are densely inhabited areas in cities (urban and sub-urban) and slightly less populated commuter zones (semi-rural and rural). With data, collected over 3 years and weighted to the current situation by employing exponential smoothing, it is possible to plot forecast demand at postcode sector level and time of day. Best forecasts are obtained for categories 1 and 2 calls for a limited period (say 12 weeks) which account for seasonality and key conditions such as holiday peaks in demand. Using such demand data by day of the week and considering weather details, it is possible to forecast ambulance requirements to potential 'hot spots' by the time of day which allow staff to locate unallocated resources throughout the territory to areas with a high probability of demand and therefore maximise the opportunity to achieve the target response times.

6.2 Resource allocation

Previously resources were located at local ambulance stations and hospitals but with the development of direct-to-vehicle communications plus vehicle tracking and tracing the control centre has real-time knowledge of each crew's location (even while they are traveling). The current thinking is to allocate resources to ambulance stations and temporary deployment points in FUAs. Deployment points are parking places for a single front line double manned ambulance awaiting a job, often located at fire or police stations, shopping centres or garages where there are suitable 'comfort' facilities for the crew.

However, based upon significantly improved analysis of demand data it is now more appropriate to allocate resources based on forecast demand. 'Hot spots' could be geo-fenced providing a forecast of potentially successful travel time to a call based upon travel time from the centre point of a hot-spot. However, the target distance to potentially travel in a defined time from the centre of a 'hot-spot' is known as a 'geo-fence' which will vary by factors such as the resource available, the road layout and the forecast demand. by season, day of the week and hour of the day—see **Figure 3**. Ambulance stations and deployment points could be provided in areas of potential 'hot spots'. Significant gaps, not covered by 'geo-fences' could be filled by activating back-up resources including shift overlaps, on-call staff, Volunteer Ambulance Crews (VAC) or Community First Responders (CFRs). Once a crew is despatched it may be necessary to backfill the location with another crew at the earliest opportunity. This form of resource allocation improves the probability of achieving ambulance response times for category one and two calls.

Recognising that 'hot spots' alter throughout the day implies relocating operating and backup resources throughout the day as both demand patterns and travel times vary. Relocation is best undertaken at the beginning of a shift, as resources become free from a completed task or at the end of a crew break.

Table 1. Demand parameters: Data sheet.

GEOGRAPHIC AND POPULATION CHARACTERISTICS					
	Parameters	Post Code Split	Area	Population Daytime	Population Night
		%	%	%	%
URBAN	Below 0.5 square miles per post code	40	2	30	25
SUB-URBAN	Between 0.5 and 2.0 square miles per post code	30	8	36	40
SEMI-RURAL	Between 2.0 and 10.0 square miles per post code	20	20	26	25
RURAL	Over 10 square miles per post code	10	70	8	10
			100	100	100
		(Data averaged and rounded up)			

FORECASTABLE VARIATIONS IN DEMAND	
Season:	Spring - Summer - Autumn - Winter
Day of the Week:	Mon - Tues - Wed - Thu - Fri - Sat - Sun - Bank Holiday
Location Issues:	Tourist Holiday Season - School Holidays
Special Events:	Sporting Fixtures - County Shows - University Freshers Week
Zone:	Travel Time Dependant by Time of Day
Temperature:	Ice - Black Ice - Below Average - Above Average - Hot - Very Hot
Weather:	Snow - Sleet - Rain - Heavy Rain - Dry

FORECASTABLE LOCATION OF DEMAND
Urban - Sub-Urban - Semi-Rural - Rural
Population Demographics including Income Levels
Industry/Work Related - Ethnic Origin/Background Related - Housing/Social Related
Availability of Health and Social Services

CALL VOLUME BY TYPE AND TIME OF DAY				CALL VOLUME BY POPULATION AGE		
Time of Day (hours)	Life Threatening Emergencies	Emergency Calls		Age Group	Total Population Split	Demand by Age Group
	%	%			%	%
00.00 to 02.00	7	9		Under 10	12	9
02.00 to 04.00	5	6		11 to 20	13	5
04.00 to 06.00	2	3		21 to 30	12	7
06.00 to 08.00	7	6		31 to 40	15	5
08.00 to 10.00	9	7		41 to 50	14	8
10.00 to 12.00	11	9		51 to 60	13	10
12.00 to 14.00	11	10		61 to 70	10	14
14.00 to 16.00	10	10		71 to 80	7	18
16.00 to 18.00	10	10		81 to 90	3	16
18.00 to 20.00	10	11		Over 90	1	8
20.00 to 22.00	9	10			100	100
22.00 to 24.00	9	9				
	100	100				

Table 1 continued

CALL VOLUME BY TYPE AND TIME OF DAY				CALL VOLUME BY POPULATION AGE		
Time of Day (hours)	Life Threatening Emergencies	Emergency Calls		Age Group	Total Population Split	Demand by Age Group
UN-FORECASTABLE VARIATIONS IN DEMAND						
Severe Weather - Pandemic						
Mass Casualty Incident - Short Term Localised Issues						
Local Events						
Requirement for Mutual Aid						

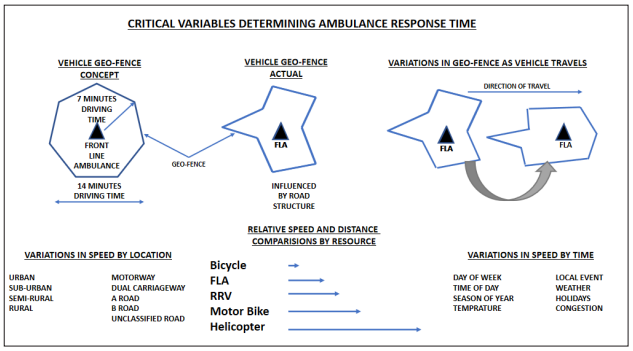

Figure 3. Critical variables determining ambulance response time.

6.3 Resource deployment

Traditionally the ambulance service has deployed the nearest available resource to a task. They have even redirected crews on-route to category 3 and 4 calls to a category 1 or 2 call if they were the nearest. However, if dispatchers adopt real-time vehicle tracking and tracing combined with geo-fencing methods they will be able to determine all potential options to attend the scene. Eglese et al. [34] indicated that the travel distance from any one point and each geo-fence structure is determined by the nature of the road speed and each vehicle geo-fence will be a different shape offering different ground coverage—see **Figure 3**. Eglese et al. [34] also showed that road speed differs between nodal points (road junctions on all except minor roads and tracks) on a specific road and that a 'road timetable' may be developed showing the estimated speed between each nodal point for each vehicle type with variations for the time of day, day of the week and season of the year. It is also practical to impose speed reductions for specific short-term events which are known to reduce vehicle travel speeds such as long-term road works.

With the use of vehicle tracking, geo-fencing based upon a relevant 'road timetable', it is possible to calculate the realistic area that may be covered in 7 minutes (for category 1 calls) or 18 minutes (for category 2 calls) from the vehicle's current location (whether static or mobile). Such an analysis of alternative vehicles and alternative routes may show the despatcher that a vehicle with the shortest travel distance could be slower than a vehicle with the shortest travel time.

It should be noted that urban and rural clusters will look different and there will be available resources traveling through each demand cluster when returning to a standby location and when outbound to a task—see **Figures 4 and 5**. The ambulance service could also use the combination of critical path programs, electronic mapping and vehicle tracking and tracing software to communicate in real-time with a caller who has a smart mobile the status and location of any outbound resource responding to their call—thus establishing a realistic expectation of an on-scene time and avoiding repeat requests for immediate ambulance services.

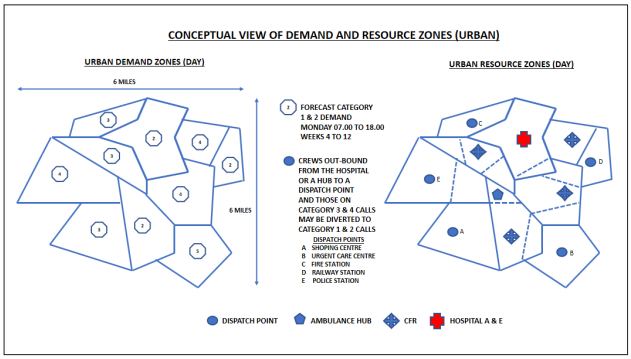

Figure 4. Conceptual view of demand and resource zones (Urban).

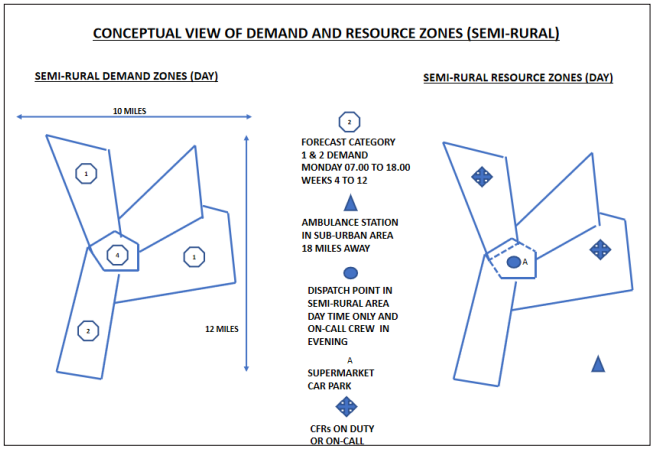

Figure 5. Conceptual view of demand and resource zones (Semi-rural).

6.4 Task review

One of the most significant benefits to a patient is the backup service provided by call-centre staff to both on-scene public before a crew arrives and the ambulance crew as they undertake their observations, conclude what actions are necessary, which pathway the patient should take and which medical facility the patient should be taken.

On-scene staff may also request assistance from senior clinicians within the call-centre or external supporting resources (for example Helicopter Emergency Medical Service—HEMS). In addition, staff may request the public on-scene to assist with immediate first-aid before an ambulance response arrives. This may take the form of advice by telephone, advice upon where to collect the nearest static defibrillator/bleed pack and how to use these resources.

Staff should be aware of all resources currently tasked, their location and when they are likely to become available (upon completion of a task or after any break) or when their shift finishes and whether it could be extended if necessary. Constant monitoring may indicate potential issues, for example, long ambulance handover times at a particular accident and emergency (A & E) department which may require further action to divert inbound ambulances to alternative accident and emergency departments or a local urgent care centre if practical.

6.5 Operating environment

To be able to improve the accuracy of vehicle running time and on-scene crew operating time any standard times for each activity must be amended to reflect the actual operating conditions at the time of the call. Such variations are achieved by monitoring, recording and updating specific operating tasks; for example:

The ‘road timetable’ is a database that forecasts the speed of a vehicle (operating with blue lights and sirens) between two nodal points at hourly intervals, by day of the week, under specific weather and traffic conditions during a specific season—an outbound travel forecast being the sum of the times between each nodal point on the route. The ‘road timetable’ is populated and updated from data gathered using the vehicle tracking and tracing system averaged to account for differed driver behaviours.

The ‘on scene operating time’ may be estimated for each AMPDS code, for each type and age of the patient, whether indoor or outdoor, at what time of day and in which geographic zone—collection of actual data over time could generate a ‘look-up’ table. Real-time monitoring against estimated will provide a clue as to whether the crew needs telephone or on-scene assistance.

Direct access (on a portable tablet) to patient records also provides the crew with a patient history, medication history and particularly which ‘primary’ and ‘secondary’ medical facilities they have visited. This may influence both questions asked during the crew’s initial observations and the decision upon an onward pathway to a medical facility. Previous patient calls to the ambulance service should be available on a database for crews to access while traveling outbound.

6.6 Data warehouse

A ‘data warehouse’ could be generated and updated from relevant data from each module 1 to 5 which allows relevant staff access 24/7/365. The data warehouse could be used to identify trends, recognise

resource deficiencies and highlight both existing and potential operating issues. Data could also represent the basis for comparisons between operations in different geographical zones supporting any necessary operational changes.

7. Simulation

To test the feasibility and practicality of developing and using the five modules a simulation was undertaken based on 24/7 operation, in a limited but representative geographical area, over the most difficult season of the year. A honeycomb pattern of adjusted hexagons was created based on a daily demand forecast at the response category level, corrected by exponential smoothing of historic demand patterns and broken down into six-hour periods. The honeycomb pattern covered an area with urban, suburban, semi-rural and rural populations. 'Hub' ambulance station locations were selected in functional urban areas, and 'deployment points' were selected in suitable facilities where there was up to 20 hours demand for 6 days each week. 'Spokes' (parking locations for Double Manned Front Line Ambulances DMFLA) were selected, throughout the rest of the territory, at other suitable facilities to cover forecast demand which was limited to specific periods in the day and days of the week.

Before the simulation was attempted a small data warehouse was established for the geographical area selected comprising three years of demand data, resources potentially available (based upon use), a deployment of resources at the starting position, data on local medical facilities, a high on-scene time by AMPDS code and a road time table (adjusted for 'blue-light' vehicles). Several basic decision rules were adopted, for example, road traffic accidents with two casualties would warrant two double manned front line vehicles (DMFLV). Additional demand was covered where known, for example, when the fire service dispatched three or more tenders to an incident one DMFLV would be dispatched to support the fire crews. No mass casualty incidents were included.

The simulation was undertaken based upon a geographically and time-limited data set broken into three years 'historic' data to produce a three-month statistical forecast of demand. Several operating rules were tested which achieved the required ambulance response times for the daily demand. These calculations were targeted to determine the maximum and minimum number and type of resources required at each hub, deployment point and spoke in the defined area. The simulation was used to determine how resources could be relocated throughout a shift pattern to meet forecast demand from the hub or deployment point to spokes and vice-versa to meet forecast demand within and between each hexagon.

The simulation was based on the defragmentation of the problem and split into four separate but interconnected principles:

Firstly, the forecast of short-term demand (expressed as potential calls by patient category and time of day) to determine the potential number of calls in each hexagon for every six hours in a rolling 24 hours. Calls were allocated an AMPDS code, day of the week and time of day based on weighted historic data. How many of these calls would fall into the 'hear and treat' and 'see and treat' groupings were estimated based on AMPDS coding. The AMPDS code would be translated into a category of patient need. A reduction factor was applied based on an estimate of how many would be duplicates or repeat calls for the same incident. Frequent caller data was identified but maintained in the dataset at category three because a response would be required. A separate forecast was calculated for calls transferred from the 111 service all of which were allocated to category two demand.

Secondly, based upon demand the selection of 'hubs', 'deployment points', 'spokes' and resources of all types would be initially allocated throughout the area. This would include a forecast of operational tasks by patient category in progress by location and percentage completion, so resources were limited at the start through a carry-over situation.

Thirdly, appropriate resources would be allocated to each call as it was forecast to occur (location, patient category by AMPDS code and time of day)—

the rules would be based upon achieving the target response time while maintaining maximum availability throughout the area. Resources that became available would be redeployed and their transit monitored.

Fourthly, all tasks would be monitored using a scheduling system with estimated task times and vehicle routing techniques to obtain operational data which would be used to determine when a task is likely to be completed and the crew available for the next task.

The simulation covered three months in the winter but excluded support for known local events, pandemics and any mass casualty occurrences. Each simulation was reviewed and run again with alternative operational rules.

The best results from several simulations indicated that 96% of the required ambulance response times would be achievable with 6% fewer resources than currently allocated in the area. However, this could only be achieved if and when resources became available they were immediately either allocated a break period or redeployed to areas of forecast demand. It was particularly important to ensure that 'hubs' would always have resources available or inbound following the completion of a task. The six most significant results include:

More than 15% of calls in FUAs were satisfied by crews being redeployed before reaching less urgent tasks or available in transit to a hub, deployment point or spoke.

Achievement for categories 1 and 2 patients was above the target emergency ambulance response time in FUAs but slightly below the target in other areas except where patients were initially attended by Community First Responders (CFRs) or on-call staff.

At periods of unusual peak demand times it would be necessary to convey category 4 patients using third-party ambulance services.

Over 20% of category 1 and 2 patients which achieved the target response time at peak times were responded to by crews from deployment points.

Less than 3% of category 1 and 2 calls required two or more crews

Spacing shift time starts, varying shift length and having a split shift for 'hub' based staff minimised the requirement to extend crew shifts to complete an allocated task.

The sensitivity of the simulation results showed that more than an 8% change in demand levels influenced whether the response time was achieved for both category 1 and category 2 even if such measures as extending crew shift time were employed.

After undertaking various sensitivity analysis runs, as stress tests based on the best simulation result several other significant conclusions arose, the six most significant were:

If hand-over times for category 2 and 3 patients at accident and emergency facilities doubled then significant local gaps appeared in resource availability at both hubs and deployment points leading to a need to convey category 4 patients employing third-party ambulance services.

The best results were obtained by having a paramedic as part of every crew because the paramedic would after observation treat certain AMPDS codes as 'see and treat'.

Utilising 'retained staff' in Rapid Response Vehicles (RRVs) from rural Primary Care surgeries and Volunteer Ambulance Crews (VAC) from rural fire, police or coastguard stations significantly improved the response time for category 1 and 2 patients in both semi-rural and rural areas.

Overall response time targets improved if crews were allocated category 3 and 4 patients at the end of their shift and shift starters were deployed to 'deployment points' and 'spokes' where they would initially be tasked with responding to category 1 and 2 patients.

Redirecting patients to either specialist medical facilities or alternative accident and emergency units (rather than the nearest one if hand-over times there exceeded the target) had little impact on the redeployment of crews or overall achievement of the target ambulance response times except where a patient could be grouped as 'hear and treat' and directed by call-centre staff to attend alternative medical facili-

ties or a pharmacy.

Following Hamet and Tremblay [35] the application of operational rules targeted at testing an Artificial Intelligence (AI) response towards testing call-centre staff efficiency by limiting resource options to those which could either achieve the target response time or were at the nearest 'hub'. These limited computing calculation time and offered the dispatcher a choice of the best results.

8. Conclusions

It has been widely understood that ambulance services in England have through their Computer Aided Dispatch (CAD), AMPDS and patient record systems collected a large amount of patient and operations data. However, updating, validating and processing this information in real-time has not been recognised as the backbone to achieving national emergency ambulance response times.

To address this problem the ambulance service could defragment the problem and using several currently available information technologies consider five key decisions in real time.

Where are the demand clusters for life-threatening and emergency calls?

How many of each type of resource are required and where to locate these resources?

How many, of which resources and when to allocate resources to each call?

To which facility (if further treatment is required) the patient should be conveyed?

Which location an ambulance should be deployed to upon completion of the allocated task?

It has been recognised that these questions may be answered by separate modules in the form of:

GIS analysis and forecasting modules to determine demand 'hot spots' and demand clusters by location and time.

A resource coverage and availability module matched to statistical forecasting of demand over a short-term time, based upon hexagons each with a radius set by travel distance over the response time requirements.

A recommended call resource allocation module based upon interpreting both a set of basic rules and past dispatch behaviour to maintain maximum availability of resources covering the territory.

A task scheduling module to provide the basis for a resource allocation and redeployment module based upon matching forecast short-term demand with shift time remaining for each operating crew and alternative resources that may be available.

A queuing theory module that monitors availability at each secondary medical facility (also defining specialisations) servicing the territory to deliver the patient to the most appropriate facility, minimise patient queuing and maximise crew turn-round.

Simulation and sensitivity analysis have proved that linking the technologies in these modules together, by utilising a data warehouse in real-time, provides an opportunity to understand short-term demand and be able to resource enough calls within the national emergency ambulance service target response times.

These developments represent the first step towards 'smart ambulance operations' by establishing the groundwork upon which information systems may be used in the decision-making process Subsequently, artificial intelligence will use a combination of activities to locate 'stand-by' crews, dispatch crews or alternative immediate assistance, select a receiving hospital, sending on-scene real-time internet video recordings to medical teams and to communicate patient observations directly from equipment in the ambulance to the hospital based medical team. Such activities are targeted to improve the medical assistance available throughout the patients' pathway and thereby improve the patient experience and outcome.

Potential progress in the application of these techniques nationwide may be limited by the ability to allocate sufficient financial support and the ability to attract staff with relevant information technology skills.

Author Contributions

This article has been researched and written by a single author.

Conflict of Interest

There is no conflict of interest.

References

[1] Cook, M., 2011. An introduction to the new ambulance clinical quality indicators. Ambulance Today. 7(5), 35-36.

[2] Heath, G., Radcliffe, J., 2007. Performance measurement and the English ambulance service. Public Money and Management. 27(3), 223-228.

[3] Heath, G., Radcliffe, J., 2010. Exploring the utility of current performance measures for changing roles and practices of ambulance paramedics. Public Money & Management. 30(3), 151-158.

[4] Gething,V (2015) .Written Statement – Clinical Review of Ambulance Response Time Targets' Cabinet Statement, Welsh Government, Health Board. https://www.gov.wales/written-statement-clinical-review-ambulance-response-time-targets

[5] Price, L., 2006. Treating the clock and not the patient: Ambulance response times and risk. BMJ Quality & Safety. 15(2), 127-130.

[6] Wankhade, P., 2011. Performance measurement and the UK emergency ambulance service: Unintended consequences of the ambulance response time targets. International Journal of Public Sector Management. 24(5), 384-402.

[7] Turner J (2017) 'How we remodelled Ambulance Services in England' Research Features, University of Sheffield, England. https://www.sheffield.ac.uk/research/features/remodelled-ambulance-service

[8] On the Day Briefing: Ambulance Response Time Programme [Internet]. NHS Providers. Available from: https://nhsproviders.org/resources/briefings/on-the-day-briefing-ambulance-response-programme#

[9] Toregas, C., Swain, R., ReVelle, C., et al., 1971. The location of emergency service facilities. Operations Research. 19(6), 1363-1373.

[10] Church, R., ReVelle, C., 1974. The maximal covering location problem. Regional Science. 32(1), 101-118.

[11] Repede, J.F., Bernardo, J.J., 1994. Developing and validating a decision support system for locating emergency medical vehicles in Louisville, Kentucky. European Journal of Operational Research. 75(3), 567-581.

[12] Gendreau, M., Laporte, G., Semet, F., 1997. Solving an ambulance location model by tabu search. Location Science. 5(2), 75-88.

[13] Doerner, K.F., Gutjahr, W.J., Hartl, R.F., et al., 2005. Heuristic solution of an extended double-coverage ambulance location problem for Austria. Central European Journal of Operations Research. 13(4), 325-340.

[14] Daskin, M.S., 1983. A maximum expected covering location model: Formulation, properties and heuristic solution. Transportation Science. 17(1), 48-70.

[15] Daskin, M., 1987. Location, Dispatching and Routing Model for Emergency Services with Stochastic Travel Times [Internet]. Available from: https://www.semanticscholar.org/paper/LOCATION%2C-DISPATCHING-AND-ROUTING-MODELS-FOR-WITH-Daskin/5bc91cb1642f023fc1958eaf31c228b291f4cde4

[16] Carter, G.M., Chaiken, J.M., Ignall, E., 1972. Response areas for two emergency units. Operations Research. 20(3), 571-594.

[17] Larson, R.C., 1974. A hypercube queuing model for facility location and redistricting in urban emergency services. Computers & Operations Research. 1(1), 67-95.

[18] Lubicz, M., Mielczarek, B., 1987. Simulation modelling of emergency medical services. European Journal of Operational Research. 29(2), 178-185.

[19] Savas, E.S., 1969. Simulation and cost-effectiveness analysis of New York's emergency ambulance service. Management Science. 15(12), B-608.

[20] Fitzsimmons, J.A., 1973. A methodology for

emergency ambulance deployment. Management Science. 19(6), 627-636.

[21] Swoveland, C., Uyeno, D., Vertinsky, I., et al., 1973. Ambulance location: A probabilistic enumeration approach. Management Science. 20, 686-698.

[22] Erkut, E., Ingolfsson, A., Budge, S., 2007. Maximum Availability Models for Selecting Ambulance Station and Vehicle Locations: A Critique [Internet]. Available from: https://citeseerx.ist.psu.edu/document?repid=rep1&type=pdf&doi=965f00e8ec5caa3d08ab916b6c71528f5908a311

[23] Inakawa, K., Furuta, T., Suzuki, A. (editors), 2010. Effect of ambulance station locations and number of ambulances to the quality of the emergency service. The Ninth International Symposium on Operations Research and Its Applications (ISORA'10); 2010 Aug 19-23; Chengdu, China. p. 340-347.

[24] Brotcorne, L., Laporte, G., Semet, F., 2003. Ambulance location and relocation models. European Journal of Operational Research. 147(3), 451-463.

[25] Fitch, J., 2005. Response times: Myths, measurement and management. Journal of Emergency Medical Services. 30, 46-56.

[26] Blackwell, T.H., Kaufman, J.S., 2002. Response time effectiveness: Comparison of response time and survival in an urban emergency medical services system. Academic Emergency Medicine. 9(4), 288-295.

[27] Henderson, S.G., Mason, A.J., 2004. Ambulance service planning: Simulation and data visualisation. Operations research and health care: A handbook of methods and applications. Springer: Berlin. pp. 77-102.

[28] Carson, Y.M., Batta, R., 1990. Locating an ambulance on the Amherst campus of the State University of New York at Buffalo. Interfaces. 20(5), 43-49.

[29] Kolesar, P., 1975. A model for predicting average fire engine travel times. Operations Research. 23(4), 603-613.

[30] Naoum-Sawaya, J., Elhedhli, S., 2013. A stochastic optimization model for real-time ambulance redeployment. Computers & Operations Research. 40(8), 1972-1978.

[31] Carter, L., 2018. Operational Productivity and Performance in English Ambulance Trusts: Unwanted Variations [Internet]. Available from: https://www.england.nhs.uk/wp-content/uploads/2019/09/Operational_productivity_and_performance_NHS_Ambulance_Trusts_final.pdf

[32] Royal Mail (2015) 'History of UK Postcodes' Royal Mail Group, London. https://www.poweredbypaf.com/the-history-of-uk-postcodes/

[33] Pidd, M., De Silva, F.N., Eglese, R.W., 1996. A simulation model for emergency evacuation. European Journal of Operational Research. 90(3), 413-419.

[34] Eglese, R., Maden, W., Slater, A., 2006. A road timetableTM to aid vehicle routing and scheduling. Computers & Operations Research. 33(12), 3508-3519.

[35] Hamet, P., Tremblay, J., 2017. Artificial intelligence in medicine. Metabolism. 69, S36-S40.

BILINGUAL PUBLISHING GROUP

Journal of Electronic & Information Systems
https://journals.bilpubgroup.com/index.php/jeis

ARTICLE

Practical Considerations for Implementing Adaptive Acoustic Noise Cancellation in Commercial Earbuds

Agustinus Oey

VizWave Inc., Seongnam, 13595, Korea

ABSTRACT

Active noise cancellation has become a prominent feature in contemporary in-ear personal audio devices. However, due to constraints related to component arrangement, power consumption, and manufacturing costs, most commercial products utilize fixed-type controller systems as the basis for their active noise control algorithms. These systems offer robust performance and a straightforward structure, which is achievable with cost-effective digital signal processors. Nonetheless, a major drawback of fixed-type controllers is their inability to adapt to changes in acoustic transfer paths, such as variations in earpiece fitting conditions. Therefore, adaptive-type active noise control systems that employ adaptive digital filters are considered as the alternative. To address the increasing system complexity, design concepts and implementation strategies are discussed with respect to actual hardware limitations. To illustrate these considerations, a case study showcasing the implementation of a filtered-x least mean square-based active noise control algorithm is presented. A commercial evaluation board accommodating a low-cost, fixed-point digital signal processor is used to simplify operation and provide programming access. The earbuds are obtained from a commercial product designed for noise cancellation. This study underscores the importance of addressing hardware constraints when implementing adaptive active noise cancellation, providing valuable insights for real-world applications.

Keywords: Active noise cancellation; Adaptive filter; DSP implementation

1. Introduction

The use of the active noise control (ANC) method to reduce ambient noise in the earbuds has achieved significant commercial success, demonstrating the

*CORRESPONDING AUTHOR:
Agustinus Oey, VizWave Inc., Seongnam, 13595, Korea; Email: oeyaugust@vizwave.net

ARTICLE INFO
Received: 7 October 2023 | Revised: 26 October 2023 | Accepted: 30 October 2023 | Published Online: 6 November 2023
DOI: https://doi.org/10.30564/jeis.v5i2.5998

CITATION
Oey, A., 2023. Practical Considerations for Implementing Adaptive Acoustic Noise Cancellation in Commercial Earbuds. Journal of Electronic & Information Systems. 5(2): 25-34. DOI: https://doi.org/10.30564/jeis.v5i2.5998

effectiveness of the method in the frequency range where the spatial control region is small in comparison to the wavelength. The problem itself can be simply considered as a one-dimensional problem—that is, the cancellation of plane waves. However, incorporating ANC into earbuds presents specific challenges, primarily due to the compact form factor essential for earbud design. These challenges include fitting all the required components into a tiny enclosure and dealing with tight spacing between the sensor and actuator, which limits the response time of an ANC system. This necessitates low-latency audio processing devices and computationally efficient control algorithms. Achieving significant noise reduction across a broad bandwidth depends on minimizing latency [1].

Another important factor to be considered for a well-performing ANC system is the variation in acoustic leakage within the acoustic control region. This variability is mainly associated with user preferences for diverse earbud fit conditions to ensure comfortable wear. On some occasions, the fit may also loosen as the user moves. Obviously, a stronger anti-noise signal is required to compensate for the increase in acoustic leakage. However, even a minor alteration in the leakage causes variability in the way ambient noise propagates into the ear. This introduces uncertainty in how a controller would respond. Consequently, controller stability and noise reduction performance must be assured within the assumed perturbed range.

One of the earliest approaches proposed to address uncertainty in active headsets is the utilization of a robust controller [2]. This method employs an algorithm based on the two Riccati equations to determine appropriate parameters for a controller with guaranteed operating margins. The resulting controller is implemented using operational amplifier circuitry. Another noteworthy alternative approach involves employing a set of stable feedback controllers with various preset gains [3]. In response to specific fitness conditions, a comparator switches to the appropriate operational controller. These studies shed light on the idea that a certain degree of controller adaptiveness is generally necessary to accommodate varying acoustic environments.

In the field of ANC applications, adaptive controllers incorporating digital filters have gained popularity for their ability to efficiently adapt to dynamic and complex acoustic environments. However, practical implementation within earbuds presents challenges due to the limited choice of computing hardware, which compromises the system's ability to perform complex calculations. High-performing processor is essential for executing sophisticated control algorithms requiring intensive and intricate digital filtering tasks [4].

Achieving effective ANC in resource-constrained earbuds demands a careful balance of design factors to ensure satisfactory noise cancellation performance. This article investigates practical considerations for implementing adaptive filters in noise cancellation, specifically utilizing a low-cost digital signal processor (DSP) suitable for earbud integration. The adaptive controller employs the well-known filtered-x least mean square algorithm (FxLMS). Details about the specifications of the speakers and microphone, as well as their spatial arrangement, are derived from a popular commercial earbud product. The overall configurations are determined based on computational resources and the functional features available within the chosen DSP. Finally, the article presents experimentation using broadband random noise to validate the proposed approach.

2. Adaptive noise control system

Figure 1(a) illustrates a simplified ANC system within earbuds. The interface unit performs signal conditioning and audio codec, as well as signal mixing and amplification. To reduce ambient noise, typically assumed to be random and broadband, a feed-forward controller is commonly adopted. This setup involves one speaker to generate the anti-noise and two microphones: one positioned upstream and another downstream to measure the reference input, $x(n)$, and the noise residue, $e(n)$, respectively. When the speaker and error microphone are placed within a sealed enclosure, two propagation paths must be con-

sidered. The first is referred to as the primary path, $P(z)$, through which noise travels from the reference microphone to the error microphone. This path is purely acoustical in nature. The other is the secondary path, $S(z)$, which exists between the controller's output and input ports. It is a propagation medium that comprises both electrical components within the circuitry of the signal interface unit, speaker, and error microphone, as well as acoustic elements within the space between the speaker and error microphone.

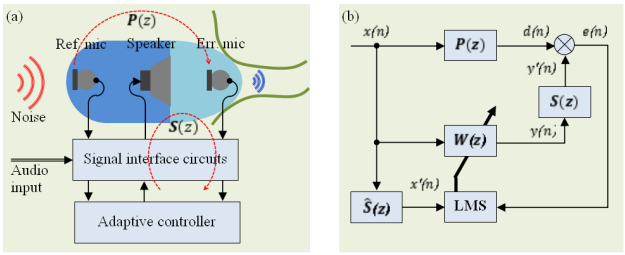

Figure 1. A system overview: (a) ANC integration in earbuds. (b) FxLMS based controller.

In practical implementation, there may be an audio signal feed from the connected device, such as a phone or audio player, that is sent to the speaker. This audio signal could potentially mix with the noise residue measured by the error microphone. However, because information about the audio signal is known, it becomes practical to separate the noise residue. Furthermore, the audio signal can be effectively utilized for both online and offline modeling of the secondary path transfer function [5]. It is important to note that the scope of this work does not encompass a discussion of the algorithm for separating the noise residue from the audio signal.

The heart of the adaptive controller is a digital filter, generally classified into two major categories: recursive and non-recursive. The former reuses a part of its output as the input, creating a feedback loop that results in a very long impulse response. While a recursive filter has the potential to reduce the computational burden, it comes with inherent drawbacks, such as response instability and local minimum solutions. In this work, the preference is for a non-recursive digital filter to facilitate convergence during adaptation. It consists of one row of unit delays, where a segment of input data is stored, and another row of coefficient memories of the same length. The output of the digital filter is the sum product of the values in the corresponding rows. Alongside an algorithm for adjusting filter coefficients, an adaptive controller is constructed.

2.1 A review of the FxLMS algorithm

In this work, the least mean square algorithm is considered. The algorithm iteratively adjusts the filter coefficients in a way that minimizes noise residue by following the negative direction of the error gradient. However, the presence of a secondary path causes a phase mismatch in the arrival of the anti-noise signal, impeding the correct filter update. Therefore, an auxiliary filter must be introduced into the control loop to compensate for the alteration of the anti-noise signal by the secondary path [6]. This auxiliary filter, often referred to as a secondary path estimate, $\hat{S}(z)$, can be obtained through transfer function modeling or measurement. This approach is known as the FxLMS algorithm.

The block diagram in **Figure 1(b)** illustrates an adaptive feed-forward controller, $W(z)$, which is implemented as a non-recursive filter with a length of L. In response to the input, $x(n)$, provided by the reference microphone, the controller generates the anti-noise signal, $y(n)$, which can be calculated using the following relationship,

$$y(n) = \sum_{l=0}^{L-1} w_l(n)x(n-l) = w^T(n)x(n) \quad (1)$$

Here, w_l denotes the l-th coefficient of the controller. The anti-noise signal is transmitted through the speaker to produce,

$$e(n) = d(n) + y'(n) = p^T(n)x(n) + s^T(n)y(n) \quad (2)$$

which is the noise residue measured by the error microphone. This equation uses a positive sign to signify the superposition of sound waves between the unknown ambient noise, $d(n) = p^T(n)x(n)$, and the anti-noise, $y'(n) = s^T(n)y(n)$, as they reach the control point.

The gradient of the error surface can be obtained by differentiating the cost function $J(n) = e^2(n)$ with re-

spect to the filter coefficients. By applying the gradient descent algorithm, the iterative process for adjusting the controller coefficients is expressed as follows,

$$w(n+1) = w(n) - \mu\, x'(n)\, e(n) \tag{3}$$

Here, notations μ and $x'(n) = \hat{s}^T(n)\, x(n)$ represent the iteration step and the filtered reference input, respectively. The iteration step, which is associated with convergence speed, is a positive coefficient that can be selected from a range of values that is not larger than,

$$\mu_{max.} = \frac{1}{\|x'(n)\|^2 (L + \delta_S)} \tag{4}$$

The notations $\mu_{max.}$ and δ_S represent the maximum applicable iteration step and the inherent delay in the secondary path, respectively. Accordingly, it is evident that the delay in the secondary path imposes a constraint on convergence speed [7]. A longer path delay leads to slower convergence.

2.2 The importance of the secondary path

If perfect noise cancellation is achievable, meaning $e(n) \rightarrow 0$ as the adaptation converges, the optimal controller, $W_o(z)$, can be derived from Equation (1) and Equation (2) as:

$$W_o(z) = -\frac{P(z)}{S(z)} \tag{5}$$

To effectively attenuate broadband random noise, the transfer function of the controller, $W(z)$, should closely match the impulse response of the optimal controller. This is achievable if the inverse of $S(z)$ exists. Therefore, it is desirable to have a secondary path that can be represented by a causal and minimum-phase transfer function. In practice, the delay in the secondary path should be shorter than that in the primary path. Additionally, when using a non-recursive filter as the controller, it should have sufficient length to accommodate the rational part of the equation. Fortunately, the control plant associated with this setup is expected to be of low order due to the relatively small acoustical volume within the earbuds.

2.3 Performance factors in noise reduction

The causality condition, which must be satisfied by any ANC system to allow a broadband noise cancellation, is met when the time required for the anti-noise to be generated and delivered to the control point is faster than the noise propagation time across the primary path. In short, it is fulfilled when the delay in the electrical path is smaller than that in the acoustical path.

The primary contributors to electrical delay include the time required for signal conditioning, data conversion, and computation process. Signal conditioning in the anti-aliasing and reconstruction filters introduces a latency that is proportional to the filter order and inversely proportional to the filter corner frequency. The time for signal conversion between analog and digital domains depends on the type of converter and the number of bits involved. For example, given the same resolution, a Delta Sigma ADC is typically slower than a SAR ADC. Computation in the controller consumes one sample period during which the processor executes an adaptive control algorithm. The latency of the speaker and microphones also contributes to electrical delay.

The delay of the acoustic primary path can be influenced by various factors. In earbuds, device fitting and enclosure provide passive isolation that can increase the delay in the primary path [8]. Intuitively, acoustic leakage reduces the delay and the lowest estimate of acoustic delay, δ_{act}, can be calculated from the direct sound propagation as follows:

$$\delta_{act} = (\Delta x_{re} - \Delta x_{ye}) \,/\, c_0 \tag{6}$$

Here, Δx_{re} represents the distance between the two microphones, Δx_{ye} represents the distance between the speaker and the error microphone, and c_0 is the sound speed, approximately 343 m/s. However, when the path of arriving noise is closer to the error microphone than the reference microphone, the acoustic delay may not be sufficient to ensure causality [9]. This condition is purely physical and is less related to the allocated filter length in the controller. Practical remedies include increasing the acoustic path delay by improving passive isolation and enhancing spatial information using the multi-reference microphone method. The sound passing through the earbuds enclosure and ear-tip can improve the

performance of the feedforward system by increasing the delay between the two microphones [10]. The use of additional reference microphones provides a comprehensive representation of noise coming from various directions [11].

Coherence in measurements defines the noise reduction performance of an ANC system because the adaptation of controller coefficients relies on two correlated pieces of information provided by the error microphone and reference microphone. Based on the analysis of random processes, the noise reduction, *0*, at a given frequency ω can be estimated as:

$$R(\omega) = 10\ log_{10}\left(1 - \gamma_{xe}^2(\omega)\right)\ \ dB$$

where $\gamma_{xe}^2(\omega)$ represents the coherence function between the output of the reference microphone and the output of the error microphone when the ANC system is inactive [12]. The coherence function has a range of values between 0 and 1, indicating the quality of signal coherence, from poor to excellent. This can be interpreted as follows: The higher the coherence between the signals provided by the microphones, the greater the noise reduction to be expected. In practice, signal coherence is primarily affected by the quality of the instrumentation system, such as microphone dynamic range, sensitivity, and directivity, as well as distortion in the signal amplification unit. Additionally, cable shielding and circuit isolation can help minimize input contamination from signal interference.

In addition to its impact on system latency, the proper positioning of the speaker and microphones is crucial for controllability. While the enclosure of earbuds is the obvious place for a speaker, the opening of the ear tip can extend beyond the ear canal open end, creating an impedance mismatch where sound waves are transmitted and reflected. Conceptually, the optimal position for the speaker is at the dominant anti-node. In terms of the reference microphone position, controller complexity can be reduced if the microphone picks up a negligible amount of the anti-noise radiated from the speaker. Therefore, it is desirable to block the acoustic feedback path through proper enclosure design. As for the error microphone, the ideal location is near the speaker, where the noise residue is present with a high correlation to the reference noise.

The performance of the controller is intricately linked to numerical accuracy, which, in turn, is dependent on the choice between floating-point and fixed-point systems in the processing hardware [13]. Floating-point systems offer the advantage of high precision, making them well-suited for applications where numerical accuracy is critical. However, typically demanding more computational resources can strain the limited processing capabilities of devices like earbuds. On the other hand, fixed-point systems, while more resource-efficient, may introduce numerical errors due to lower precision, which can potentially impact the accuracy of controller operations. The causes of numerical error in fixed-point systems are primarily related to the limited number of bits available for representing numbers and rounding during arithmetic operations. To address these errors, careful consideration of scaling, quantization, and rounding techniques can be employed in fixed-point implementations to enhance the accuracy of controller calculations.

3. Implementation of adaptive ANC

Developing high-performance noise-canceling earbuds involves considering numerous aspects [14], such as the comprehensive acoustic design to produce favorable characteristics in the earbuds, which significantly impacts noise cancellation performance. Earbuds for ANC applications require careful integration of components such as speakers, microphones, controllers, and partitions. The arrangement of these components within a compact, well-shaped enclosure defines the interaction between noise and anti-noise. Additionally, it is crucial to incorporate low-latency electroacoustic components into the system.

While the design of the earbuds is a critical factor, this study does not cover every aspect of creating the perfect earbuds. It primarily focuses on realizing the adaptive controller. Therefore, for the experimentation, earbuds sourced from the Bose QC30 are used.

Originally, these components were connected to the main board in the neckband via cables. Each unit of the earbuds has approximate dimensions of 28 × 30 × 20 mm and is equipped with two 4 mm electret microphones and one 15 mm speaker with an impedance of 32 Ω. To gain access to the internal parts, a few modifications were made: the earbuds need to be separated from the main board and the connecting cables must be traced to identify the internal parts.

Two compartments can be found within the earbuds. The first one houses the error microphone and the speaker, facing inward toward the ear tunnel. It is isolated from the second compartment where the reference microphone is set. The reference microphone is facing outward to pick up ambient noise entering the ear. The distance between the reference microphone and the error microphone and the distance between the speaker and the error microphone is 8.5 mm and 2 mm, respectively, resulting in an acoustic delay of approximately 19 μs in this setup.

High-performance DSP is essential for controller development in ANC applications, particularly for earbuds. However, implementing ANC in earbuds can have a significant impact on device operation time. In short, the DSP should be compact, require minimal components to support its operation, energy-efficient, and cost-effective. These qualifications hold especially true when considering processor choices for mid and upper-range commercial earbuds. For example, options like the Qualcomm S5 Sound Platform and the Apple H2 BT5.3 Audio-SoC offer functionality for audio processing, voice services, and device connectivity in a single SoC component, all while operating with low power consumption.

For performing general experimentation, several commercial DSP options with the corresponding development boards are available, including the CS47L85, i.MX RT1020, and TMS320C5517. Concerning the computational speed, it must ensure that the delay in the electrical path is shorter than in the acoustical path. Theoretically, assuming a 19 μs acoustic delay, any DSP working at a sample rate of 96 kHz or higher is sufficient. A minimum of two input channels and one output channel are required. In this study, the evaluation board EVAL-ADAU1787Z from Analog Devices, depicted in **Figure 2(a)**, is employed. This choice aligns with the study objectives as it addresses the challenge posed by the limitation of computational resources. Additionally, the small DSP footprint makes it a practical choice for integration into earbuds.

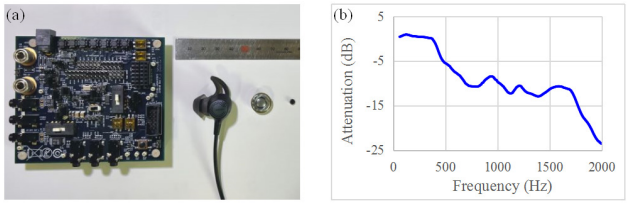

Figure 2. Device selection: (a) DSP board and earbuds. (b) Passive noise isolation in earbuds.

The evaluation board is equipped with four ADC channels, two DAC channels, a low-power audio codec, and two fixed-point DSP cores. The first core is the FastDSP audio processing engine, offering built-in features such as biquad filters, signal limiters, mixers, and volume controls. When passing a signal from the ADC input to the DAC output at a sampling frequency of 768 kHz, a group delay of 5 μs can be expected [15]. This particular core can be programmed to perform specific tasks using no more than 64 instruction cycles. Here, group delay represents the time shift of a packet of oscillating waves centered around one frequency that travels together. An instruction cycle denotes a discrete step a processor takes to execute a single machine-level instruction.

The second core in the processor is the 28-bit SigmaDSP audio processing core, offering additional built-in functions, including FIR filters and many custom algorithms. For this particular core, the maximum number of instruction cycles varies depending on the sampling frequency, ranging from 32 instructions at 768 kHz to 512 instructions at 48 kHz. Moreover, the core supports a high-performance mode achieved by overclocking, which doubles the number of available instruction cycles. It is worth to note the aforementioned active noise algorithm is implemented here using one DSP core, which is, the SigmaDSP core at the normal clock mode.

3.1 Software development tool

For programming the SigmaDSP product lineup, Analog Devices provides SigmaStudio, which is a graphical programming environment for creating and deploying signal processing programs on the evaluation board. It comprises two fundamental frameworks, the first one offers access at the DSP register level to assign built-in operational features, including power management, signal conditioning filters, data interpolation and decimation, and channel routing between input and output (I/O) ports and the DSP cores.

The second framework involves schematic tools that allow the assembly of functional blocks to perform signal manipulation and control. These composed schematics establish operational flow in the device, which is called repeatedly at the start of each sampling period. Each schematic block consumes computational resources in terms of instruction cycles and memory usage. Given the limited instruction capacity at high sampling frequencies, it is crucial to know the minimum feasible sampling frequency and utilize computationally efficient blocks accordingly. Fortunately, memory resources are relatively abundant.

There are scenarios where essential schematic blocks for ANC applications cannot be used due to their high instruction cycle demands. For instance, the built-in L-tap FIR filter function consumes 13 instruction cycles for function overhead and $L + 8$ instruction cycles for sub-routine overhead. Moreover, modifying the filter coefficients during program execution is also not feasible. Therefore, to implement an efficient ANC program, it becomes necessary to employ custom code that grants access to low-level functionality such as shift registers, multiply and accumulate (MAC) operations, as well as the memory read and the memory write operations. With custom code, an L-tap FIR filtering can be accomplished in L cycles of MAC instructions and 1 cycle of memory transfer. The shifting of filter data is automatically managed in the shift register at the start of each sampling period. Detailed discussions of low-level programming are beyond the scope of this article.

3.2 Design of the controller

A reasonable target performance of the controller must be defined, such as the desired minimum noise attenuation within a given bandwidth. One way to determine these parameters is by assessing the passive noise isolation provided by the earbuds. To evaluate this, measurement was conducted in a controlled listening environment using an artificial head and torso (HEAD Acoustic HTB V) with a loudspeaker as the sound source. The loudspeaker was positioned one meter in front of the ear. A broadband, uniformly distributed random noise served as the excitation signal. By comparing the internal microphone responses with and without the earbuds attached to the ears, the passive noise isolation plot displayed in **Figure 2(b)** was obtained. From the data, one may say the passive noise attenuation below 750 Hz is poor. Therefore, the target to achieve in this work is a significant noise reduction of at least 10 dB in the operating bandwidth extending up to 1 kHz.

Considering that the earbuds are sourced from an external commercial product and cannot be modified, it is crucial to ensure the system is causal. To do this, initial data about acoustic paths in the earbuds was collected through measurements using the mentioned test equipment. A sine-sweep signal served as the excitation source. In the primary path measurement, the signal was directed towards an external loudspeaker, and the impulse response function between the two microphones was recorded. In the case of the secondary path, the signal was directed to the speaker in the earbuds, and the path response was captured from the DSP output port, which is directly connected to the earbuds error microphone.

Taking into account the assumed 19 μs acoustic delay, the DSP sampling rate option that meets the minimum requirement is 96 kHz. The measurement results at this specific sampling frequency are depicted in **Figure 3(a)**. One can notice that the leading peak in the impulse response function of the primary path exhibits a lower amplitude compared to the secondary path, which is expected due to higher path attenuation. It is worth noting that the first peak in the primary path impulse response follows that of

the secondary path, indicating the system is causal. In conclusion, the arrangement of microphones and the speaker within the earbuds, along with the choice selection of a 96 kHz DSP sampling rate, confirms system causality.

Based on the initial assessment, the programming work for creating the adaptive feedforward controller can begin. Running at 96 kHz, the SigmaDSP core at its normal clock rate can handle a maximum of 256 instruction cycles. Approximately 43 instruction cycles are reserved for core housekeeping. This means the entire algorithm, along with I/O port assignments, must fit within a total of 213 instruction cycles. The bare minimum noise cancellation program comprises built-in functions and custom code. The built-in functions handle essential tasks such as ADC input, signal generator, two-state logic switching, and DAC output. On the other hand, the custom functions are responsible for signal conditioning in the upstream path, reference input filtering, and adaptive control. After allocating computational resources to the built-in functions, 200 instruction cycles remain available for reference input filtering and adaptive control. It is important to optimize the filter lengths for these functions to ensure efficient use of this allocated resource.

There are three functional blocks in the FxLMS algorithm that handle: anti-noise calculation, as represented by Equation (1), reference input filtering, and coefficient adaptation following Equation (3). The first two blocks, essentially filters, consume one instruction cycle per filter coefficient, while the last block consumes three instruction cycles per filter coefficient. **Table 1** provides a summary of the distribution of instruction allocations for three potential design scenarios. In the first column, the controller and the secondary path estimates are non-recursive filters. Referring to **Figure 3(a)**, it is evident that a substantial filter length is required when using a non-recursive filter to represent the secondary path estimate, approximately 100 taps to cover the first microsecond. This condition restricts the length of the controller to no more than 25 coefficients.

The second scenario involves using a recursive filter to model the secondary path estimate, which has proven advantageous as it significantly reduces the required filter length without compromising controller stability. The optimal filter length for the secondary path estimate is determined using the line search method, which is 16 coefficients in the feed-forward part and 19 coefficients in the feedback part. **Figure 3(b)** provides a comparison between the impulse response functions of the measured the secondary path and secondary path estimate. The length of the controller is significantly expanded to 40 coefficients.

The optimal controller can be used to determine an appropriate controller length. **Figure 4(a)** displays an estimate of the impulse response function of the optimal controller. This calculation, performed without regularization, utilizes the measured acoustic paths. Although not entirely precise, this estimate

Table 1. Basic computational requirements for various programming schemes.

Computation process	**Computation cost (instruction cycle)**			**Notes**
	FxLMS [(a)]	**FxLMS [(b)]**	**FuLMS [(c)]**	
Core housekeeping	43	43	43	(a). $W(z)$ and $\hat{S}(z)$ are non recursive filters (b). $W(z)$ is non recursive filter, $\hat{S}(z)$ is recursive filter (c). $W(z)$ and $\hat{S}(z)$ are Recursive filters Notations WA and WB in the table indicate filter association to the feedback and the feed-forward parts, respectively
ADC: Reference signal	2	2	2	
ADC: Error signal	2	2	2	
DAC: Control signal	2	2	2	
Controller output	$LWB + 1$	$LWB + 1$	$(LWB + LWA) + 1$	
Filtering of input	$SWB + 1$	$(SWB + SWA) + 1$	$(SWB + SWA) + 1$	
Filtering of output	-	-	$(SWB + SWA) + 1$	
Controller adaptation	$2 + 3\ LWB$	$2 + 3\ LW$	$4 + 3(SWB + SWA)$	

serves as an initial approximation for determining the required length of the controller filter. It becomes evident that the first microsecond of the impulse response function carries over 90% of the signal power. While it is conceivable to set the controller length near 100 to mimic the dominant optimal response, this proves unrealistic because the remaining resources support only 40 coefficients.

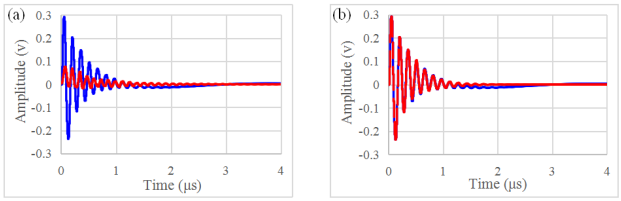

Figure 3. The modeling of secondary paths: (a) The measured impulse response functions of the earbud's primary path (red) and secondary path (blue). (b) Comparison between impulse response functions of the measured (blue) and the modeled (red, dashed) secondary paths.

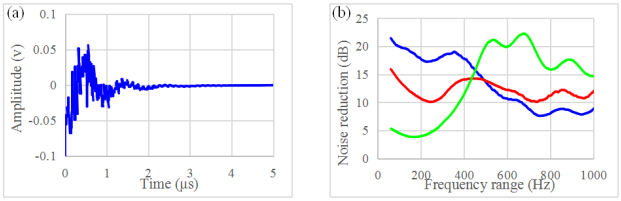

Figure 4. Design of the controller: (a) A non-regularized impulse response function of the optimal controller estimate. (b) The performance of the controller in terms of noise reduction at a given multi-rate factor $N_d = n$ (green), $N_d = 2n$ (red), $N_d = 4n$ (blue).

While one may suggest an alternative approach involving a recursive filter as the controller, it is essential to note that, as detailed in the third column of **Table 1**, additional resources must be allocated for output filtering during the adaptation of the feedback filter. The feedback loop may potentially put controller stability at risk during adaptation. Nevertheless, there is some potential, considering recent developments in alternative algorithms that aim to address stability [16]. Another suggestion, applied here, is based on multi-rate signal processing [17]. It is a straightforward approach that involves decimating the signals. The processes for filter adaptation and anti-noise generation are performed at different rates.

In summary, the final configuration is as follows: a 40-tap non-recursive filter for the controller and a 35-tap recursive filter as the secondary path estimate, which corresponds to a total of 248 instruction cycles. A few more instruction cycles were allocated for a second-order recursive filter, inserted upstream for input signal treatment. The performance of the controller to cancel broadband random noise is depicted in **Figure 4(b)**. Interestingly, the slopes of the plots at different multi-rate factors, denoted as N_d, show variations around 450 Hz. It is believed that with a smaller multi-rate factor, the observation time in the controller becomes shorter, making it challenging for the controller to regulate the low-frequency components, and vice versa. When N_d is set to $2n$, an average noise reduction exceeding 10 dB is achieved in the frequency range up to 1 kHz, satisfies the given design target.

The experimentation showcases adaptive controller design by limiting DSP capability. Greater noise reduction over a wider frequency range becomes attainable with additional resources. For instance, running the DSP board in overclock mode doubles the total instruction cycles to 512. Furthermore, utilizing Biquad filters in the FDSP core to model the secondary path estimate frees up more instruction cycles. Some signal processing functions, such as multi-rate signal processing, are performable by the hardware. These additional resources offer the feasibility of expanding controller length and implementing sophisticated algorithms for improved noise cancellation.

4. Conclusions

The study discussing the development of active noise control systems for earbuds has been presented, emphasizing the significance of maintaining low latency to ensure causality for effective broadband noise cancellation. Nevertheless, when working within the constraints of earbuds, the available hardware resources are limited, hindering the utilization of sophisticated adaptive control algorithms. To overcome these limitations, optimization of filter configuration is employed, along with implementing a computationally efficient program. Moreover, multi-rate signal processing techniques provide practical solutions for achieving the desired noise reduction.

Conflict of Interest

I declare that there is no conflict of interest regarding the publication of this paper.

Funding

This research received no external funding.

Acknowledgement

The author extends gratitude to Dr. Ji-Ho Chang of the Korea Research Institute of Standards and Science, Daejeon, and Prof. Sung-Hwan Shin of Kookmin University, Seoul, for providing access to the test facility and experimental equipment.

References

[1] Liebich, S., Fabry, J., Jax, P., et al. (editors), 2018. Signal processing challenges for active noise cancellation headphones. Speech Communication; 13th ITG-Symposium; 2018 Oct 10-12; Oldenburg. Berlin: VDE. p. 1-5.

[2] Bai, M., Lee, D., 1997. Implementation of an active headset by using the H∞ robust control theory. The Journal of the Acoustical Society of America. 102(4), 2184-2190.

[3] Goldstein, A.L. (inventor), 2016. Adaptive feedback control for earbuds headphones and handset. Patent Application Publication. US patent. 2016/0300562 A1.

[4] Kim, Y., Park, Y., 2019. CPU-GPU architecture for active noise control. Applied Acoustics. 153, 1-13.

[5] Gan, W.S., Kuo, S.M., 2002. An integrated audio and active noise control headset. IEEE Transactions on Consumer Electronics. 48(2), 242-247.

[6] Morgan, D., 1980. An analysis of multiple correlation cancellation loops with a filter in the auxiliary path. IEEE Transactions on Acoustics, Speech, and Signal Processing. 28(4), 454-467.

[7] Kuo, S.M., Morgan, D.R. (editors), 2000. Review of DSP algorithms for active noise control. IEEE International Conference on Control Applications. Conference Proceedings (Cat. No. 00CH37162); 2000 Sep 27; Anchorage. New York: IEEE. p. 243-248.

[8] Zhong, X., Zhang, D., 2021. Latency prediction of earmuff using a lumped parameter model. Applied Acoustics. 176, 107870.

[9] Zhang, L., Qiu, X., 2014. Causality study on a feedforward active noise control headset with different noise coming directions in free field. Applied Acoustics. 80, 36-44.

[10] Rafaely, B., Jones, M., 2002. Combined feedback—feedforward active noise-reducing headset—The effect of the acoustics on broadband performance. The Journal of the Acoustical Society of America. 112(3), 981-989.

[11] Iwai, K., Kinoshita, S., Kajikawa, Y., 2019. Multichannel feedforward active noise control system combined with noise source separation by microphone arrays. Journal of Sound and Vibration. 453, 151-173.

[12] Hansen, C., Snyder, S., Qiu, X., et al., 2012. Active control of noise and vibration. CRC Press: Boca Raton.

[13] Chang, C.Y., 2009. Efficient active noise controller using a fixed-point DSP. Signal Processing. 89(5), 843-850.

[14] Huang, C.H., Pawar, S.J., Hong, Z.J., et al., 2012. Earbud-type earphone modeling and measurement by head and torso simulator. Applied Acoustics. 73(5), 461-469.

[15] Four ADC, Two DAC, Low Power Codec with Audio DSPs ADAU1787 [Internet]. Analog Devices; 2020. Available from: https://www.analog.com/media/en/technical-documentation/data-sheets/adau1787.pdf

[16] Mohammed, J.R., Singh, G. (editors), 2007. An efficient RLS algorithm for output-error adaptive IIR filtering and its application to acoustic echo cancellation. 2007 IEEE Symposium on Computational Intelligence in Image and Signal Processing; 2007 Apr 1-5; Honolulu. New York: IEEE. p. 139-145.

[17] Graf, J., Reithmeier, E., 2009. Computationally efficient active noise reduction in headsets. Journal of Computer and Systems Sciences International. 48, 567-573.

BILINGUAL PUBLISHING GROUP

Journal of Electronic & Information Systems
https://journals.bilpubgroup.com/index.php/jeis

ARTICLE

Control and Treatment of Bone Cancer: A Novel Theoretical Study

***Ali Soltani Sharif Abadi*[1,2*], *Mansour Rafeeyan*[3], *Vahid Abootalebi*[4]**

[1] *Institute of Automatic Control and Robotics, Faculty of Mechatronics, Warsaw University of Technology, Warsaw, 00-664, Poland*

[2] *Institute of Electronic Systems, Faculty of Electronics and Information Technology, Warsaw University of Technology, Warsaw, 00-664, Poland*

[3] *Faculty of Mechanics, Yazd University, Yazd, 8915818411, Iran*

[4] *Faculty of Electrical Engineering, Yazd University, Yazd, 8915818411, Iran*

ABSTRACT

The human body has symmetric bones. This paper uses control engineering concepts to design a suitable controller to synchronize two symmetric bones of the human body to control and treat bone cancer. A Nonsingular Terminal Sliding Mode Control (NTSMC) method will be employed to design the proposed control inputs. The control inputs can be the chemical drugs that can be used to treat bone cancer. The dynamical equations of bone cancer will be used to apply the designed control method and test it. For testing the designed controller, Simulink/MATLAB software will be used. The proposed controller is chattering-free, robust against uncertainties and external disturbances, and finite-time stable in the control engineering view. Bone cancer will be treated for almost one year using the proposed control method.

Keywords: Bone cancer; Synchronization; Finite-time stability; Biomedical engineering

1. Introduction

The human bones are composed of two types of cells: Osteoblast (OB) and Osteoclast (OC). This collection is called a Basic Multicellular Unit (BMU) [1,2]. Bone diseases are diverse, one of them is

*CORRESPONDING AUTHOR:
Ali Soltani Sharif Abadi, Institute of Automatic Control and Robotics, Faculty of Mechatronics, Warsaw University of Technology, Warsaw, 00-664, Poland; Institute of Electronic Systems, Faculty of Electronics and Information Technology, Warsaw University of Technology, Warsaw, 00-664, Poland; Email: ali.soltani_sharif_abadi.dokt@pw.edu.pl

ARTICLE INFO
Received: 9 October 2023 | Revised: 4 November 2023 | Accepted: 7 November 2023 | Published Online: 17 November 2023
DOI: https://doi.org/10.30564/jeis.v5i2.6004

CITATION
Abadi, A.S.S., Rafeeyan, M., Abootalebi, V., 2023. Control and Treatment of Bone Cancer: A Novel Theoretical Study. Journal of Electronic & Information Systems. 5(2): 35-44. DOI: https://doi.org/10.30564/jeis.v5i2.6004

bone cancer. Bone cancer happens when the growth rate order of the bone cells (OB or OC) is disrupted, which grows into cancer cells (CCs) [1-3]. Osteosarcoma (OS) is a type of bone disease. When the OS happens in the bone, the discipline of the growth of the bone cells disorganizes. OS is more likely to happen at 13-16 years old and after 55 years old. This sickness more occurs in boy children [3,4]. OB cells are responsible for the remodeling of bone, and OC cells are for bone growth. If the order of growth and reproduction of these cells is lost, OB cells will grow more and cause CCs [5,6]. In the healthy bone (bone without cancer), OB and OC cells multiply clearly and periodically. However, in sick bone (cancerous bone), there is no systematic growth and reproduction [1].

Bones are the skeleton of the human body, and almost all of them are symmetrical. If one of the human bones becomes cancerous, the closest value of the parameters is its symmetric bone. Therefore, symmetric bone parameters can be used for the reconstruction and treatment of cancerous bone. This fact can be used to model, design, and control cancerous bones. This concept in control engineering is called "synchronization". In the synchronization problem, the variables and parameters of the "slave" system will be the same as the variables and parameters of the "master" system [7]. In the synchronization of two human bones, the cancerous bone (slave) will be the same as the healthy bone (master). For synchronization, the systems need to apply control inputs to the system. These control inputs in the synchronization of the human bones can be considered as the effect of the dose of the chemical drugs. Recently, many control efforts have been made using the synchronization concept in different fields, such as synchronizing communication systems [8,9], chaotic systems [10,11], and chemical systems [12,13].

The Nonsingular Terminal Sliding Mode Control (NTSMC) method is a robust finite-time control strategy that guarantees that the system states reach zero at a finite time. The NTSMC is an extended version of Finite-time Sliding Mode Control methods that have been used in controlling different applications. This method has been used to solve the stability and tracking problems of rigid manipulators, high-order nonlinear systems, and robotic surgery [14-16]. It is used for controlling some practical systems such as manipulator robots [17], perturbed nonlinear systems [18], DC-DC buck converters [19], Quadrotor unmanned aerial vehicles [20], underactuated underwater robots [21], acute Leukemia therapy [22]. Recently control engineering methods have been used to increase biomedical applications such as drug delivery in cancerous tumors [23], tumor treatment immunity [24], cancer chemotherapy [25], control the tumor growth [26], and angiogenic inhibition therapy [27]. An extended adaptive NTSMC using fractional disturbance observer has been presented to accelerate system response without resulting in chattering [28]. Also, the NTSMC has been used to deal with the time delay for controlling the integrating processes [29].

One of the challenges in the designed controller by NTSMC is the chattering phenomenon. The chattering phenomenon is because of the high frequency switching gain in the controller. Chattering is a very harmful phenomenon in control applications. It can reduce the actuators' age and add unwanted noise to the system. In biomedical applications, especially cancer treatment, the chattering causes to control inputs will be uncreatable. It means that the chattered control inputs cannot be created in the practical tests. Some types of control methods are developed to remove, eliminate or reduce the chattering from the control input signals [30-33].

This paper proposes three control signals to synchronize two symmetrical human bones to control bone cancer. It is assumed that one of the human bones (arm or leg bones) is cancerous with cancer, and it will be treated by applying the proposed control inputs, which are the effect of the chemical drugs. The proposed control inputs will be designed by the NTSMC control method. The control inputs are designed using the chattering-free concepts. Below are the most important features of the proposed control method:

- Robustness against model uncertainties and external disturbances,

- Chattering-free control of the bone cancer,
- Accurate tracking of the healthy cells,
- Smooth control of the system,
- Fast tracking of the master states,
- Implementable results in control signals.

2. Mathematics

Definition 1. Function $sig^a(x)$ with the relation between absolute function $|x|$ and symbol-function for $sig^a(x) = |x|^a sign(x)$ is defined. Function $sign(x)$ is defined as follows [34,35]:

$$sign(x) = \begin{cases} 1 \ ; \ x > 0 \\ 0 \ ; \ x = 0 \\ -1 \ ; \ x < 0 \end{cases} \quad (1)$$

Definition 2. The relation between absolute and signum function is as $|x| = xsign(x)$ [34].

Lemma 1. For a nonlinear system $\dot{x} = f(x), f(0) = 0, x \in D \subseteq \Re^n, x(0) = x_0$ by assuming the constants ρ_1 to ρ_4 as $\rho_1 > 0, \rho_2 > 0, \rho_3 > 1, \rho_4 = 1 - \frac{1}{2\rho_3}, \rho_5 = 1 + \frac{1}{2\rho_3}$ and Lyapunov function $V(x): \Re^n \to \Re^+ \cup \{0\}$, as a scalar continuous radially unbounded function therefore if $\dot{V}(x) \leq -\rho_1 V^{p4}(x) - \rho_2 V^{p5}(x)$ so the equilibrium $x = 0$ of this system will be globally finite-time stable, and state variables of this system converge from each initial condition to zero, and the upper bound of its settling time is for $T \leq \pi\rho_3(\sqrt{\rho_1\rho_2})^{-1}$ [36].

Lemma 2. Considering scalars $a_1, a_2, ..., a_n \in \Re$ and choosing $0 < q < 2$ then will have $|a_1|^q + |a_2|^q + ... + |a_n|^q \geq \left(a_1^2 + a_2^2 + ... + a_n^2\right)^{\frac{q}{2}}$ [37].

3. Explanation of the purpose

This paper aims to synchronize the OBs and OCs cells of the cancerous bone to OBs and OCs cells of the symmetrical healthy bone and destroy the CCs. The model of bone OBs, OCs cells, and CCs for cancerous and healthy bones are the same, and only the parameter values are different [1]. The provided bone model and the values of its parameters for healthy and cancerous bone are published [1,2,38] for Mixed Lesion and Osteolytic Lesion diseases. These are the most common cancerous bone diseases. This model is called the Komarova model, which is presented in Equation (2).

$$\begin{cases} \dot{u} = \alpha_1 u v^{\gamma_1} - \beta_1 u + \sigma_1 u\omega \\ \dot{v} = \alpha_2 v u^{\gamma_2} - \beta_2 v + \sigma_2 v\omega \\ \dot{\omega} = \alpha_3 \left(1 - \frac{\omega}{K}\right)\omega + (\sigma_3 u^{\gamma_2} + \sigma_4 v^{\gamma_1})\omega - \beta_3\omega \end{cases} \quad (2)$$

where u, v and ω are the density of OC, OB and CC cells, respectively. α_i, β_i, $i = (1, 2, 3)$ multiplication rate of OC, OB and CCs and are fixed parameters and positive. σ_j, $j = (1, 2, 3, 4)$ coefficients constant for the relationship between OC, OB and CCs that σ_1, σ_3 are positive and σ_2, σ_4 are negative or positive. γ_1, γ_2 are the rate of signaling between OBs and OCs that are coefficient and $\gamma_1 < 0$, $\gamma_2 > 0$ and K is the ability to carry CCs. As well as the model of bone mass is as follows [2]:

$$\dot{z} = -k_1\sqrt{\max\{u - \overline{u}, 0\}} + k_2\sqrt{\max\{v - \overline{v}, 0\}} \quad (3)$$

where z is the bone mass and k_1, k_2 are normalized activities of bone formation that are constant and positive. $\overline{v}$, $\overline{u}$ are steady-state of the OB and OC cells that are presented as follows:

$$\begin{aligned} \overline{u} &= \left(\frac{\beta_2}{\alpha_2}\right)^{\frac{1}{\gamma_2}} \\ \overline{v} &= \left(\frac{\beta_1}{\alpha_1}\right)^{\frac{1}{\gamma_1}} \end{aligned} \quad (4)$$

For healthy bone, the values of parameters are presented as follows:

$$\begin{aligned} &\alpha_{1m} = 0.3, \alpha_{1m} = 0.1, \beta_{1m} = 0.2, \beta_{2m} = 0.02, \\ &\gamma_{1m} = -0.3, \gamma_{2m} = 0.5, k_{1m} = 0.07, k_{2m} = 0.0022, \\ &\alpha_{3m} = 0.045, \beta_{3m} = 0.05, \sigma_{1m} = 0.001, \sigma_{2m} = -0.00005, \\ &\sigma_{3m} = 0.005, \sigma_{4m} = 0.005, \sigma_{4m} = 0, K_m = 300 \end{aligned} \quad (5)$$

In addition, for the Fixed Lesion disease, these parameters have values as follows:

$$\begin{aligned} &\alpha_{1s} = 0.3, \alpha_{2s} = 0.1, \beta_{1s} = 0.2, \beta_{2s} = 0.02, \gamma_{1s} = -0.3, \\ &\gamma_{2s} = 0.5, k_{1s} = 0.023, k_{2s} = 0.0023, \alpha_{3s} = 0.055, \\ &\beta_{3s} = 0.05, \sigma_{1s} = \sigma_{2s} = -0.005, \sigma_{3s} = 0.001, \sigma_{4s} = 0, K_s = 3 \end{aligned} \quad (6)$$

For the synchronization of two healthy and cancerous bones, the synchronization errors are defined as $e_1 = u_s - u_m$, $e_2 = v_s - v_m$, $e_3 = \omega_s - \omega_m$ where m is the abbreviation of the master system (healthy bone), also s is the abbreviation of the slave system (cancerous bone). This paper aims to reach these errors to zero at a finite time.

The error dynamic will be as follows:

$$\begin{cases} \dot{e_1} = f_{1s} - f_{1m} + D_1 + U_1 \\ \dot{e_2} = f_{2s} - f_{2m} + D_2 + U_2 \\ \dot{e_3} = f_{3s} - f_{3m} + D_3 + U_3 \end{cases} \quad (7)$$

where

$$\begin{cases} f_{1m} = \alpha_{1m} u_m v_m^{\gamma_{1m}} - \beta_{1m} u_m + \sigma_{1m} u_m \omega_m \\ f_{2m} = \alpha_{2m} v_m u_m^{\gamma_{2m}} - \beta_{2m} v_m + \sigma_{2m} v_m \omega_m \\ f_{3m} = \alpha_{3m} \left(1 - \frac{\omega_m}{K_m}\right) \omega_m + \left(\sigma_{3m} u_m^{\gamma_{2m}} + \sigma_{4m} v_m^{\gamma_{1m}}\right) \omega_m - \beta_{3m} \omega_m \end{cases} \quad (8)$$

and

$$\begin{cases} f_{1s} = \alpha_{1s} u_s v_s^{\gamma_{1s}} - \beta_{1s} u_s + \sigma_{1s} u_s \omega_s \\ f_{2s} = \alpha_{2s} v_s u_s^{\gamma_{2s}} - \beta_{2s} v_s + \sigma_{2s} v_s \omega_s \\ f_{3s} = \alpha_{3s} \left(1 - \frac{\omega_s}{K_s}\right) \omega_s + \left(\sigma_{3s} u_s^{\gamma_{2s}} + \sigma_{4s} v_s^{\gamma_{1s}}\right) \omega_s - \beta_{3s} \omega_s \end{cases} \quad (9)$$

U_i, i = (1, 2, 3) are the models of the control inputs that will be designed in the next section and D_i are the models of unknowns and uncertainties. Assuming that the upper bounds for D_i are available as follows:

$$\begin{aligned} |D_i| &\le \eta_{i1} \\ |\dot{D}_i| &\le \eta_{i2} \end{aligned} \quad (10)$$

4. Designing the control inputs

Designing the controller using the NTSMC method consists of two parts. The first part is designing the sliding surfaces and proof of their stability, and the second part is proof of reaching the sliding surface. Since this paper aims for finite-time stability, must both these parts prove at a finite time to ensure the finite-time stability.

Theorem 1: Consider system Equation (7), defined sliding surfaces Equation (11), and control inputs Equation (12). So the states of this system reach zero in a finite time.

$$\begin{cases} s_1 = \dot{e}_1 + c_{11} sig^{\alpha_{11}}(e_1) + c_{12} sig^{\alpha_{12}}(e_1) \\ s_2 = \dot{e}_2 + c_{21} sig^{\alpha_{21}}(e_2) + c_{22} sig^{\alpha_{22}}(e_2) \\ s_3 = \dot{e}_3 + c_{31} sig^{\alpha_{31}}(e_3) + c_{32} sig^{\alpha_{32}}(e_3) \end{cases} \quad (11)$$

where c_{i1}, c_{i2} are positive control parameters and α_{i1}, α_{i2} are positive constants as $\begin{cases} \alpha_{i1} = N \\ \alpha_{i2} = \frac{N}{2-N} \end{cases}$ and $N \in (1, 2)$.

$$\begin{cases} U_i = U_{eq_i} + U_{r_i} \\ U_{eq_i} = f_{im} - f_{is} - c_{i1} sig^{\alpha_{i1}}(e_i) - c_{i2} sig^{\alpha_{i2}}(e_i) \\ \dot{U}_{r_i} = -k_{i1} sig^{\beta_{i1}}(s_i) - k_{i2} sig^{\beta_{i2}}(s_i) - \eta_{i2} sign(s_i) \end{cases} \quad (12)$$

In these control inputs k_{i1}, k_{i2} are positive constants and β_{i1}, β_{i2} are positive and smaller than one constant.

Proof: It has been shown that sliding surfaces Equation (11) have finite-time stability, provided that c_{i1}, c_{i2} are chosen so polynomial of $p^2 + c_{i2}p + c_{i1} = 0$ is Hurwitz [39]. For prooving the reaching phase (second part), consider the Lyapunov function $V = \sum_{i=1}^{3} \frac{1}{2} s_i$ which has conditions of the Lyapunov function of Lemma 1. Then will have $\dot{V} = \sum_{i=1}^{3} s_i \dot{s}_i$ and with applying the control inputs to the system also putting up $\dot{s}_i$ in $\dot{V}$ so can be written $\dot{V} = \sum_{i=1}^{3} s_i (\dot{U}_{r_i} + \dot{D}_i)$ as follows:

$$\dot{V} = \sum_{i=1}^{3} s_i \left(-k_{i1} sig^{\beta_{i1}}(s_i) - k_{i2} sig^{\beta_{i2}}(s_i) - \eta_{i2} sign(s_i) + \dot{D}_i\right) \quad (13)$$

by simplifying:

$$\dot{V} = \sum_{i=1}^{3} -k_{i1} |s_i|^{1+\beta_{i1}} - k_{i2} |s_i|^{1+\beta_{i2}} - \eta_{i2} |s_i| + \dot{D}_i s_i \quad (14)$$

since the $\dot{D}_i s_i \le |\dot{D}_i| |s_i|$ also $|\dot{D}_i| \le \eta_{i2}$ so:

$$\dot{V} \le \sum_{i=1}^{3} -k_{i1} |s_i|^{1+\beta_{i1}} - k_{i2} |s_i|^{1+\beta_{i2}} \quad (15)$$

due to the Lemma 2:

$$\dot{V}(x) \le \sum_{i=1}^{3} -\left(\sqrt{2}\right)^{\beta_{i1}+1} k_{i1} s_i^{\frac{\beta_{i1}+1}{2}} - \left(\sqrt{2}\right)^{\beta_{i2}+1} k_{i2} s_i^{\frac{\beta_{i2}+1}{2}} \quad (16)$$

with the selection of parameters values as follows:

$$r_1 = \left(\sqrt{2}\right)^{\beta_{i1}+1} k_{i1} > 0, r_2 = \left(\sqrt{2}\right)^{\beta_{i2}+1} k_{i2} > 0, r_4 = \beta_{i1} = 1 - \frac{1}{r_3}, r_5 = \beta_{i2} = 1 + \frac{1}{r_3} \quad (17)$$

where $r_3 > 1$:

$$\dot{V}(x) \le -r_1 V^{r_4} - r_2 V^{r_5} \quad (18)$$

due to the Lemma 1, the system Equation (2) is stable for a finite time, and the settling time is $T \le \pi r_3 \left(\sqrt{(r_1 r_2)}\right)^{-1}$. Theorem 1 is proved.

5. Simulation

The aim of this paper was to show that OB and OC cells of cancerous bone track the OB and OC cells of healthy bone as well as eliminate the CCs of the cancerous bone. The simulation was conducted in MATLAB software. The control parameters are selected as follows:

$$c_{i1} = 0.02, c_{i2} = 0.0001, k_{i1} = 0.01,$$
$$k_{i2} = 0.01, N = 0.9, r_3 = 0.5 \quad (19)$$

Figure 1 shows the curves of the OC cells, and **Figure 2** shows the OB cells of the healthy and cancerous bones. **Figure 3** shows the curve of the CCs for cancerous bone. As well as **Figure 4** illustrates the curves of the designed control inputs. In this simulation, the initial conditions of healthy bone are (u_0, v_0, ω_0) = (10, 5, 1). Since the cancerousness happens, the distances of the OC and CCs cells are more than a healthy bone, and the distance of the OB cells is less than, so the initial conditions of cancerous bone are selected as (u_0, v_0, ω_0) = (40, 1, 5).

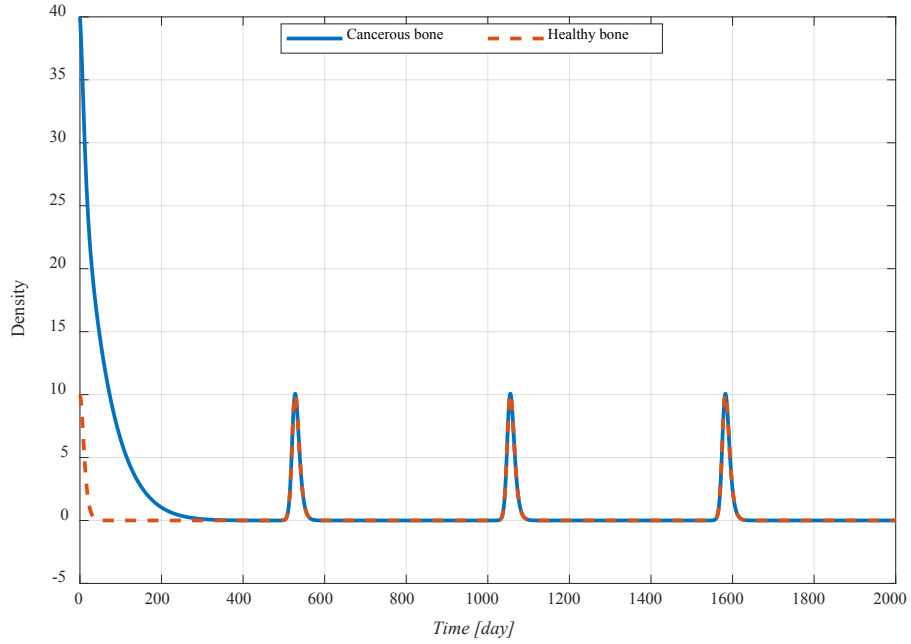

Figure 1. The curves of the OC cells of cancerous and healthy bone.

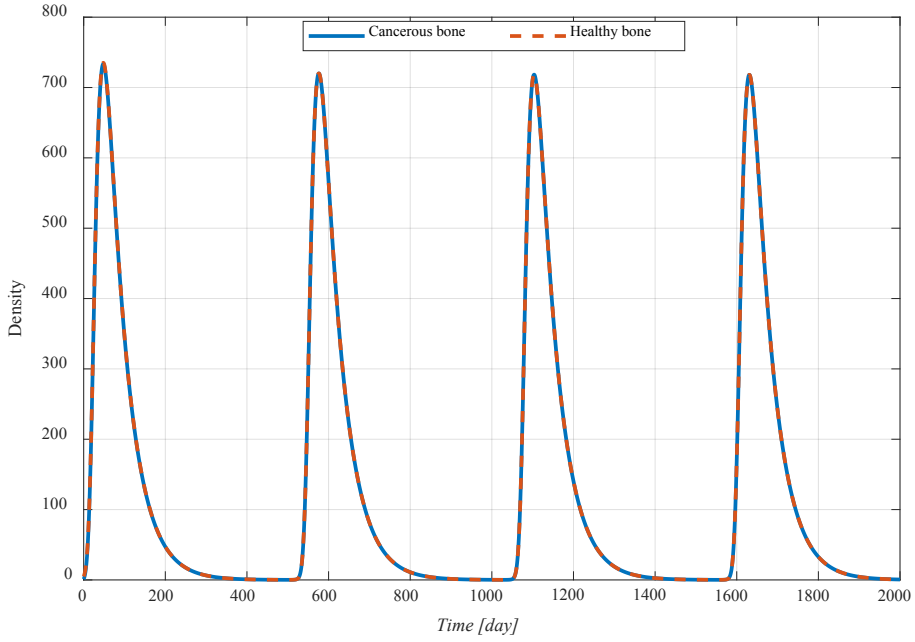

Figure 2. The curves of the OB cells of cancerous and healthy bone.

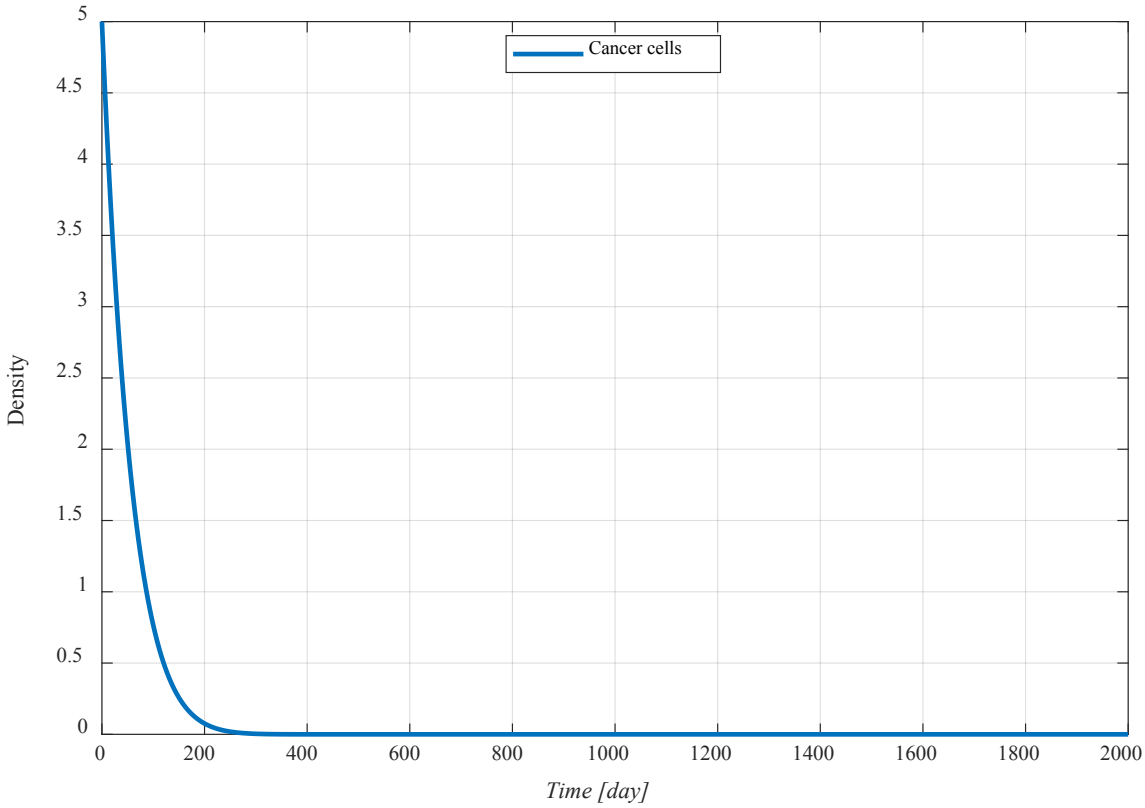

Figure 3. The curves of the CCs of cancerous bone.

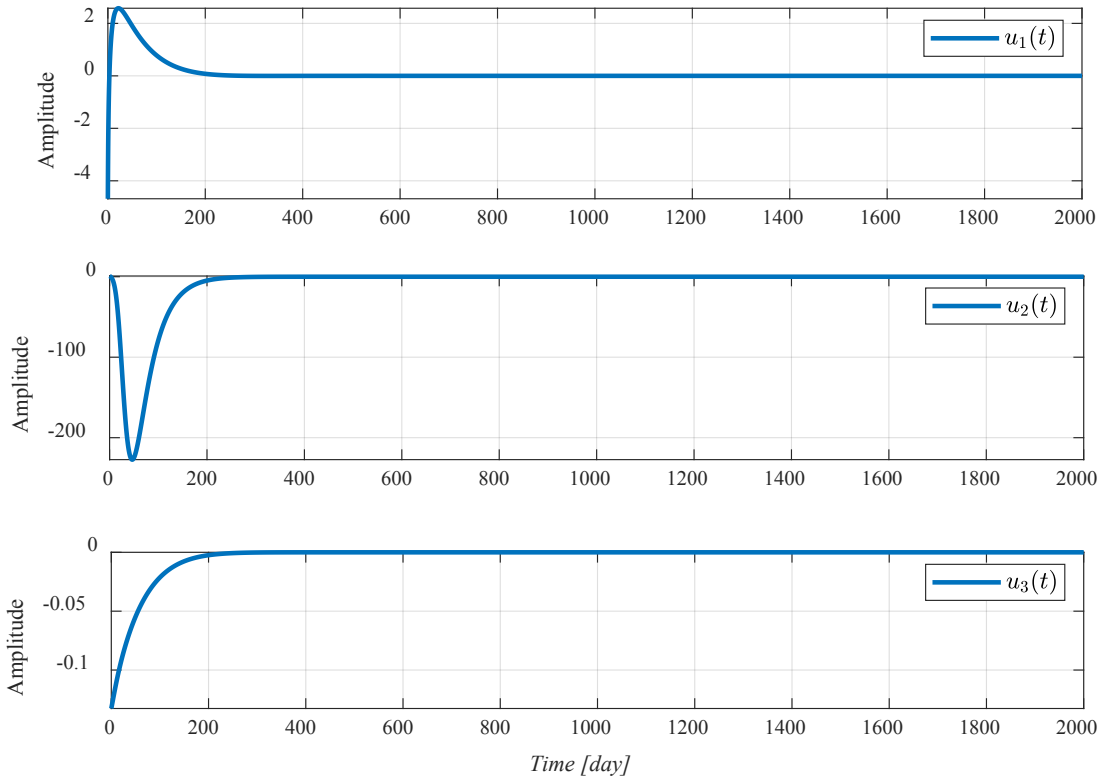

Figure 4. The curves of the control inputs.

6. Discussion

As the figures are precise, after about 300 days (almost one year), the OC cells of cancerous bone have tracked the OC cells of healthy bone until the CCs have disappeared. In the OB cells, because the initial conditions of cancerous bone and healthy bone are close and the amplitude of the figure is big, the result is not clear correctly. **Figure 5** shows the curve of the OB cells in 30 days (zoomed in). The period of OS treatment is almost five years in the real world. This is the reason for selecting the final time of the simulation as 2000 days. The control inputs are smooth. They are possible to implement in real tests. The smoothness happened because of the chattering-free design.

In brief, all the required features of a controller for controlling bone cancer have been considered in designing the proposed controller. The controller is robust, chatter-free, accurate, smooth, fast, and implementable. The results presented in **Figures 1-5** show the power of the proposed controller.

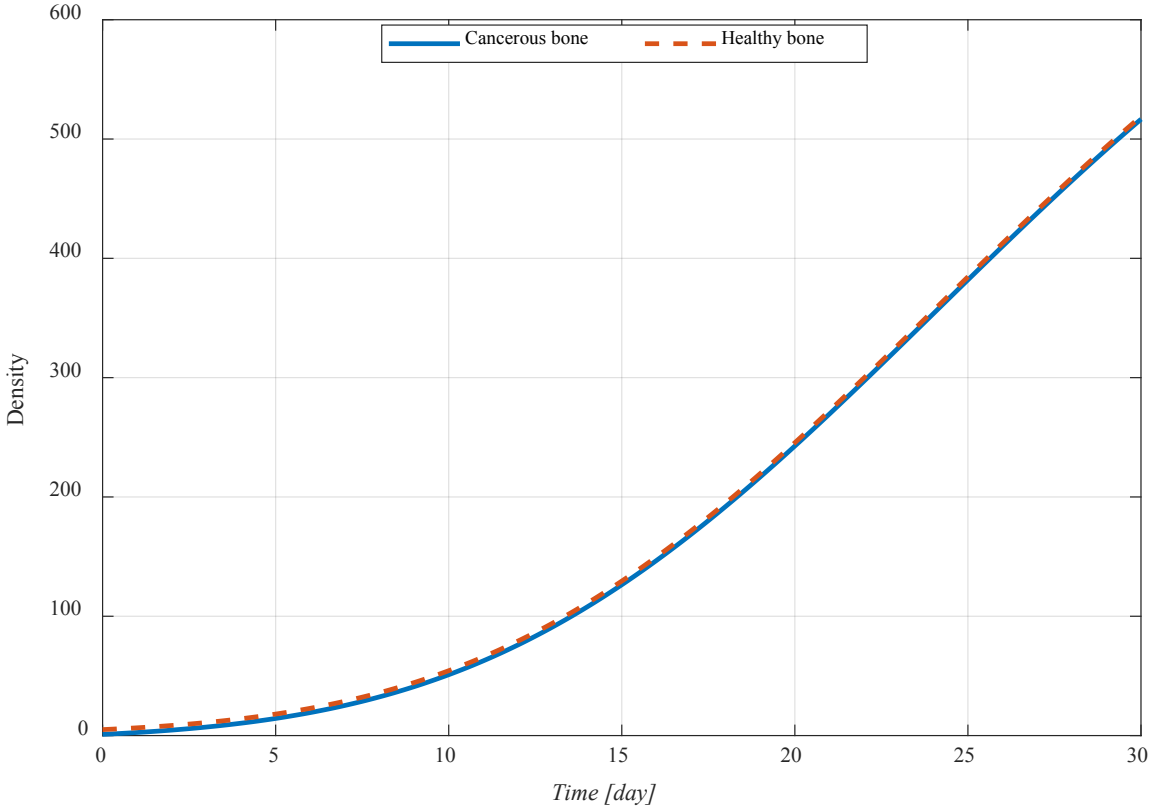

Figure 5. The curve of the OB cells of cancerous and healthy bone in 30 days.

7. Conclusions

In this paper, the NTSMC control method is employed to synchronize two human body bones. One of these bones was cancerous bone, and the other bone was healthy. This paper was a theoretical study that controlled and treated bone cancer with a theoretical method. Three designed control inputs have the features of chattering-free, finite-time stability and robustness against unknowns and uncertainties, which can be used in practical tests. These control inputs can be the effects of doses of medicines or the power of X-rays. After about a year, it was shown that the CCs had disappeared, and the cancerous bone looked like symmetrical healthy bone. For the subsequent studies, it is suggested to work on implementing these types of studies in real tests for the treatment of some animals' bone cancer.

Authors' Contributions

Ali Soltani Sharif Abadi: conceptualization, methodology, software, validation, formal analysis, investigation, resources, data curation, writing, review and editing, visualization, and funding.

Mansour Rafeeyan: conceptualization, methodology, validation, formal analysis, investigation, resources, data curation, writing, review and editing, visualization, supervision.

Vahid Abootalebi: conceptualization, methodology, validation, formal analysis, investigation, resources, data curation, writing, review and editing, visualization, supervision.

Conflict of Interest

There is no conflict of interest.

Data Availability Statement

Not applicable.

Funding

Ali Soltani Sharif Abadi acknowledges support from Warsaw University of Technology (WUT), grant No: 504440200003.

Acknowledgement

Ali Soltani Sharif Abadi acknowledges support from the WUT.

References

[1] Jerez, S., Camacho, A., 2018. Bone metastasis modeling based on the interactions between the BMU and tumor cells. Journal of Computational and Applied Mathematics. 330, 866-876. DOI: https://doi.org/10.1016/j.cam.2016.12.026

[2] Buenzli, P.R., Pivonka, P., Gardiner, B.S., et al., 2012. Modelling the anabolic response of bone using a cell population model. Journal of Theoretical Biology. 307, 42-52. DOI: https://doi.org/10.1016/j.jtbi.2012.04.019

[3] Han, Y., Kang, Y., 2022. Bone niche and bone metastases. Bone sarcomas and bone metastases-from bench to bedside. Academic Press: Cambridge. pp. 107-119.

[4] Ottaviani, G., Jaffe, N., 2010. The epidemiology of osteosarcoma. Pediatric and adolescent osteosarcoma. Springer: Berlin. pp. 3-13.

[5] Pivonka, P., Zimak, J., Smith, D.W., et al., 2008. Model structure and control of bone remodeling: A theoretical study. Bone. 43(2), 249-263. DOI: https://doi.org/10.1016/j.bone.2008.03.025

[6] Chen-Charpentier, B.M., Diakite, I., 2016. A mathematical model of bone remodeling with delays. Journal of Computational and Applied Mathematics. 291, 76-84. DOI: https://doi.org/10.1016/j.cam.2014.11.025

[7] Abadi, A.S.S., Hosseinabadi, P.A., Mekhilef, S., et al., 2020. Chattering-free fixed-time sliding mode control for bilateral teleoperation under unknown time-varying delay via disturbance and state observers. Advanced Control for Applications: Engineering and Industrial Systems. 2(4), e52. DOI: https://doi.org/10.1002/adc2.52

[8] D'Amico, A.A., Colavolpe, G., Foggi, T., et al., 2022. Timing synchronization and channel estimation in free-space optical OOK communication systems. IEEE Transactions on Communications. 70(3), 1901-1912. DOI: https://doi.org/10.1109/TCOMM.2022.3142134

[9] Mohadeszadeh, M., Pariz, N., 2022. An application of adaptive synchronization of uncertain chaotic system in secure communication systems. International Journal of Modelling and Simulation. 42(1), 143-152. DOI: https://doi.org/10.1080/02286203.2020.1848281

[10] Chantawat, C., Botmart, T., 2022. Finite-time H∞ synchronization control for coronary artery chaos system with input and state time-varying delays. Plos One. 17(4), e0266706. DOI: https://doi.org/10.1371/journal.pone.0266706

[11] Izadbakhsh, A., Gholizade-Narm, H., Deylami,

A., 2022. Observer-based adaptive controller design for chaos synchronization using Bernstein-type operators. International Journal of Robust and Nonlinear Control. 32(7), 4318-4335.
DOI: https://doi.org/10.1002/rnc.6026

[12] Khan, A., Khan, T., Chaudhary, H., 2022. Chaos controllability in chemical reactor system via active controlled hybrid projective synchronization method. AIP Conference Proceedings. 2435(1).
DOI: https://doi.org/10.1063/5.0084689

[13] Vaidyanathan, S., 2015. Adaptive synchronization of novel 3-D chemical chaotic reactor systems. Parameters. 1, 4.

[14] Feng, Y., Yu, X., Han, F., 2013. On nonsingular terminal sliding-mode control of nonlinear systems. Automatica. 49(6), 1715-1722.
DOI: https://doi.org/10.1016/j.automatica.2013.01.051

[15] Feng, Y., Yu, X., Man, Z., 2002. Non-singular terminal sliding mode control of rigid manipulators. Automatica. 38(12), 2159-2167.
DOI: https://doi.org/10.1016/S0005-1098(02)00147-4

[16] Soltani Sharif Abadi, A., Ordys, A., Kukielka, K., et al., 2023. Review on challenges for robotic eye surgery; surgical systems, technologies, cost-effectiveness, and controllers. The International Journal of Medical Robotics and Computer Assisted Surgery. e2524.
DOI: https://doi.org/10.1002/rcs.2524

[17] Cruz-Ortiz, D., Chairez, I., Poznyak, A., 2022. Non-singular terminal sliding-mode control for a manipulator robot using a barrier Lyapunov function. ISA Transactions. 121, 268-283.
DOI: https://doi.org/10.1016/j.isatra.2021.04.001

[18] Alattas, K.A., Vu, M.T., Mofid, O., et al., 2022. Adaptive nonsingular terminal sliding mode control for performance improvement of perturbed nonlinear systems. Mathematics. 10(7), 1064.
DOI: https://doi.org/10.3390/math10071064

[19] Wang, S., Li, S., Su, J., et al., 2023. Extended state observer-based nonsingular terminal sliding mode controller for a DC-DC buck converter with disturbances: Theoretical analysis and experimental verification. International Journal of Control. 96(7), 1661-1671.
DOI: https://doi.org/10.1080/00207179.2022.2063192

[20] Alattas, K.A., Mofid, O., Alanazi, A.K., et al., 2022. Barrier function adaptive nonsingular terminal sliding mode control approach for quad-rotor unmanned aerial vehicles. Sensors. 22(3), 909.
DOI: https://doi.org/10.3390/s22030909

[21] Guo, L., Liu, W., Li, L., et al., 2022. Neural network non-singular terminal sliding mode control for target tracking of underactuated underwater robots with prescribed performance. Journal of Marine Science and Engineering. 10(2), 252.
DOI: https://doi.org/10.3390/jmse10020252

[22] Islam, Y., Ahmad, I., Zubair, M., et al., 2022. Adaptive terminal and supertwisting sliding mode controllers for acute Leukemia therapy. Biomedical Signal Processing and Control. 71, 103121.
DOI: https://doi.org/10.1016/j.bspc.2021.103121

[23] Khalili, P., Vatankhah, R., Taghvaei, S., 2018. Optimal sliding mode control of drug delivery in cancerous tumour chemotherapy considering the obesity effects. IET Systems Biology. 12(4), 185-189.
DOI: https://doi.org/10.1049/iet-syb.2017.0094

[24] Sarhaddi, M., Yaghoobi, M., 2020. A new approach in cancer treatment regimen using adaptive fuzzy back-stepping sliding mode control and tumor-immunity fractional order model. Biocybernetics and Biomedical Engineering. 40(4), 1654-1665.
DOI: https://doi.org/10.1016/j.bbe.2020.09.003

[25] Dey, B.S., Bera, M.K., & Roy, B.K. (editors), 2018. Super twisting sliding mode control of cancer chemotherapy. 2018 15th International Workshop on Variable Structure Systems (VSS); 2018 Jul 9-11; Graz, Austria. New York: IEEE. p. 343-348.
DOI: https://doi.org/10.1109/VSS.2018.8460228

[26] Shahri, A.P., Haghighatnia, S., Moghaddam,

R.K., et al., 2017. Control the tumour growth via sliding mode control. International Journal of Medical Engineering and Informatics. 9(2), 101-109.
DOI: https://doi.org/10.1504/IJMEI.2017.083093

[27] Doruk, R.Ö., 2020. Angiogenic inhibition therapy, a sliding mode control adventure. Computer Methods and Programs in Biomedicine. 190, 105358.
DOI: https://doi.org/10.1016/j.cmpb.2020.105358

[28] Alyoussef, F., Kaya, I., 2023. Improved adaptive dynamic non-singular terminal sliding mode controller with fractional disturbance observer. Information Sciences. 641, 119110.
DOI: https://doi.org/10.1016/j.ins.2023.119110

[29] Alyoussef, F., Kaya, I., 2023. A new dynamic sliding mode controller with disturbance observer for controlling integrating processes with time delay. International Journal of Control. 1-21.
DOI: https://doi.org/10.1080/00207179.2023.2201649

[30] Cai, G., Ding, Y., Chen, Q., 2019. SMC Chaos control of a novel hyperchaotic finance system using a new chatter free sliding mode control. Journal of Physics: Conference Series. 1187(3), 032103.
DOI: https://doi.org/10.1088/1742-6596/1187/3/032103

[31] Adamiak, K., 2020. Chattering-free reference sliding variable-based SMC. Mathematical Problems in Engineering. 3454090.
DOI: https://doi.org/10.1155/2020/3454090

[32] Abadi, A.S.S., 2023. A novel control system for synchronizing chaotic systems in the presence of communication channel time delay; case study of Genesio-Tesi and Coullet systems. Nonlinear Analysis: Hybrid Systems. 50, 101408.
DOI: https://doi.org/10.1016/j.nahs.2023.101408

[33] Abadi, A.S.S., Ordys, A., Pierscionek, B. (editors), 2023. Controlling a teleoperated robotic eye surgical system under a communication channel's unknown time delay. 2023 27th International Conference on Methods and Models in Automation and Robotics (MMAR); 2023 Aug 22-25; Międzyzdroje, Poland. New York: IEEE. p. 211-215.
DOI: https://doi.org/10.1109/MMAR58394.2023.10242556

[34] Alinaghi Hosseinabadi, P., Soltani Sharif Abadi, A., Mekhilef, S., et al., 2020. Chattering-free trajectory tracking robust predefined-time sliding mode control for a remotely operated vehicle. Journal of Control, Automation and Electrical Systems. 31(5), 1177-1195.
DOI: https://doi.org/10.1007/s40313-020-00599-4

[35] Abadi, A.S.S., Ordys, A., Pierscionek, B., 2023. Novel off-line self-tuning controller with guaranteed stability. International Journal of Automotive Technology. 24(3), 851-862.
DOI: https://doi.org/10.1007/s12239-023-0069-7

[36] Abadi, A.S.S., Hosseinabadi, P.A., Mekhilef, S., 2018. Two novel approaches of NTSMC and ANTSMC synchronization for smart grid chaotic systems. Technology and Economics of Smart Grids and Sustainable Energy. 3, 1-14.
DOI: https://doi.org/10.1007/s40866-018-0050-0

[37] Abadi, A.S.S., Hosseinabadi, P.A., Mekhilef, S., 2020. Fuzzy adaptive fixed-time sliding mode control with state observer for a class of high-order mismatched uncertain systems. International Journal of Control, Automation and Systems. 18, 2492-2508.
DOI: https://doi.org/10.1007/s12555-019-0650-z

[38] Komarova, S.V., Smith, R.J., Dixon, S.J., et al., 2003. Mathematical model predicts a critical role for osteoclast autocrine regulation in the control of bone remodeling. Bone. 33(2), 206-215.
DOI: https://doi.org/10.1016/S8756-3282(03)00157-1

[39] Feng, Y., Han, F., Yu, X., 2014. Chattering free full-order sliding-mode control. Automatica. 50(4), 1310-1314.
DOI: https://doi.org/10.1016/j.automatica.2014.01.004

BILINGUAL PUBLISHING GROUP

Journal of Electronic & Information Systems
https://journals.bilpubgroup.com/index.php/jeis

ARTICLE

Enhancing Semantic Segmentation through Reinforced Active Learning: Combating Dataset Imbalances and Bolstering Annotation Efficiency

Dong Han, Huong Pham, Samuel Cheng*

School of Electrical and Computer Engineering, University of Oklahoma, Tulsa, OK, 74135, USA

ABSTRACT

This research addresses the challenges of training large semantic segmentation models for image analysis, focusing on expediting the annotation process and mitigating imbalanced datasets. In the context of imbalanced datasets, biases related to age and gender in clinical contexts and skewed representation in natural images can affect model performance. Strategies to mitigate these biases are explored to enhance efficiency and accuracy in semantic segmentation analysis. An in-depth exploration of various reinforced active learning methodologies for image segmentation is conducted, optimizing precision and efficiency across diverse domains. The proposed framework integrates Dueling Deep Q-Networks (DQN), Prioritized Experience Replay, Noisy Networks, and Emphasizing Recent Experience. Extensive experimentation and evaluation of diverse datasets reveal both improvements and limitations associated with various approaches in terms of overall accuracy and efficiency. This research contributes to the expansion of reinforced active learning methodologies for image segmentation, paving the way for more sophisticated and precise segmentation algorithms across diverse domains. The findings emphasize the need for a careful balance between exploration and exploitation strategies in reinforcement learning for effective image segmentation.

Keywords: Semantic segmentation; Active learning; Reinforcement learning

1. Introduction

Semantic segmentation involves assigning a class label to each pixel within an image, effectively dividing the image into segments that carry semantic

*CORRESPONDING AUTHOR:
Samuel Cheng, School of Electrical and Computer Engineering, University of Oklahoma, Tulsa, OK, 74135, USA; Email: samuel.cheng@ou.edu

ARTICLE INFO
Received: 1 November 2023 | Revised: 25 November 2023 | Accepted: 27 November 2023 | Published Online: 4 December 2023
DOI: https://doi.org/10.30564/jeis.v5i2.6063

CITATION
Han, D., Pham, H., Cheng, S., 2023. Enhancing Semantic Segmentation through Reinforced Active Learning: Combating Dataset Imbalances and Bolstering Annotation Efficiency. Journal of Electronic & Information Systems. 5(2): 45-60. DOI: https://doi.org/10.30564/jeis.v5i2.6063

meaning. Unlike image classification, which assigns a single class label to the entire image, semantic segmentation is a more granular task, amounting to pixel-level classification [1]. Over the past few years, the computer vision community has heavily relied on effective deep neural networks (DNNs) designed for semantic segmentation, as evidenced by recent research [2-11]. These efficient DNNs are characterized by their low computational demands and quick inference times [12], and their widespread adoption has significantly influenced applications in various fields such as autonomous driving [13,14], semantic segmentation enables precise scene understanding, allowing the vehicle to identify and differentiate between various objects on the road, such as pedestrians, vehicles, traffic signs, and obstacles. This technology aids in real-time decision-making, helping the vehicle navigate complex environments and ensure the safety of passengers and pedestrians; robot manipulation [15,16], for robots to interact intelligently with their environment, they require a comprehensive understanding of the objects and structures in their surroundings. Semantic segmentation facilitates this by enabling robots to identify and differentiate between different objects and their corresponding spatial relationships. This capability is crucial for tasks such as object manipulation, navigation in dynamic environments, and human-robot collaboration, enhancing the overall efficiency and safety of robotic systems; and biomedical image analysis [17,18], this technology assists healthcare professionals in diagnosing diseases, monitoring the progression of conditions, and planning effective treatment strategies. By providing detailed insights into complex biological structures, semantic segmentation contributes to advancements in medical research, patient care, and disease management. where advanced computer vision systems are paramount. For these models to operate effectively, however, they typically rely on a substantial volume of pixel-level annotations, a process that often necessitates expensive human labor.

Semantic segmentation datasets, with their pixel-wise annotations for each image, have been instrumental in advancing computer vision tasks. However, they are not without their limitations. Here are some of the key limitations associated with semantic segmentation datasets: 1) Extensive pixel-level annotations. Semantic segmentation models often require a large volume of accurately labeled training data, where each pixel in the image is assigned a corresponding class label. This process demands meticulous and precise annotations, which can be time-consuming and resource-intensive. Obtaining such detailed annotations for diverse datasets can be challenging, particularly for complex scenes with numerous objects and intricate boundaries. 2) Labor-intensive annotation process. The pixel-wise annotation process for semantic segmentation datasets is a labor-intensive task, often requiring significant human effort and time [19]. This manual labeling process is labor-intensive, time-consuming, and can be prone to human error, especially when dealing with large datasets. As a result, the creation of high-quality annotated datasets requires significant human resources and can be a bottleneck in the development of accurate and robust semantic segmentation models. 3) Data imbalance and variability. Semantic segmentation datasets may suffer from data imbalance and variability in the distribution of classes within the dataset. Certain classes may be underrepresented, leading to biased model predictions and reduced performance in specific classes. Handling such data imbalance and variability is crucial to ensure that the model can generalize effectively across different scenarios and accurately segment diverse objects in various contexts. 4) Generalization and robustness. Semantic segmentation models must be capable of generalizing well to unseen data and diverse environments. Achieving robust performance across different lighting conditions, viewpoints, and environmental changes remains a significant challenge. Ensuring that the model can accurately segment objects in various real-world scenarios is essential for its practical deployment in applications such as autonomous driving, robotics, and biomedical image analysis.

This aspect gains prominence during the process of collecting annotated data under human supervi-

sion for the creation of either a novel dataset or the supplementation of an existing one. Mitigating the challenges entails the systematic and efficient selection of image regions warranting annotation. Active learning (AL) represents a well-established research discipline explicitly focused on this area. Its primary objective is the identification of the most informative samples for annotation, with the overarching goal of enhancing the performance of learning algorithms with a minimized data requirement, in contrast to a non-selective approach where the entire dataset undergoes indiscriminate labeling. Active learning methodologies can be broadly categorized into two main groups: (i) methodologies that integrate various manually crafted active learning strategies [20-22], and (ii) data-centric active learning approaches [23-25]. Notwithstanding the heightened cost and time associated with acquiring labels for semantic segmentation in comparison to image classification, the realm of active learning for semantic segmentation has garnered relatively less attention [26-28], primarily emphasizing the development of manually engineered strategies.

How can reinforced active learning be effectively employed to enhance semantic segmentation, specifically addressing challenges posed by dataset imbalances and improving annotation efficiency? The latest active learning techniques leveraging reinforcement learning primarily concentrate on annotating one sample at each step [29-31], progressing until a predetermined label budget is fulfilled. Inspired by the AL-RL model by Casanova et al. [32], the proposed approach expedites the annotation process by selectively choosing informative and representative images to accelerate model learning. Additionally, we tackle the issue of imbalanced datasets. For instance, in clinical contexts, biases related to age and gender can arise due to constraints on the diversity of medical image contributors. In natural images, certain categories may be significantly more abundant than others, potentially skewing the model's performance towards the most frequently represented category. We investigate strategies to mitigate these biases with the aim of enhancing efficiency and accuracy in semantic segmentation analysis.

Furthermore, we conduct an in-depth exploration of various Reinforced Active Learning methodologies for image segmentation to optimize the precision and efficiency of segmentation tasks across diverse domains. To achieve this, we implement a robust framework that integrates various Reinforcement Learning (RL) techniques, including Dueling Deep Q-Networks (DQN) [33], Prioritized Experience Replay [34], Noisy Networks [35], Emphasizing Recent Experience [36], Soft Update Target Network [37], and Adaptive Epsilon Greedy [38]. We test the proposed method in the CamVid [39] dataset. Our results illustrate both improvements and limitations associated with various approaches in terms of overall accuracy and efficiency in image segmentation tasks.

2. Related work

Active learning serves as a dedicated methodology focused on optimizing performance gains with a minimal number of labeled samples. Its primary goal is to identify the most informative samples from the unlabeled dataset, subsequently presented to an oracle, such as a human annotator, for labeling. This process effectively minimizes labeling costs while ensuring sustained performance. Active learning approaches can be classified into membership query synthesis [40,41], stream-based selective sampling [42,43], and pool-based [44] strategies, each derived from diverse application scenarios [45]. Certain methodologies amalgamate various techniques to enhance the overall performance of active learning. For example, Shui et al. [46] take into account the diversity and uncertainty of query samples, and try to discover a balance between those two approaches. Further investigation into traditional query strategies is undertaken [47]. Despite the considerable volume of existing research on active learning, it continues to grapple with the challenge of extending its applicability to high-dimensional data, such as images, text, and videos [48]. Consequently, the majority of active learning studies tend to focus on low-dimensional problems [49]. Several methodologies integrate various techniques to enhance the performance of

artificial intelligence, such as leveraging the exploration-exploitation trade-off [50], on a bandit formulation [21] and reinforcement learning [51].

In recent times, there has been a growing interest in reinforcement learning as an approach to acquiring a labeling policy that directly optimizes the performance of the active learning algorithm. For example, Dhiman et al. [29] proposed an automated annotation model for Multimedia Streaming Applications (MAS) to address the existing challenges of slow speeds and inefficiencies in accessing multimedia content. By leveraging Multi-modal Active Learning (MAL) and Convolutional Recurrent Neural Network (CRNN) in tandem with Deep Reinforcement Learning (DRL), the model demonstrates superior retrieval accuracy and performance metrics. Gong et al. [52] proposed Meta Agent Teaming Active Learning (MATAL) framework that effectively minimizes the laborious efforts involved in pose annotations. Sadigh et al. [53] present an active learning method for Inverse Reinforcement Learning (IRL) that relies on human-provided preferences between two sample trajectories. In a similar vein, Kunapuli et al. [54] incorporate human expert information through preference elicitation for actions in a designated state. Ezzeddine et al. [55] integrate feedback from a human trainer, particularly in cases where the provided demonstrations are less than optimal. Liu et al. [56] utilize expert knowledge derived from oracle policies to develop a labeling policy. In contrast, Pang et al. [57] employ policy gradient methods to acquire knowledge for the function. In an alternative strategy, certain techniques aggregate all labeled data in a single comprehensive step. Contardo et al. [58] employ a bi-directional RNN to select all samples simultaneously, particularly for the task of one-shot learning. Meanwhile, Sener et al. [59] suggest choosing a batch of representative samples that maximize coverage across the entire unlabeled set.

Recent active learning work has also looked at semantic segmentation [60]. Uncertainty-driven active learning identifies data samples with elevated aleatoric uncertainty. Entropy [61], which estimates uncertainty, serves as a commonly employed baseline in active learning selection. This function calculates per-pixel entropy for the predicted output and utilizes the averaged entropy as the final score. BALD [62] frequently serves as a baseline in previous studies. It is applied in segmentation by integrating dropout layers into the decoder module of the segmentation model and subsequently computing pixel-wise mutual information through multiple forwards passes. Kampffmeyer et al. [63] strive to optimize the average standard deviation of the predicted probabilities. Jain et al. [64] integrate metrics, defined by manually engineered heuristics, to promote the diversity and representativeness of labeled samples. Certain methodologies leverage unsupervised super pixel-based over segmentation [65,66], relying heavily on the precision of the super-pixel segmentation. Others concentrate on foreground-background segmentation of biomedical images [67,68], employing similarly crafted heuristics. Golestaneh et al. [69] focus on self-consistency that uses simple transformations should not change the observation in active learning for semantic segmentation. Mackowiak et al. [70] concentrate on cost-effective strategies, emphasizing that the labeling cost for an image is not uniformly treated across all images.

The advent of DQN marked a significant milestone; however, numerous constraints associated with this algorithm have surfaced, leading to the proposal of various extensions. Double DQN [71] mitigates the overestimation bias of Q-learning [72] by separating the selection and evaluation of the bootstrap action. Prioritized experience replay [34] enhances data efficiency by prioritizing more frequent replay of informative transitions. The dueling network architecture [33] aids in action generalization by independently representing state values and action advantages. Learning from multi-step bootstrap targets, as seen in A3C [73], adjusts the bias-variance trade-off and accelerates the propagation of newly observed rewards to earlier visited states. Noisy DQN [35] introduces stochastic network layers to facilitate exploration. To the best of our knowledge, our work is the first to examine an agent that integrates all the aforementioned components to the problem of active

learning for semantic segmentation. Emphasizing recent experience [36] typically refers to assigning greater importance to recent observations and actions when making decisions or updating the learning model. ERE is often driven by the recognition that the environment is non-stationary, implying that the optimal policy might evolve over time.

3. Methods

3.1 Active learning with reinforcement learning for semantic segmentation

Followed by Casanova et al. [32], we use their architecture for training segmentation networks. We frame the active learning problem as a Markov decision process (MDP). The proposed process entails an iterative active learning strategy for enhancing the performance of a segmentation network, denoted as f and parameterized by θ, within a limited labeled sample budget, B. At each iteration, a query network, represented by π and parameterized by φ, selectively picks K regions from the large unlabeled set, U_t. These regions are then submitted to an oracle for labeling, subsequently augmenting the labeled set, $\mathcal{L}_t$. The segmentation network f is trained using the enriched $\mathcal{L}_t$, and its performance is evaluated based on the Intersection-over-Union (IoU) metric. This iterative procedure continues until the designated budget B is attained. By strategically selecting informative regions for labeling, this process optimizes the performance of the segmentation network, thus efficiently leveraging a limited labeled dataset to achieve superior segmentation results. This data-centric approach enables the model to acquire selection strategies purely from past active learning encounters.

In the setting, we employ four distinct data partitions. For training the query network π, we designate a portion of labeled data D_T, utilizing it for multiple iterations of the active learning process to acquire an effective acquisition function that optimizes performance within a B region budget. The evaluation of the query network takes place on a separate data split D_V. Moreover, we utilize a distinct subset D_R to generate the reward signal, which involves evaluating the segmentation network's performance on this set. Additionally, the set D_S (with D_S being not larger than D_T) is utilized for constructing the representation of the current state.

A Markov Decision Process (MDP) is defined as a tuple (S, A, r, T, γ) where S stands for a set of states; A for actions, the composed action, consisting of K sub-actions, relies on the segmentation network, along with the labeled and unlabeled sets. Each sub-action entails requesting the labeling of a particular region; r, $S \times A \rightarrow R$, for the function based on improvement in mean IoU per class of taking an action in a state; T, $S \times A \times S \rightarrow R$, for the state-transition function; and r, for the discount factor implying that a reward obtained in the future is worth a smaller amount than an immediate reward. **Figure 1** describes this training workflow. In our approach, the episode concludes upon reaching the designated budget B for labeled regions. Post-episode termination, we reset the weights of the segmentation network, denoted as f, to the initial weights θ_0, and initiate a new episode. The training process for the query policy π involves the simulation of multiple episodes, with weight updates occurring at each time step through the sampling of transitions $\{(s_t, a_t, r_{t+1}, s_{t+1})\}$ from the experience replay buffer ε.

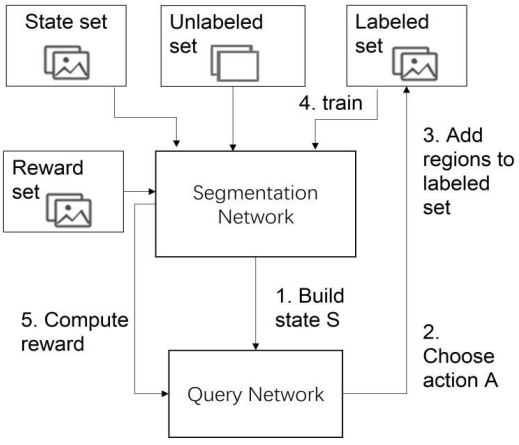

Figure 1. The overall workflow of active learning with reinforcement learning in semantic segmentation.

3.2 Extensions to DQN

The evolution of Deep Q-Networks (DQN) has

given rise to several significant extensions, each addressing specific limitations and enhancing the algorithm's overall performance. Individually, each of these algorithms leads to significant performance enhancements. Given that they tackle fundamentally different issues and share a common framework, there is a plausible opportunity for their integration. We suggest six extensions, each designed to overcome a specific limitation, contributing to an overall improvement in performance. To maintain a manageable selection size, we have chosen extensions that address distinct concerns.

Double deep Q-Learning

Following the prior work [32], we set double DQN as our baseline architecture. One issue with the DQN algorithm is that it tends to overestimate the true rewards, leading to inflated Q-values. To address this, the Double DQN algorithm [71] introduces a modification to the Bellman equation used in DQN. Instead of using the same equation, the action selection and action evaluation are decoupled in the following way:

$$Q(s,a;\theta) = r + \gamma Q\left(s', argmax_{a'} Q\left(s', a'; \theta\right); \theta'\right) \quad (1)$$

Here, the main neural network, θ, determines the best next action, a', while the target network is used to evaluate this action and compute its Q-value. This simple change has been shown to reduce over-estimations and lead to better final policies.

Dueling deep Q-Learning

The Dueling DQN algorithm introduced by Wang et al. [33] seeks to improve upon traditional DQN by decomposing the Q-values into two separate components: the value function, $V(s)$, and the advantage function, A(s, a). The value function represents the expected reward for a given state, s, while the advantage function reflects the relative advantage of taking a particular action, a, compared to other actions. By combining these two functions, it is possible to compute the full Q-values for each state-action pair.

To implement this decomposition, the Dueling DQN algorithm introduces a neural network with two separate output layers, one for the value function and one for the advantage function. These outputs are then combined to produce the final Q-values. This modification allows the network to learn more efficiently in situations where the exact values of individual actions are not as important, as it can focus on learning the value function for the state.

Prioritized experience replay

The proposition by Schaul et al. [34] in 2015 introduces a resolution termed prioritized experience replay (PER). This approach involves the utilization of an added data structure that maintains the priority of each transition. Subsequently, experiences are sampled based on their respective priorities.

$$P(i) = \frac{p_i^\alpha}{\sum_k p_k^\alpha} \quad (2)$$

The hyperparameter alpha determines the degree of sampling bias desired. The priorities correspond to the temporal difference error of the agent during its most recent training on that particular experience. This strategy enables the agent to emphasize learning from its less accurate predictions, thereby refining its weak areas and significantly improving sample efficiency. New transitions are incorporated into the replay buffer with the highest priority, introducing a bias toward recent transitions. It is essential to recognize that stochastic transitions may also receive preference, even when there is limited remaining knowledge to be gained from them.

Emphasizing recent experience

Primarily conceived to expedite the convergence speed of Soft Actor Critic (SAC) [36], this methodology can conceivably be extended to a wide array of algorithms and tasks that inherently profit from accelerated learning of recent experiences, particularly those involving multiple components. The fundamental concept entails, during the parameter update phase, sampling the initial mini batch from the entire dataset within the replay buffer. Subsequently, for each subsequent mini batch, the sampling range is gradually narrowed, enabling a more pronounced focus on recent data points. This scheme revolves around two fundamental aspects: (i) a heightened sampling frequency for more recent data, and (ii) a systematic arrangement of updates ensuring that older data does not overwrite the more recent ones. The introduction of Experience Replay Emphasis (ERE)

establishes a straightforward yet effective sampling technique that enables the agent to prioritize recent transitions without disregarding previously learned policies.

Adaptive epsilon greedy

The epsilon-greedy technique serves as a means to strike a balance between exploration and exploitation in the process of training reinforcement learning policies. For instance, when epsilon is set to 0.3, the output action is randomly chosen from the action space with a probability of 0.3, and with a probability of 0.7, the output action is selected greedily based on argmax (Q).

A refined version of the epsilon-greedy method is referred to as the Adaptive-epsilon-greedy approach [38]. In this approach, for instance, the policy is trained over N epochs/episodes, a value contingent upon the specific problem. Initially, the algorithm sets epsilon to p_{init} (e.g., $p_{\text{init}} = 0.6$), gradually reducing it to reach $\epsilon = p_{\text{end}}$ (e.g., $p_{\text{end}} = 0.1$) over a designated number of training epochs/episodes (n_{step}). Primarily, during the initial training phase, the model is granted increased exploration freedom with a higher probability (e.g., $p_{\text{init}} = 0.6$), followed by a gradual epsilon decrease at a rate r over the training epochs/episodes, adhering to the subsequent formula:

$$r = max\left(\frac{N - n_{\text{step}}}{N}, 0\right) \tag{3}$$

$$\epsilon \leftarrow (p_{\text{init}} - p_{\text{end}})r + p_{\text{end}} \tag{4}$$

This adaptable approach concludes with a notably low exploration probability, p_{end}, after n_{step}, thereby facilitating a transition towards an increased emphasis on exploitation (i.e., a greedier approach) during the latter stages of the training process. Despite this shift, a minimal exploration probability persists, ensuring the ability to explore even as the policy nears convergence.

Noisy network

Noisy networks are often utilized instead of the epsilon-greedy method to promote more effective and dynamic exploration during training. Unlike the epsilon-greedy approach, which only adjusts the exploration probability, noisy networks introduce stochasticity directly into the network's parameters, enabling a more nuanced and continuous exploration process. The Noisy Network [35] introduces a novel concept of a noisy linear layer, integrating both deterministic and noisy components.

$$y = (b + Wx) + \left(b_{\text{noisy}} \odot \epsilon^b + \left(W_{\text{noisy}} \odot \epsilon^w\right)x\right) \tag{5}$$

where ϵ^w and ϵ^b are random variables, and $\odot$ denotes the element-wise product. With time, the network can gradually disregard the noisy stream, albeit at varying rates across distinct regions of the state space, thereby enabling state-specific exploration with a form of intrinsic self-annealing. This dynamic exploration strategy allows for a more fine-grained balance between exploration and exploitation, facilitating improved learning efficiency and adaptability in complex environments.

Soft update for target network

The soft update target network is a key concept in the field of deep reinforcement learning [37]. It refers to a technique used to stabilize and improve the training of deep neural networks in reinforcement learning tasks. Unlike hard updates, which involve periodically copying the parameters of the main network to the target network, soft updates gradually blend the parameters of the target network towards those of the main network. This process helps to mitigate the issue of drastic changes in the target network, which can lead to instability during the learning process. The value of τ is used. In the paper, it proposed an algorithm called DPG. They used $\tau = 0.001$. The target network is updated as follows.

$$\theta^{target} = \theta \times \tau + \theta^{target} \times (1 - \tau) \tag{6}$$

Due to the small value of the parameter τ, the target network smoothly adjusts towards the Q-network's value. To ensure the noticeable impact of this adjustment, frequent updates are required. By employing a soft update strategy, the target network can more smoothly track the changes in the main network, enabling a more stable and effective learning process. This technique has proven to be particularly useful in complex reinforcement learning tasks where maintaining stability during the training phase is crucial for achieving optimal performance.

4. Results

This section describes the setup of our experiments, including the dataset, evaluation methods, and the baselines for comparison.

4.1 Experimental setup

Data collections

The dataset we primarily used in our experiments is the Cambridge-driving Labeled Video Database or CamVid [34] with samples shown in **Figure 2**. This public dataset comprises 360 × 480 street scene color images or frames, each annotated with ground truth semantic labels for pixels across 32 classes. The images were captured from a moving automobile using high-resolution cameras placed on the streets, allowing for the observation of various objects. In this study, our focus is on the segmentation of 11 key classes. Given the urban context, the Road, Building, and Sky classes collectively constitute most frame pixels, accounting for approximately 15.81% and 27.35%, and appearing in almost all frames. Other significant classes, such as Car and Pedestrian, are consistently present throughout the frame sequence but occupy smaller portions, approximately 3.93% and 0.64%, respectively. Additionally, our analysis includes other classes depicted in **Table 1**. The accompanying table illustrates a significant imbalance among the different classes, a challenge that we address in our study. The video sequences were shot during the daytime and at dusk, where the objects in the scene can still be recognized but appear darker than in other sequences. Daylight sequences were captured in sunny weather conditions, featuring mixed urban and residential surroundings.

For a fair comparison between different methods, the segmentation networks of all methods have been pre-trained on the GTA dataset [74], which comprises extensive synthetic images with pixel-level semantic annotations. These images are generated through the open-world video game Grand Theft Auto 5, depicting scenes from a car perspective within virtual cities designed in an American style, like our primary testing dataset introduced earlier.

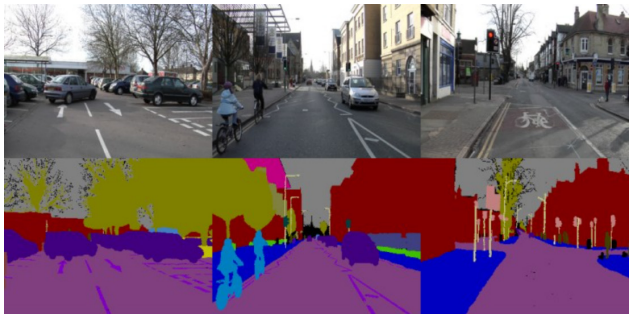

Figure 2. Labeled frames from the video at 1 Hz.

Table 1. Statistics for each class used in this study: "%" shows the ratio of pixels and "Occurrence" shows the number of occurrences over all images.

Class name	Percentage	Occurrence
Road	27.3	701
Building	22.7	687
Sky	15.8	699
Tree	10.4	636
Sidewalk	6.33	672
Car	3.4	643
Column_Pole	0.98	698
Fence	1.43	363
Pedestrian	0.64	640
Bicyclist	0.53	365
Sign_Symbol	0.12	416

Data collection instruments

The CamVid dataset was captured using a digital film camera under fixed conditions without auto zooming, focus, or adjustments during the collecting process. The camera's focus was adjusted to infinity, and both gain and shutter speed were fixed. At the outset, the aperture was widened to its maximum extent while ensuring that white objects in the scene did not become overexposed.

Data analysis

In a real-world scenario where we have unlabeled data, it's possible to involve a human annotator to label the necessary dataset based on active learning recommendations. Nevertheless, in this paper, as a proof of concept, we opted to work with fully labelled data and selectively concealed portions of it to assess the active learning algorithm's performance on the segmentation task.

The dataset we primarily used in our experiments is CamVid [39] discussed earlier. The training, val-

idation, and test sets consist of 370, 104, and 234 images, respectively. In the training set, we used 100 labelled images for building D_T to train the DQN network for several episodes and learn a good acquisition function that maximizes performance with a budget of B regions. A set of 10 images or D_S is used to construct the state representation. For the baseline evaluation set D_V, we utilized 260 images. D_S has a similar class distribution to D_T to represent it. The original validation set was used to build D_R. The dataset's test set was employed to train the model to obtain the final segmentation results. Each image was divided into K regions (in this case, K = 24) with a resolution of 80 × 90. For implementation, we executed 5 different runs with random seeds to calculate the mean and standard deviation. Horizontal flips and random crops of 224 × 224 were applied for data augmentation.

Evaluation

We trained the active learning agent on DT with approximately 0.5 k regions to learn the selection of regions that would improve performance in data-scarce scenarios. Subsequently, we evaluated the model using DV, where the model could access an increasing number of images within different fixed budgets. Once the fixed budget was reached, the segmentation network was trained with LT until it met the early stopping condition in DR. The segmentation network f for all algorithms was pre-trained with the GTA dataset [74], a synthetic dataset, and DT. Finally, we measured the segmentation model's performance on the CamVid test set using the Intersection over Union (IoU) score.

Hardware usage

The models were trained using a single NVIDIA RTX A5000 GPU with 24 GB of VRAM. Training the active learning agents took approximately 18 hours for 5 runs, and training the segmentation models to test the active learning algorithm required a total of 8 hours for 5 runs at each of the 6 budgets.

4.2 Experiment results

In **Figures 3 and 4**, we compare various methods across increasing budgets of labeled 128 × 128 pixel regions. The x-axis, labeled as "Budget", represents the additional number of regions in thousands and the percentage of utilized unlabeled data. The plots include means and standard deviations of 5 runs. The segmentation network utilized in these methods has been pre-trained with the GTA dataset and part of their respective target datasets. The dashed line represents 96% of the best performance (Intersection Over Union) achieved by the segmentation network trained with all available labels. Given that the performance of the preceding work [32] surpasses that of the other baseline models, we will adopt it as the new baseline model for comparisons with other methods.

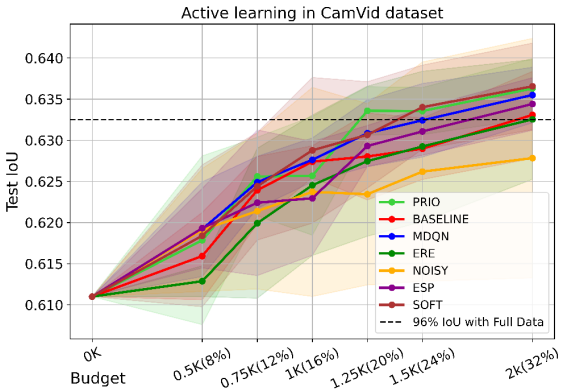

Figure 3. Comparisons of various active learning methods.

In detail, **Figure 3** illustrates the performance of various methods, including Prioritized Experience Replay (PRIO) [34], the reproduced DQN baseline (BASELINE) [32], Dueling Deep Q-network (MDQN) [33], Emphasizing Recent Experiences (ERE) [36], and Noisy Network (NOISY) [35], Adaptive Epsilon Greedy (ESP) [38], Soft Update for Target Network [37]. It's important to note that at 1.5 k regions, the performance of some methods exceeds 96% of the maximum achieved with fully supervised training (having access to all labels). In these experiments, the NOISY model performs the worst, suggesting that acquiring new labels does not provide significant additional information to the model. PRIO and SOFT outperform the other methods, including the baseline, in all budget scenarios, except for the 1K case for the PRIO method. They achieve this without overfitting the training model,

while the other methods yield similar results. This suggests that effective active learning, through selective labeling or additional information, can assist the segmentation model in avoiding local minima and achieving better performance.

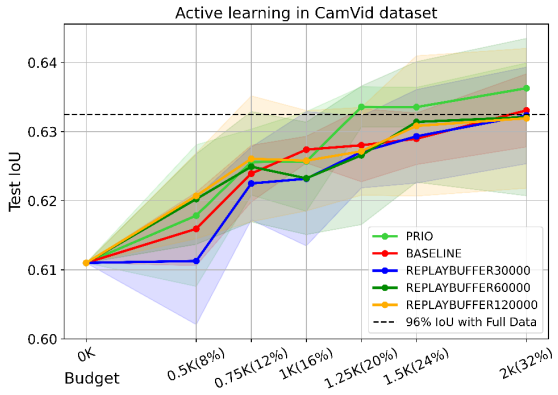

Figure 4. Compare the PRIO method with varying replay buffer sizes.

In **Figure 4**, a comparison is made between the baseline and PRIOR methods, considering different replay buffer pool sizes: 600, 30,000, 60,000, and 120,000. Performance remains relatively stable for both 60,000 and 120,000. Interestingly, PRIOR, despite having a smaller replay buffer (around 600 compared to 30,000, 60,000, and 120,000), outperforms the others by a significant margin.

4.3 Discussion

Implications and suggestions

In this section, we examine the primary findings from the experiments. As the experiment results show, implementing a soft target network update can improve performance. This is due to the smoother tracking of changes in the main network by the target network through the use of soft updates. Consequently, a more stable learning process is achieved, and the algorithm is able to converge to a better policy, resulting in improved performance reflected in better results and more reliable Q-value estimations. The Dueling DQN algorithm improves upon earlier models by decoupling value and advantage functions in Q-value estimation. This allows for better recognition of action importance in varying states, thereby enhancing learning and generalization. The resulting architecture enables more effective comprehension of state value and action advantage, leading to improved action selection and overall performance. Moreover, this division reduces the variability in learned action values, stabilizes learning, and provides more precise estimates. This solves the problems of overestimation or underestimation of Q-values. Prioritized Experience Replay (PER) improves reinforcement learning by enhancing sample efficiency, stabilizing the learning process, and promoting effective exploration of the state space. PER prioritizes experiences based on higher probabilities for transitions with greater TD errors, accelerating convergence and fostering efficient learning. Emphasizing rare events also aids agents in handling critical scenarios adeptly. The learning process stability is ensured by policy updates that efficiently lead to rapid learning and enhanced convergence. Emphasizing transitions with high learning potential aids the thorough exploration of the state space, resulting in improved overall performance and decision-making by the agent. PER usage reduces bias from uniform sampling and mitigates high variance issues, resulting in more accurate and stable Q-value updates. This enhances the learning process and improves performance in various reinforcement learning tasks.

Our experiments showed that certain techniques, like incorporating noisy networks to encourage diverse segmentation strategies, had a negative impact on segmentation performance by introducing instability in the learning process, resulting in decreased accuracy in certain scenarios. In intricate settings with sparse rewards or high-dimensional state spaces, challenges arise where adjusting the exploration rate alone may prove ineffective. Poor adjustment of the exploration rate adaptation and disregard for specific learning dynamics can disturb the balance between exploration and exploitation, despite the use of adaptable epsilon-greedy approaches, creating difficulties in obtaining the ideal exploration-exploitation equilibrium, especially in some settings. Overemphasizing recent experiences in a DQN can hinder reinforcement learning performance by re-

ducing sample efficiency, impeding generalization, introducing increased variance, and destabilizing the learning process. It also limits exploration across the state space, restricting the discovery of critical, infrequently encountered states and thereby compromising the agent's convergence to an optimal policy. Thus, in order to improve performance, it is crucial to achieve a balance between prioritizing recent experiences and maintaining a varied set of samples that support efficient learning and exploration across the entire state space.

Limitations and future work

We have illustrated the successful integration of various enhancements into the DQN, enhancing the semantic segmentation model to achieve state-of-the-art performance. Furthermore, our findings indicate that certain components within the integrated algorithm yield distinct performance advantages. While numerous algorithmic components couldn't be incorporated in this study, they stand as promising candidates for future experiments involving integrated agents. Below, we discuss several of these potential candidates.

Policy-based methods directly parameterize the policy, allowing for more flexible and complex policies compared to value-based approaches like DQN. Investigating the application of policy-based methods to active learning in semantic segmentation could provide valuable insights into optimizing decision-making strategies. Actor-critic methods combine the strengths of both policy and value-based approaches by maintaining separate networks for policy and value estimation. Exploring the integration of actor-critic methods in our active learning framework may offer advantages in terms of stability and efficiency. N-step methods extend the traditional DQN by incorporating multiple consecutive states and actions. Evaluating the impact of N-step methods on active learning performance in semantic segmentation could enhance our understanding of the temporal dynamics involved. Distributional RL models the distribution of returns rather than focusing solely on expected values. Introducing distributional RL techniques into our framework may contribute to a more nuanced understanding of uncertainty and risk management in the active learning process. Imitation learning leverages expert demonstrations to guide the learning process. Integrating imitation learning into active learning for semantic segmentation could offer a valuable mechanism for initializing the model and accelerating the learning curve.

The exploration of these alternative RL techniques represents a promising direction for future research. Investigating how those methods can be tailored to the specific challenges of active learning in semantic segmentation is essential. The strengths of different RL paradigms could be harnessed by exploring the combination of these techniques in hybrid models or ensembles. Moreover, the transferability and generalization of learned policies across diverse datasets and domains require attention in future investigations.

5. Conclusions

In conclusion, our study provides a comprehensive comparison of different DQN extensions designed to improve active learning in semantic segmentation through reinforcement learning. Our primary objective is to mitigate the labour-intensive task of obtaining pixel-wise labels with human intervention. Our results demonstrate that the NOISY model performs the worst, showing rapid overfitting, therefore implying that acquiring new labels does not significantly enhance the model's information. Notably, prioritized experience replay and soft update outperform all other methods, including the baseline, in all budget scenarios. Importantly, these methods achieve superior performance without overfitting, while the other techniques yield similar results. Additionally, the comparison of the baseline and PER methods, considering different replay buffer pool sizes, indicates that PRIOR outperforms others despite having a smaller replay buffer. This emphasizes the importance of utilizing information effectively to improve the segmentation process. This highlights the effectiveness of selective labelling or including additional information to help the segmentation model avoid local minimum and achieve better per-

formance. These findings highlight the prospect of utilizing sophisticated DQN extensions to enhance active learning in semantic segmentation, resulting in streamlined label acquisition and improved model performance.

Author Contributions

Conceptualization, D.H. and S.C.; methodology, D.H. and S.C.; investigation, D.H.; validation, D.H. and P.H.; data curation, D.H. and P.H.; writing, D.H. and P.H.; review and editing, S.C.; supervision, S.C.

Conflict of Interest

There is no conflict of interest.

Funding

This work is partially supported by the Vice President for Research and Partnerships of the University of Oklahoma, the Data Institute for Societal Challenges, and the Stephenson Cancer Center through DISC/SCC Seed Grant Award.

References

[1] Szeliski, R., 2022. Computer vision: Algorithms and applications. Springer Nature: Berlin.

[2] Li, H., Xiong, P., Fan, H., et al., 2019. DFANet: Deep Feature Aggregation for Real-Time Semantic Segmentation [Internet]. Available from: https://openaccess.thecvf.com/content_CVPR_2019/papers/Li_DFANet_Deep_Feature_Aggregation_for_Real-Time_Semantic_Segmentation_CVPR_2019_paper.pdf

[3] Liu, M., Yin, H., 2019. Feature pyramid encoding network for real-time semantic segmentation. arXiv preprint arXiv:1909.08599.
DOI: https://doi.org/10.48550/arXiv.1909.08599

[4] Li, X., You, A., Zhu, Z., et al. (editors), 2020. Semantic flow for fast and accurate scene parsing. Computer Vision-ECCV 2020: 16th European Conference; 2020 Aug 23-38; Glasgow, UK. Cham: Springer International Publishing. p. 775-793.
DOI: https://doi.org/10.1007/978-3-030-58452-8_45

[5] Yang, X., Wu, Y., Zhao, J., et al., 2020. Dense Dual-Path Network for Real-time Semantic Segmentation [Internet]. Available from: https://openaccess.thecvf.com/content/ACCV2020/papers/Yang_Dense_Dual-Path_Network_for_Real-time_Semantic_Segmentation_ACCV_2020_paper.pdf

[6] Orsic, M., Kreso, I., Bevandic, P., et al., 2019. In Defense of Pre-Trained ImageNet Architectures for Real-Time Semantic Segmentation of Road-Driving Images [Internet]. Available from: https://openaccess.thecvf.com/content_CVPR_2019/papers/Orsic_In_Defense_of_Pre-Trained_ImageNet_Architectures_for_Real-Time_Semantic_Segmentation_CVPR_2019_paper.pdf

[7] Zhang, H., Tang, W., Na, W., et al., 2020. Implementation of generative adversarial network-CLS combined with bidirectional long short-term memory for lithium-ion battery state prediction. Journal of Energy Storage. 31, 101489.
DOI: https://doi.org/10.1016/j.est.2020.101489

[8] Zhang, H., Na, W., Kim, J. (editors), 2018. State-of-charge estimation of the lithium-ion battery using neural network based on an improved thevenin circuit model. 2018 IEEE Transportation Electrification Conference and Expo (ITEC); 2018 Jun 13-15; Long Beach, CA, USA. New York: IEEE. p. 342-346.
DOI: https://doi.org/10.1109/ITEC.2018.8450162

[9] Zhang, H., Cheng, S., El Amm, C., et al., 2023. Efficient pooling operator for 3D morphable models. IEEE Transactions on Visualization and Computer Graphics. 1-9.
DOI: https://doi.org/10.1109/TVCG.2023.3255820

[10] Han, D., Wang, S., Jiang, C., et al., 2015. Trends in biomedical informatics: Automated topic analysis of JAMIA articles. Journal of the American Medical Informatics Association. 22(6), 1153-1163.
DOI: https://doi.org/10.1093/jamia/ocv157

[11] Han, D., Mulyana, B., Stankovic, V., et al., 2023. A survey on deep reinforcement learning algorithms for robotic manipulation. Sensors. 23(7), 3762.
DOI: https://doi.org/10.3390/s23073762

[12] Sze, V., Chen, Y.H., Yang, T.J., et al., 2017. Efficient processing of deep neural networks: A tutorial and survey. Proceedings of the IEEE. 105(12), 2295-2329.
DOI: https://doi.org/10.1109/JPROC.2017.2761740

[13] Wang, W., Fu, Y., Pan, Z., et al., 2020. Real-time driving scene semantic segmentation. IEEE Access. 8, 36776-36788.
DOI: https://doi.org/10.1109/ACCESS.2020.2975640

[14] Papadeas, I., Tsochatzidis, L., Amanatiadis, A., et al., 2021. Real-time semantic image segmentation with deep learning for autonomous driving: A survey. Applied Sciences. 11(19), 8802.
DOI: https://doi.org/10.3390/app11198802

[15] Mahe, H., Marraud, D., Comport, A.I. (editors), 2019. Real-time rgb-d semantic keyframe slam based on image segmentation learning from industrial cad models. 2019 19th International Conference on Advanced Robotics (ICAR); 2019 Dec 2-6; Belo Horizonte, Brazil. New York: IEEE. p. 147-154.
DOI: https://doi.org/10.1109/ICAR46387.2019.8981549

[16] Bruce, J., Balch, T., Veloso, M. (editors), 2000. Fast and inexpensive color image segmentation for interactive robots. Proceedings. 2000 IEEE/RSJ International Conference on Intelligent Robots and Systems (IROS 2000) (Cat. No. 00CH37113); 2000 Oct 31-Nov 5; Takamatsu, Japan. New York: IEEE. p. 2061-2066.
DOI: https://doi.org/10.1109/IROS.2000.895274

[17] Du, X., Nie, Y., Wang, F., et al., 2022. AL-Net: Asymmetric lightweight network for medical image segmentation. Frontiers in Signal Processing. 2, 842925.
DOI: https://doi.org/10.3389/frsip.2022.842925

[18] Lou, A., Guan, S., Loew, M., 2023. Cfpnet-m: A light-weight encoder-decoder based network for multimodal biomedical image real-time segmentation. Computers in Biology and Medicine. 154, 106579.
DOI: https://doi.org/10.1016/j.compbiomed.2023.106579

[19] Cordts, M., Omran, M., Ramos, S., et al., 2016. The Cityscapes Dataset for Semantic Urban Scene Understanding [Internet]. Available from: https://openaccess.thecvf.com/content_cvpr_2016/papers/Cordts_The_Cityscapes_Dataset_CVPR_2016_paper.pdf

[20] Gal, Y., Islam, R., Ghahramani, Z., 2017. Deep Bayesian Active Learning with Image Data [Internet]. Available from: https://proceedings.mlr.press/v70/gal17a/gal17a.pdf

[21] Chu, H.M., Lin, H.T. (editors), 2016. Can active learning experience be transferred? 2016 IEEE 16th International Conference on Data Mining (ICDM); 2016 Dec 12-15; Barcelona, Spain. New York: IEEE. p. 841-846.
DOI: https://doi.org/10.1109/ICDM.2016.0100

[22] Hsu, W.N., Lin, H.T., 2015. Active learning by learning. Proceedings of the AAAI Conference on Artificial Intelligence. 29(1).
DOI: https://doi.org/10.1609/aaai.v29i1.9597

[23] Yoo, D., Kweon, I.S., 2019. Learning Loss for Active Learning [Internet]. Available from: https://openaccess.thecvf.com/content_CVPR_2019/papers/Yoo_Learning_Loss_for_Active_Learning_CVPR_2019_paper.pdf

[24] Lookman, T., Balachandran, P.V., Xue, D., et al., 2019. Active learning in materials science with emphasis on adaptive sampling using uncertainties for targeted design. npj Computational Materials. 5(1), 21.
DOI: https://doi.org/10.1038/s41524-019-0153-8

[25] Fasel, U., Kutz, J.N., Brunton, B.W., et al., 2022. Ensemble-SINDy: Robust sparse model discovery in the low-data, high-noise limit, with active learning and control. Proceedings of the Royal Society A. 478(2260), 20210904.
DOI: https://doi.org/10.1098/rspa.2021.0904

[26] Hu, Z., Bai, X., Zhang, R., et al., 2022. Lidal: Inter-frame uncertainty based active learning for 3d lidar semantic segmentation. European

Conference on Computer Vision. 13687, 248-265.
DOI: https://doi.org/10.1007/978-3-031-19812-0_15

[27] Lenczner, G., Chan-Hon-Tong, A., Le Saux, B., et al., 2022. Dial: Deep interactive and active learning for semantic segmentation in remote sensing. IEEE Journal of Selected Topics in Applied Earth Observations and Remote Sensing. 15, 3376-3389.
DOI: https://doi.org/10.1109/JSTARS.2022.3166551

[28] Xie, B., Yuan, L., Li, S., et al., 2022. Towards Fewer Annotations: Active Learning via Region Impurity and Prediction Uncertainty for Domain Adaptive Semantic Segmentation [Internet]. Available from: https://openaccess.thecvf.com/content/CVPR2022/papers/Xie_Towards_Fewer_Annotations_Active_Learning_via_Region_Impurity_and_Prediction_CVPR_2022_paper.pdf

[29] Dhiman, G., Kumar, A.V., Nirmalan, R., et al., 2023. Multi-modal active learning with deep reinforcement learning for target feature extraction in multi-media image processing applications. Multimedia Tools and Applications. 82(4), 5343-5367.
DOI: https://doi.org/10.1007/s11042-022-12178-7

[30] Zhou, W., Li, J., Zhang, Q., 2022. Joint communication and action learning in multi-target tracking of UAV swarms with deep reinforcement learning. Drones. 6(11), 339.
DOI: https://doi.org/10.3390/drones6110339

[31] Hu, M., Zhang, J., Matkovic, L., et al., 2023. Reinforcement learning in medical image analysis: Concepts, applications, challenges, and future directions. Journal of Applied Clinical Medical Physics. 24(2), e13898.
DOI: https://doi.org/10.1002/acm2.13898

[32] Casanova, A., Pinheiro, P.O., Rostamzadeh, N., et al., 2020. Reinforced active learning for image segmentation. arXiv preprint arXiv:2002.06583.
DOI: https://doi.org/10.48550/arXiv.2002.06583

[33] Wang, Z., Schaul, T., Hessel, M., et al., 2016. Dueling Network Architectures for Deep Reinforcement Learning [Internet]. Available from: https://proceedings.mlr.press/v48/wangf16.pdf

[34] Schaul, T., Quan, J., Antonoglou, I., et al., 2015. Prioritized experience replay. arXiv preprint arXiv:1511.05952.
DOI: https://doi.org/10.48550/arXiv.1511.05952

[35] Fortunato, M., Azar, M.G., Piot, B., et al., 2017. Noisy networks for exploration. arXiv preprint arXiv:1706.10295.
DOI: https://doi.org/10.48550/arXiv.1706.10295

[36] Wang, C., Ross, K., 2019. Boosting soft actor-critic: Emphasizing recent experience without forgetting the past. arXiv preprint arXiv:1906.04009.
DOI: https://doi.org/10.48550/arXiv.1906.04009

[37] Lillicrap, T.P., Hunt, J.J., Pritzel, A., et al., 2015. Continuous control with deep reinforcement learning. arXiv preprint arXiv:1509.02971.
DOI: https://doi.org/10.48550/arXiv.1509.02971

[38] Tokic, M., Palm, G., 2011. Value-difference based exploration: Adaptive control between epsilon-greedy and softmax. Annual conference on artificial intelligence. Springer: Berlin. pp. 335-346.
DOI: https://doi.org/10.1007/978-3-642-24455-1_33

[39] Brostow, G.J., Shotton, J., Fauqueur, J., et al. (editors), 2008. Segmentation and recognition using structure from motion point clouds. Computer Vision-ECCV 2008: 10th European Conference on Computer Vision; 2008 Oct 12-18; Marseille, France. Berlin: Springer. p. 44-57.
DOI: https://doi.org/10.1007/978-3-540-88682-2_5

[40] Angluin, D., 1988. Queries and concept learning. Machine Learning. 2, 319-342.
DOI: https://doi.org/10.1023/A:1022821128753

[41] King, R.D., Whelan, K.E., Jones, F.M., et al., 2004. Functional genomic hypothesis generation and experimentation by a robot scientist. Nature. 427(6971), 247-252.
DOI: https://doi.org/10.1038/nature02236

[42] Dagan, I., Engelson, S.P. (editors), 1995. Committee-based sampling for training probabilis-

tic classifiers. Machine Learning Proceedings 1995; 1995 Jul 9-12; Tahoe, California. p. 150-157.
DOI: https://doi.org/10.1016/B978-1-55860-377-6.50027-X

[43] Krishnamurthy, V., 2002. Algorithms for optimal scheduling and management of hidden Markov model sensors. IEEE Transactions on Signal Processing. 50(6), 1382-1397.
DOI: https://doi.org/10.1109/TSP.2002.1003062

[44] Lewis, D.D., 1995. A Sequential Algorithm for Training Text Classifiers: Corrigendum and Additional Data [Internet]. Available from: https://dl.acm.org/doi/pdf/10.1145/219587.219592

[45] Ren, P., Xiao, Y., Chang, X., et al., 2021. A survey of deep active learning. ACM Computing Surveys (CSUR). 54(9), 1-40.
DOI: https://doi.org/10.1145/3472291

[46] Shui, C., Zhou, F., Gagné, C., et al., 2020. Deep Active Learning: Unified and Principled Method for Query and Training [Internet]. Available from: https://proceedings.mlr.press/v108/shui20a/shui20a.pdf

[47] Settles, B., 2012. Active learning, volume 6 of synthesis lectures on artificial intelligence and machine learning. Morgan & Claypool.

[48] Settles, B., 2011. From Theories to Queries: Active Learning in Practice [Internet]. Available from: https://proceedings.mlr.press/v16/settles11a/settles11a.pdf

[49] Hernández-Lobato, J.M., Adams, R., 2015. Probabilistic Backpropagation for Scalable Learning of Bayesian Neural Networks [Internet]. Available from: http://proceedings.mlr.press/v37/hernandez-lobatoc15.pdf

[50] Osugi, T., Kim, D., Scott, S. (editors), 2005. Balancing exploration and exploitation: A new algorithm for active machine learning. Fifth IEEE International Conference on Data Mining (ICDM'05); 2005 Nov 27-30; Houston, TX, USA. New York: IEEE.
DOI: https://doi.org/10.1109/ICDM.2005.33

[51] Long, C., Hua, G., 2015. Multi-Class Multi-Annotator Active Learning with Robust Gaussian Process for Visual Recognition [Internet]. Available from: https://openaccess.thecvf.com/content_iccv_2015/papers/Long_Multi-Class_Multi-Annotator_Active_ICCV_2015_paper.pdf

[52] Gong, J., Fan, Z., Ke, Q., et al., 2022. Meta Agent Teaming Active Learning for Pose Estimation [Internet]. Available from: https://openaccess.thecvf.com/content/CVPR2022/papers/Gong_Meta_Agent_Teaming_Active_Learning_for_Pose_Estimation_CVPR_2022_paper.pdf

[53] Sadigh, D., Dragan, A.D., Sastry, S., et al., 2017. Active preference-based learning of reward functions. UC Berkeley: Berkeley.
DOI: https://doi.org/10.15607/rss.2017.xiii.053

[54] Kunapuli, G., Odom, P., Shavlik, J.W., et al. (editors), 2013. Guiding autonomous agents to better behaviors through human advice. 2013 IEEE 13th International Conference on Data Mining; 2013 Dec 7-10; Dallas, TX, USA. New York: IEEE. p. 409-418.
DOI: https://doi.org/10.1109/ICDM.2013.79

[55] Ezzeddine, A., Mourad, N., Araabi, B.N., et al., 2018. Combination of learning from non-optimal demonstrations and feedbacks using inverse reinforcement learning and Bayesian policy improvement. Expert Systems with Applications. 112, 331-341.
DOI: https://doi.org/10.1016/j.eswa.2018.06.035

[56] Liu, M., Buntine, W., Haffari, G. (editors), 2018. Learning how to actively learn: A deep imitation learning approach. Proceedings of the 56th Annual Meeting of the Association for Computational Linguistics (Volume 1: Long Papers); 2018 Jul 15-20; Melbourne, Australia. p. 1874-1883.
DOI: https://doi.org/10.18653/v1/P18-1174

[57] Pang, K., Dong, M., Wu, Y., et al., 2018. Meta-learning transferable active learning policies by deep reinforcement learning. arXiv preprint arXiv:1806.04798.
DOI: https://doi.org/10.48550/arXiv.1806.04798

[58] Contardo, G., Denoyer, L., Artières, T., 2017.

A meta-learning approach to one-step active learning. arXiv preprint arXiv:1706.08334.
DOI: https://doi.org/10.48550/arXiv.1706.08334

[59] Sener, O., Savarese, S., 2017. Active learning for convolutional neural networks: A core-set approach. arXiv preprint arXiv:1708.00489.
DOI: https://doi.org/10.48550/arXiv.1708.00489

[60] Mittal, S., Niemeijer, J., Schäfer, J.P., et al., 2023. Revisiting deep active learning for semantic segmentation. arXiv preprint arXiv:2302.04075.
DOI: https://doi.org/10.48550/arXiv.2302.04075

[61] Shannon, C.E., 1948. A mathematical theory of communication. The Bell System Technical Journal. 27(3), 379-423.
DOI: https://doi.org/10.1002/j.1538-7305.1948.tb01338.x

[62] Houlsby, N., Huszár, F., Ghahramani, Z., et al., 2011. Bayesian active learning for classification and preference learning. arXiv preprint arXiv:1112.5745.
DOI: https://doi.org/10.48550/arXiv.1112.5745

[63] Kampffmeyer, M., Salberg, A.B., Jenssen, R., 2016. Semantic Segmentation of Small Objects and Modeling of Uncertainty in Urban Remote Sensing Images Using Deep Convolutional Neural Networks [Internet]. Available from: https://www.cv-foundation.org//openaccess/content_cvpr_2016_workshops/w19/papers/Kampffmeyer_Semantic_Segmentation_of_CVPR_2016_paper.pdf

[64] Jain, S.D., Grauman, K., 2016. Active Image Segmentation Propagation [Internet]. Available from: https://openaccess.thecvf.com/content_cvpr_2016/papers/Jain_Active_Image_Segmentation_CVPR_2016_paper.pdf

[65] Vezhnevets, A., Buhmann, J.M., Ferrari, V. (editors), 2012. Active learning for semantic segmentation with expected change. 2012 IEEE Conference on Computer Vision and Pattern Recognition; 2012 Jun 16-21; Providence, RI, USA. New York: IEEE. p. 3162-3169.
DOI: https://doi.org/10.1109/CVPR.2012.6248050

[66] Konyushkova, K., Sznitman, R., Fua, P., 2015. Introducing Geometry in Active Learning for Image Segmentation [Internet]. Available from: https://openaccess.thecvf.com/content_iccv_2015/papers/Konyushkova_Introducing_Geometry_in_ICCV_2015_paper.pdf

[67] Aklilu, J., Yeung, S., 2022. ALGES: Active Learning with Gradient Embeddings for Semantic Segmentation of Laparoscopic Surgical Images [Internet]. Available from: https://proceedings.mlr.press/v182/aklilu22a

[68] Shu, X., Yang, Y., Xie, R., et al., 2022. ALS: Active learning-based image segmentation model for skin lesion.
DOI: http://dx.doi.org/10.2139/ssrn.4141765

[69] Golestaneh, S.A., Kitani, K.M., 2020. Importance of self-consistency in active learning for semantic segmentation. arXiv preprint arXiv:2008.01860.
DOI: https://doi.org/10.48550/arXiv.2008.01860

[70] Mackowiak, R., Lenz, P., Ghori, O., et al., 2018. Cereals-cost-effective region-based active learning for semantic segmentation. arXiv preprint arXiv:1810.09726.
DOI: https://doi.org/10.48550/arXiv.1810.09726

[71] Van Hasselt, H., Guez, A., Silver, D., 2016. Deep reinforcement learning with double q-learning. Proceedings of the AAAI Conference on Artificial Intelligence. 30(1).
DOI: https://doi.org/10.1609/aaai.v30i1.10295

[72] Hasselt, H., 2010. Double Q-learning. Advances in Neural Information Processing Systems. 23, 2613-2621.

[73] Babaeizadeh, M., Frosio, I., Tyree, S., et al., 2016. Reinforcement learning through asynchronous advantage actor-critic on a gpu. arXiv preprint arXiv:1611.06256.
DOI: https://doi.org/10.48550/arXiv.1611.06256

[74] Richter, S.R., Vineet, V., Roth, S., et al. (editors), 2016. Playing for data: Ground truth from computer games. Computer Vision-ECCV 2016: 14th European Conference; 2016 Oct 11-14; Amsterdam, The Netherlands. Cham: Springer International Publishing. p. 102-118.
DOI: https://doi.org/10.1007/978-3-319-46475-6_7

BILINGUAL PUBLISHING GROUP

Journal of Electronic & Information Systems
https://journals.bilpubgroup.com/index.php/jeis

ARTICLE

Development of Technology and Equipment for Non-destructive Testing of Defects in Sewing Mandrels of a Three-roll Screw Mill 30-80

Shatalov Roman Lvovich [*], ***Zagoskin Egor Evgenievich***

Moscow Polytechnic University, Moscow, 115280, Russian Federation

ABSTRACT

The conditions of heating and cooling of piercing mandrels made of 4X5MFS steel of a three-roll screw mill 30-80 in the production of a closed cavity of steel vessels of small volume are determined. It is established that multiple cycles of heating up to 600 °C and cooling with water up to 80 °C for about 7 seconds/1 cycle lead to the formation of ridges, shells and cracks on the surface and in the volume of the tool. The loss of structural strength of the material leads to the breakdown of the mandrel during the stitching process. The technique and equipment of magnetic powder control have been developed to establish the dynamics of the growth of internal and external defects of mandrels. An equation is obtained that allows determining the increase in the number of defects in the sewing tool of a screw rolling mill. The technology of non-destructive testing made it possible to develop a rational plan for replacing the sewing mandrels, which allows for predicting the appearance of defects leading to a complex breakdown of the deforming tool at the NPO Pribor machine-building enterprise.

Keywords: Screw rolling mill 30-80; Piercing mandrel made of 4X5MFS steel; Vessel made of 50 steel; Temperature; Crack; Magnetic powder control of hidden defects

1. Introduction

Automation of rolling production in mechanical engineering and metallurgy makes it possible to ensure high quality and low cost of flat, round and shaped rolled products [1,2]. One of the most popular types of rolled products for quality control today is steel vessels of the responsible purpose of small internal volume. That is why for the hot production of semi-finished products, lines consisting of screw

*CORRESPONDING AUTHOR:
Shatalov Roman Lvovich, Moscow Polytechnic University, Moscow, 115280, Russian Federation; Email: mmomd@mail.ru

ARTICLE INFO
Received: 7 October 2023 | Revised: 4 November 2023 | Accepted: 6 December 2023 | Published Online: 12 December 2023
DOI: https://doi.org/10.30564/jeis.v5i2.6000

CITATION
Lvovich, S.R., Evgenievich, Z.E., 2023. Development of Technology and Equipment for Non-destructive Testing of Defects in Sewing Mandrels of a Three-roll Screw Mill 30-80. Journal of Electronic & Information Systems. 5(2): 61-66. DOI: https://doi.org/10.30564/jeis.v5i2.6000

rolling mills with a sewing mandrel installed along the axis are increasingly used [3-5].

The technology provides for significant heating temperatures of the initial bars-blanks to ensure the continuity of the process of screw rolling, stitching and final heat treatment of products. The high temperature of about 2/3 of the melting makes it possible to ensure the high plasticity of the deformed material [5,6].

The heating of semi-finished products affects the deforming tool by heat transfer of the contacting surfaces [7,8]. The outer surface of the heated metal comes into contact with massive rolling rolls, which are continuously cooled by water. For this reason, their heating rarely exceeds critical values that reduce mechanical properties and lead to the formation of thermal stresses and defects on the surface and in the volume of the rolls [9,10]. The inner surface of a small volume vessel is formed by a mandrel with a low mass, without the possibility of cooling during flashing [11-13]. The time of the piercing cycle and the subsequent extraction of the mandrel from the vessel cavity is not infrequently sufficient to warm up the material to the temperature of the beginning of phase rearrangements [14]. Intensive cooling with water allows us to exclude the influence of temperature on the mandrel at the moment of inactivity. However, in this case, there is a risk of the formation of thermal stresses due to the reverse rearrangement of the crystal lattice leading to the formation of cracks in the volume of the tool [15,16]. Multiple cycles of intensive heating and cooling increase the risk of tool breakage and failure of the process line [17,18]. Therefore, this work was aimed at developing technology and equipment for non-destructive testing of unacceptable defects in sewing mandrels.

The purpose of the work was the development of technology and equipment for non-destructive testing of defects in sewing mandrels of a three-roll screw mill 30-80.

2. The methodology of the experiment

The experiment was carried out during the hot production of vessels made of steel 50 on the production line of the BF JSC NPO Pribor, which includes heating equipment, a three-roll screw mill 30-80 with a rotating mandrel installed along the axis with the possibility of moving along the axis of the firmware. The vessel was extracted with a "P" shaped stop. The initial rod-blank had dimensions of a length of 70 mm diameter of 40 mm. The rolling speed was 1.2 m/s. The rhythm of rolling and stitching, including the extraction of the vessel from the mandrel, is about 7 seconds. The deformed vessel was diverted along the stream and fell into the quenching tank. **Figure 1** shows the main line of the screw rolling mill 30-80.

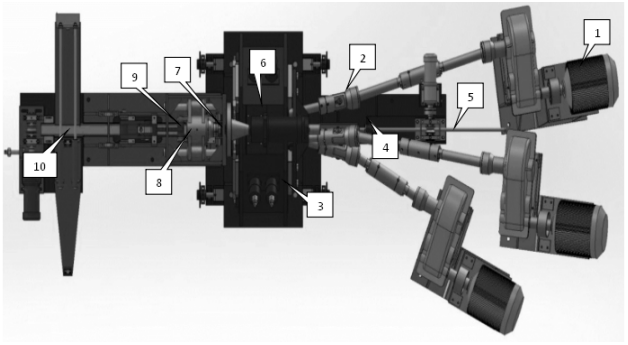

Figure 1. The main line of the screw rolling mill is 30-80.

The rolling mill line consisted of 1—asynchronous motor with a power of 50 kW each with a rotation speed of 1250 revolutions per minute, 2—gimbals transmitting the moment of rotation, 3—gearboxes, 4—guide chutes, 5—pusher rod, 6—rolling cage, 7—rotating mandrel, 8—mechanism fixing the position of the mandrel relative to rolling axes, 9—stop removing the vessel from the mandrel, 10—diverting stream.

The scheme of production of steel vessels on the production line: The initial rod-billet was heated in an induction and resistance furnace to a temperature of about 1160 °C, after which it was rolled and not completely stitched with a rotating mandrel, after which it was removed with a U-shaped stop and diverted to the quenching tank along the gutter. Water cooling of the rolling rolls was carried out continuously, and the mandrels were at the time of extraction from the cavity of the vessel.

Figure 2 shows the geometric dimensions of the deforming tool and steel vessels at the outlet of the processing line.

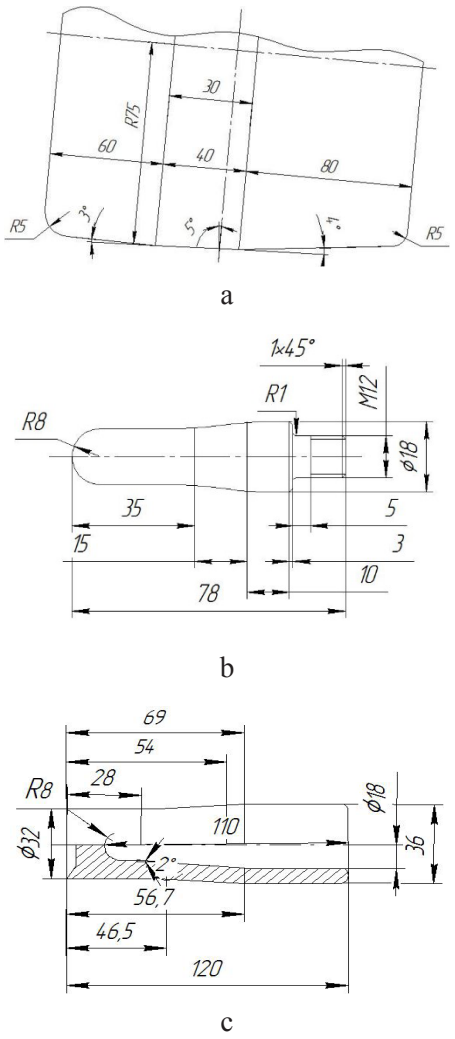

Figure 2. Geometric dimensions: a—rolling rolls, b—sewing mandrel, c—steel vessel at the outlet of the processing line.

Figure 2a shows the permissible geometric dimensions of 3 pieces of identical rolling rolls made of 35 HGSA steel that are part of the equipment of the rolling mill 30-80, **Figure 2b** shows the geometric dimensions of the working part of the piercing mandrel made of 4X5MFS steel, **Figure 2c** shows the geometric dimensions of the completed product in the form of a vessel made of ST50 material. Permissible deviations from the dimensions in **Figure 2** are not more than ± 0.1 mm.

The heating temperature of the mandrel was determined using an optical pyrometer SEM 1600 after its extraction from the vessel cavity.

The magnetic particle inspection method is a universal way of detecting defects in a deforming tool. The method is based on the occurrence of magnetic field inhomogeneity in places of discontinuity of ferromagnetic material, including steel and iron-based alloys.

The formation of internal defects of the sewing mandrel was investigated in accordance with GOST 56512-2015 "Non-destructive testing. Magnetic powder method". For this purpose, the design of the mandrel magnetization equipment was developed. **Figure 3** shows the developed magnetization setup of the sewing mandrels.

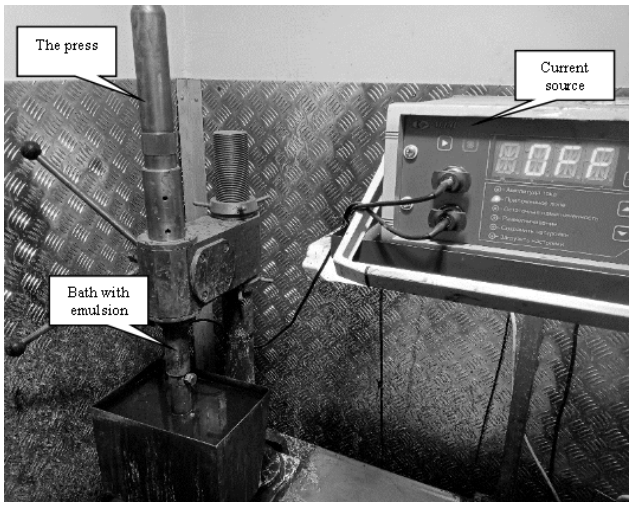

Figure 3. Installation of magnetization of sewing mandrels.

MD-I was used as a direct current source. The magnetization parameters were a current of 2 V, and a voltage of 160 A. Iron powder with a particle size not exceeding 0.001 mm was used as an indicator. The amount of powder was about 1/8 of the carrier liquid, which included: 1/3 kerosene, 1/3 soap solution, and the rest of industrial oil and 20. Defects on the surface of the mandrel were determined after the release of a batch of vessels from 250 to 1200 pieces.

The sequence of technological operations when checking the sewing mandrel for hidden defects:

- mechanical cleaning of the surface from dirt and scale layer with sandpaper grain size 80.
- preparation of the suspension consists of intensive mixing in the bathroom.
- the mandrel was installed on the lower electrode, the upper electrode was moved along the screw of the press all the way to the opposite part of the mandrel.

● magnetization took place in 2 seconds between the electrodes immersed in the suspension, under the action of the applied field, the particles moved in the area of magnetic disturbances, which indicate external and internal defects of the material.

● defects of mandrels were determined visually.

Measurements of traces of accumulations of iron powder were carried out with an electronic calliper.

3. The results of the experiment and their discussion

The heating temperature of the sewing mandrel was studied at an interval of 10 mm from the toe of the mandrel. Its bow is taken as the beginning of the countdown. **Figure 4** shows the results of measurements of the heating of the mandrel of the screw mill 30-80.

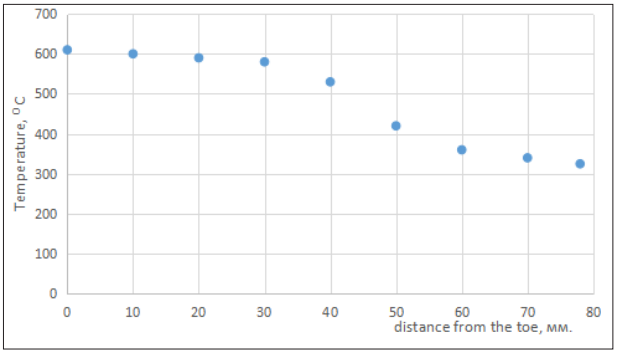

Figure 4. The results of measurements of the heating temperature of the screw machine mandrel 30-80.

Based on the temperature measurements carried out, it can be assumed that the main formation of mandrel defects will occur in the nasal region and further decrease due to the cyclical heating modes shown in **Figure 4** and cooling with water up to 80 °C.

The stitching mandrel of a three-roll screw mill 30-80 was examined after the formation of the vessel cavity. The check interval was every 250 pieces of vessels. **Figure 5** shows the development of defects in the outer surface and inner volume of the sewing mandrel after the formation of the vessel cavity.

The defects shown in **Figure 5** indicate the influence of heating cycles up to 600 °C and cooling to 80 °C at intervals of 7 seconds. After the release of 250 pieces. there are no accumulations of powder on the surface of the mandrel, its surface is smooth. After the release of 500 pieces in the transition area of the diameter from 16 to 18 mm, a longitudinal risk is visible with a length of about 9 mm and a depth of up to 1.2 mm. After the release of 750 pieces of semi-finished products, external shells with a depth of up to 1.1 mm and a diameter of about 3 mm are added to the longitudinal risks in the same area. In the nasal part, there is a pitted surface in small and frequent shells. With the release of 1000 pieces, a pronounced accumulation of magnetized powder is observed in the nasal vessels at a distance of about 10 mm, which suggests the formation of through fistulas. On the side surface of the mandrel, external defects do not grow in length, but their depth increases by about 30%. After the release of 1200 pieces, the mandrel toe collapsed at a distance of about 5 mm and a crack formed at a distance of about 20 mm. The experiment was stopped.

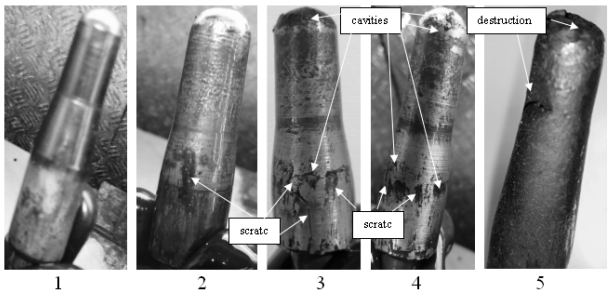

Figure 5. The development of defects in the outer surface and inner volume of the sewing mandrel after the formation of the vessel cavity: 1—250 pieces, 2—500 pieces, 3—750 pieces, 4—1000 pieces, and 5—1200 pieces.

The evolution of the growth of defects in a 4X5MFS steel sewing mandrel during the release of steel vessels, with an interval of 250 pieces. The area of defect formation was measured, as well as determined in the area of their formation at a distance of 50 mm from the toe of the mandrel. The total surface area at this length was 2811 mm^2. The sum of the outer area of powder accumulations indicating the formation of internal defects was taken into account. **Figure 6** shows the effect of the number of rolled vessels on the area of defects on the surface of the sewing mandrel.

Based on the measurements carried out, it can be concluded that with an increase in the firmware

cycles, the number of defects increases and reaches maximum values of about 12% of the studied outer surface with the release of 1000 pieces of vessels. The increase in the number of defects is subject to the developed second-order polynomial equation with a determination coefficient equal to 99%.

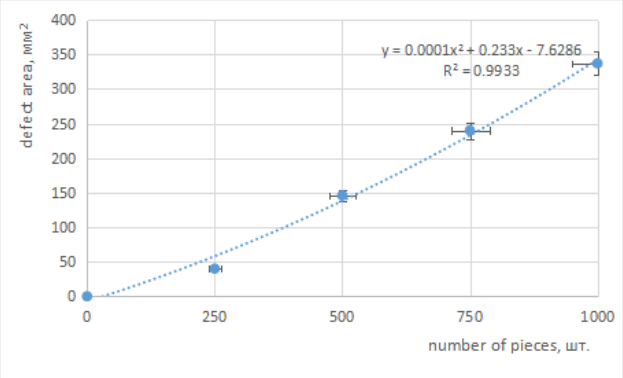

Figure 6. The effect of the number of rolled vessels on the area of defects on the surface of the sewing mandrel.

4. Conclusions

1) Testing of the design and technology of magnetic powder inspection of defects of the piercing mandrel made of 4X5MFS steel of a three-roll screw mill 30-80 was carried out. It has been established that with an increase in the number of rolled products, there is an increase in the number of external and internal defects. A rationally planned interval of replacement of mandrels for the production of steel vessels of about 1000 pieces has been determined.

2) A significant influence of the number of rolled vessels on the growth of the area of shells and cracks on the sewing mandrel has been established. It is shown that the critical area of defects at which the destruction of the deforming tool can occur is about 12% of the total area of the mandrel under study. A second-order polynomial equation is obtained that allows determining the increase in the number of defects of the mandrel surface with a determination coefficient equal to 99%.

3) The development of a system and technology for non-destructive quality control of the screw mill mandrel allowed us to develop a rational plan for replacing the piercing mandrels, which allows us to predict the appearance of defects leading to complex breakage of the deforming tool at the 30-80 mill, which ensured an increase in the efficiency of production of steel vessels at the NPO Pribor machine-building enterprise.

Author Contributions

The contribution of the authors consists of the developed methodology and equipment for checking the quality of the mandrel surface. An equation has been developed to determine the growth of defects in the mandrel surface from the number of vessel cavities formed. The technology of non-destructive testing of the presence of mandrel defects made it possible to develop a forecast for the replacement of the deforming tool.

Conflict of Interest

There is no conflict of interest.

References

[1] Muhin, U., Belskij, S., Makarov, E., et al., 2016. Simulation of accelerated strip cooling on the hot rolling mill run-out roller table. Frattura ed Integrita Strutturale. 10(37), 305-311. DOI: https://doi.org/10.3221/IGF-ESIS.37.40

[2] Belskiy, S., Mazur, I., Lezhnev, S., et al., 2016. Distribution of linear pressure of thin-sheet rolling across strip width. Journal of Chemical Technology and Metallurgy. 51(4), 371-378.

[3] Orlov, D.A., Gamin, Y.V., Goncharuk, A.V., et al., 2021. Development and investigation of piercing process using cooled guide shoes. Metallurgist. 65(3-4), 389-399. DOI: https://doi.org/10.1007/s11015-021-01168-z

[4] Лубе, И.И., Трутнев, Н.В., Тумашев, С.В., et al., 2020. Повышение стойкости оправок прошивного стана при производстве бесшовных труб из нержавеющей стали мартенситного класса марки типа 13Cr в линии ТПА. ЧЕРНАЯ МЕТАЛЛУРГИЯ. (Russian) [Mastering of production of seamless pipes of type 13 Cr martensite class stainless steel at TPA 159-426 of JSC VTZ.] Бюллетень

научно-технической и экономической информации. 76(12), 1259-1264.
DOI: https://doi.org/10.32339/0135-5910-2020-12-1259-1264

[5] Zorin, I.V., Dubtsov, Y.N., Sokolov, G.N., et al., 2017. Piercing mandrel strengthening by surfacing with nickel aluminide-based alloy. IOP Conference Series: Materials Science and Engineering. 177(1), 012101.

[6] Shatalov, R.L., Zagoskin, E.E., Medvedev, V.A., 2023. Influence of temperature unevenness on hardness, structures and defects of the stitching mandrel of a three-roll screw rolling mill 30-80. Ferrous Metals. 3, 46-52.
DOI: https://doi.org/10.17580/chm.2023.03.08

[7] Vydrin, A.V., Neroznikov, V.L., Zvonarev, D.Yu., et al., 2022. АНАЛИЗ ВЛИЯНИЯ НАСТРОЕЧНЫХ ПАРАМЕТРОВ ПРОШИВНОГО СТАНА НА ИЗМЕНЕНИЕ ДИАМЕТРА И ТОЛЩИНЫ СТЕНКИ ГИЛЬЗЫ (Russian) [Analysis of the influence of setting parameters washing machine on the change of case wall diameter and thickness]. Bulletin of the South Ural State University. Ser. Metallurgy. 22(1), 42-52.
DOI: http://dx.doi.org/10.14529/met220105

[8] Tsubouchi, K., Akiyama, M., Okuyama, T., 1997. Development and optimization of carbide-reinforced tools and application to hot rolling of stainless steel. Journal of Tribology. 119(4), 687-693.
DOI: https://doi.org/10.1115/1.2833870

[9] Shatalov, R.L., Medvedev, V.A., 2019. Effect of deformed workpiece temperature inhomogeneity on mechanical properties of thin-walled steel vessels during treatment in a rolling and pressing line. Metallurgist. 63(1-2), 176-182.
DOI: https://doi.org/10.1007/s11015-019-00807-w

[10] Shatalov, R.L., Shelest, A.E., Medvedev, V.A., 2020. Electromagnetic device for nondestructive control of the mechanical properties of thin-walled steel vessels. Russian Metallurgy (Metally). (3), 259-264.
DOI: https://doi.org/10.1134/S003602952003012X

[11] Romantsev, B.A., Aleshchenko, A.S., Tsyutsyura, V.Y., et al., 2017. Features of piercing mill TPA 50-200 working roll wear during rolling continuously-cast and hot-rolled billets. Metallurgist. 60, 1062-1069.
DOI: https://doi.org/10.1007/s11015-017-0408-x

[12] Shatalov, R.L., Medvedev, V.A., 2022. Deformation temperature conditions providing prescribed property uniformity for steel vessels and a device for non-destructive control. Metallurgist. 65(9-10), 1117-1124.
DOI: https://doi.org/10.1007/s11015-022-01254-w

[13] Shatalov, R.L., Medvedev, V.A., Bogdanov, S.V., 2022. Development and use of an electromagnetic unit for controlling the mechanical properties along the steel vessel height at the exit from a rolling—pressing line. Russian Metallurgy (Metally). (6), 628-633.
DOI: https://doi.org/10.1134/S0036029522060210

[14] Gamin, Y.V., Skripalenko, M.M., Romantsev, B.A., et al., 2021. Prediction of billet fracture at two-high screw rolling piercing. Metallurgist. 64, 1020-1028.
DOI: https://doi.org/10.1007/s11015-021-01093-1

[15] Goncharuk, A.V., Gamin, Y.V., Sharafanenko, I.K., et al., 2020. Piercing of a billet in a mill with guide disks. Russian Metallurgy (Metally). 1637-1642.
DOI: https://doi.org/10.1134/S003602952013011X

[16] Romantsev, B.A., Gamin, Y.V., Goncharuk, A.V., et al., 2017. Innovative equipment for producing cost-effective hollow billets for mechanical-engineering parts of small diameter. Metallurgist. 61, 217-222.
DOI: https://doi.org/10.1007/s11015-017-0480-2

[17] Aleshchenko, A.S., Quang, N., 2022. Studying the wear resistance of the mandrels of a two-high screw rolling mill. Metallurgist. 66(5-6), 650-656.
DOI: https://doi.org/10.1007/s11015-022-01372-5

[18] Iskhakov, R.V., Gamin, Y.V., Kadach, M.V., et al., 2020. Development of radial-shear rolling mill special stands for continuous cast billets deformation. IOP Conference Series: Materials Science and Engineering. 966(1), 012074.
DOI: https://doi.org/10.1088/1757-899X/966/1/012074

BILINGUAL PUBLISHING GROUP

Tel:+65 65881289
E-mail: contact@bilpublishing.com
Website:https://journals.bilpubgroup.com

2661-3204
02
9 772661 320230